NTNU

Norwegian University of
Science and Technology

Erosion in the Arctic: A Thermoabrasion Model to Predict Shoreline Change After an Extreme Event

Mohammad Akhsanul Islam

Coastal and Marine Engineering and Management
Submission date: July 2018
Supervisor: Raed Khalil Lubbad, IBM

Norwegian University of Science and Technology
Department of Civil and Environmental Engineering

ERASMUS +: ERASMUS MUNDUS MOBILITY PROGRAMME

Master of Science in

COASTAL AND MARINE ENGINEERING AND MANAGEMENT

CoMEM

EROSION IN THE ARCTIC: A THERMOABRASION MODEL TO PREDICT SHORELINE CHANGE AFTER AN EXTREME EVENT

Norwegian University of Science and Technology
16 July 2018

Mohammad Akhsanul Islam

The Erasmus+: Erasmus Mundus MSc in Coastal and Marine Engineering and Management is an integrated programme including mobility organized by five European partner institutions, coordinated by Norwegian University of Science and Technology (NTNU).

The joint study programme of 120 ECTS credits (two years full-time) has been obtained at two or three of the five CoMEM partner institutions:

- Norges Teknisk- Naturvitenskapelige Universitet (NTNU) Trondheim, Norway
- Technische Universiteit (TU) Delft, The Netherlands
- Universitat Politècnica de Catalunya (UPC). BarcelonaTech. Barcelona, Spain
- University of Southampton, Southampton, Great Britain
- City University London, London, Great Britain

During the first three semesters of the programme, students study at two or three different universities depending on their track of study. In the fourth and final semester an MSc project and thesis has to be completed. The two-year CoMEM programme leads to a multiple set of officially recognized MSc diploma certificates. These will be issued by the universities that have been attended by the student. The transcripts issued with the MSc Diploma Certificate of each university include grades/marks and credits for each subject.

Information regarding the CoMEM programme can be obtained from the programme coordinator:

Øivind A. Arntsen, Dr.ing.
Associate professor in Marine Civil Engineering
Department of Civil and Environmental Engineering
NTNU Norway
Mob.: +4792650455 Fax: + 4773597021
Email: oivind.arntsen@ntnu.no

CoMEM URL: https://www.ntnu.edu/studies/mscomem

CoMEM Thesis

This thesis was completed by
Mohammad Akhsanul Islam

Under supervision of
Dr Raed Lubbad
Associate Professor
Department of Civil and Environmental Engineering
Norwegian University of Science and Technology

As a requirement to attend the degree of
Erasmus+: Erasmus Mundus Master in Coastal and Marine Engineering and Management (CoMEM)

Taught at the following educational institutions:

Norges Teknisk- Naturvitenskapelige Universitet (NTNU)
Trondheim, Norway

Technische Universiteit (TU) Delft
Delft, The Netherlands

At which the student has studied from August 2016 to July 2018.

NORWEGIAN UNIVERSITY OF SCIENCE AND TECHNOLOGY
DEPARTMENT OF CIVIL AND ENVIRONMENTAL ENGINEERING

Report Title: Erosion in the Arctic: a thermoabrasion model to predict shoreline change after an extreme event	Date: 16 July 2018 Number of pages (incl. appendices): xx			
	Master Thesis	X	Project Work	
Name: Mohammad Akhsanul Islam				
Professor in charge/supervisor: Dr Raed Lubbad, Associate Professor, Department of Civil and Environmental Engineering, NTNU				
Other external professional contacts/supervisors:				

Abstract:

Erosion process in the Arctic is broadly classified into two categories: thermoabrasion and thermodenundation. The study completed under this MS framework is focused on thermoabrasion process. A numerical model is developed to predict the shoreline erosion during an extreme event like a storm.

A conceptual model identified the thermoabrasion erosion as a combination of three separate physical processes (1) storm surge flooding, (2) wave cut niche growth and (3) bluff collapse. For each physical process, a separate numerical module was developed. The numerical modules dynamically interact with each other and estimate erosion rate. The model developed under the study is 1D and uses a probabilistic approach by considering distribution patterns of the input parameters. The results were found to be in good agreement with field measurements of Baydara Bay, Russia.

A sensitivity analysis was performed to demonstrate the relative impact of the input parameters on the model. Thermoabrasion erosion rate was found to be greatly dependent on sustained wind speed during the storm, inundation depth at the base of the bluff from storm surge and ice wedge polygon size. In conclusion, the limitations of the model and the scope of future research are outlined.

Keywords:

1. Coastal Erosion
2. CoMEM
3. Thermoabrasion
4. Numerical Model

NTNU
Faculty of Engineering Science
Department of Civil and Environmental Engineering

MASTER THESIS

(TBA4920 Marine Civil Engineering, master thesis)

Spring 2018
for
Student: Mohammad Akhsanul Islam

Erosion in the Arctic: a thermoabrasion model to predict shoreline change after an extreme event

BACKGROUND

Almost one-fourth of the land surface of the northern hemisphere is permafrost. (Fiona, 2013). Thawing of the permafrost will release carbon dioxide and methane in the order of hundreds of gigaton. Permafrost is found near the Arctic and high altitudes. However, only Arctic permafrost are susceptible to erosion caused by global temperature rises. According to Overeem, the exposure of permafrost bluffs to seas water increased by a factor of 2.5 from 1979 to 2009 for northern Alaska. (Overeem et al., 2011). Worldwide, the annual rate of erosion of the coastline is 0-2meter for 90% of the cases. (Lantuit et al., 2011)

Arctic region is responding to climate change more severely than any other regions. Temperature increase is almost twice as the global rate (Serreze et al., 2000). As a result, permafrost is thawing rapidly and the sea ice extent is reducing. Arctic coastal communities are highly affected by the rapid coastline retreats and valuable resources are lost. Recent studies, e.g., (David Lawrence 2014), found that during episodes of rapid sea-ice loss, the rate of Arctic land warming is 3.5 times greater than the average 21st-century warming rates predicted in global climate models. While this warming is largest over the ocean, the simulations suggest that it can penetrate as far as 900 miles inland. The simulations also indicate that the warming acceleration during such events is especially pronounced in autumn. The decade during which a rapid sea-ice loss event occurs could see autumn temperatures warm by as much as 5 degrees Celsius along the Arctic coasts of Russia, Alaska, and Canada.

To predict Arctic coastal erosion, we need to understand the morphodynamics of the permafrost and seawater. Numerical tools and models that were developed for the temperate climate is not useful here. Arctic coastal erosion is unique in nature considering the fact that this erosion is result of various coupled physical processes. Unlike soil erosion in low latitudes region, erosion in the high Arctic is caused by both thermal and mechanical processes. Permafrost exhibits significantly higher strength than thawed soil with pores filled with water. So to induce mechanical erosion, a pre-requisite is melting of permafrost. Moreover, there is

another way of permafrost so-called erosion-frozen permafrost can be eroded as broken bluffs. Two important process includes the erosion are (1) heat transfer to allow permafrost to thaw and (2) mechanical erosion by energy coming from waves. Nairn et al. (1998) identify three key factors which differentiate erosion of permafrost coastlines from those in temperate climates: (1) Melting of exposed frozen sediment by seawater. (2) Eroded material consisting of ice and fine sediment cannot be reconstituted in the littoral zone and thus will not contribute to the sediment balance. (3) Littoral zone subsidence due to melting.

We can divide the general erosion process of the high Arctic coastal into two broad categories: thermo-abrasion and thermo-denudation. In this thesis, focus is placed on the thermoabrasion process. Generally, this process is triggered by an extreme event such as storm surges.

TASK DESCRIPTION

Description of task

As mentioned above, a model describing the thermoabrasion process will be developed. To understand the current status of the know-how of the thermal process, a literature review will be conducted. A conceptual model will be developed based on the known physical processes. The conceptual model may be divided into (1) storm surge (2) niche growth (3) bluff erosion and (4) shoreline erosion models. A proper dynamics of these processes need to be established. Analytical solutions will also be sought out. Finally, a numerical model will be developed to verify the model with field data.

Subtasks and research questions

How to assess the stability of coastal bluffs and predict shoreline erosion in the Arctic after an extreme event?

• Task 1: A Literature review

-subtask 1: a review of the arctic erosion rates and processes

-subtask 2: a review of the tools (models, software) that are available to analyze and predict coastal erosion

• Task 2: Theoretical Model of thermo-abrasion

– subtask 1: Prepare storm surge model (theoretical)

– subtask 2: Establish a niche growth model (physical process based thermal model, considering laws of conversations (mass, energy))

– subtask 3: Proper bluff erosion model (based on geometry, static and dynamic equilibrium of internal friction and external forces, not empirical)

– subtask 4: Shore erosion model

• Task 3: Numerical solutions to the conceptual models

– subtask 1: identify what parameters are most important in this process. Evaluation of existing empirical formula

– subtask 2: Prepare numerical schemes for niche growth and bluff erosion model

– subtask 3: Coupling of niche growth and bluff erosion with storm surge model

• Task 4: Verification of the established model

– subtask 1: Identify location/field data which is facing erosion after an extreme event

– subtask 2: Preparation of the field data for the model

– subtask 3: Validation of the model

– subtask 4: Comparison of the prediction and field data

• Task 5: Conclusion and Recommendation

– subtask 1: issues/limitation of the model that is developed

– subtask 2: conclusion of the analysis
– subtask 3: Recommendation for further development

General about content, work and presentation
The text for the master thesis is meant as a framework for the work of the candidate. Adjustments might be done as the work progresses. Tentative changes must be done in cooperation and agreement with the professor in charge at the Department.

In the evaluation thoroughness in the work will be emphasized, as will be documentation of independence in assessments and conclusions. Furthermore, the presentation (report) should be well organized and edited; providing clear, precise and orderly descriptions without being unnecessary voluminous.

The report shall include:

- Standard report front page (from DAIM, http://daim.idi.ntnu.no/)
- Title page with abstract and keywords. (MScTitlePage[IBM]).
  CoMEM students must include CoMEM as one of the keywords.
- CoMEM page (Only CoMEM students) (CoMEM MSc title Page templateNTNU).
- Preface
- Summary and acknowledgement. The summary shall include the objectives of the work, explain how the work has been conducted, present the main results achieved and give the main conclusions of the work.
- Table of content including list of figures, tables, enclosures and appendices.
- A list explaining important terms and abbreviations should be included.
- List of symbols should be included
- The main text.
- Clear and complete references to material used, both in text and figures/tables. This also applies for personal and/or oral communication and information.
- Thesis task description (these pages) signed by professor in charge as Attachment 1.
- The report musts have a complete page numbering.

The thesis can as an alternative be made as a scientific article for international publication, when this is agreed upon by the Professor in charge. Such a report will include the main points as given above, but where the main text includes both the scientific article and a process report.

Submission procedure
Procedures relating to the submission of the thesis are described in IV faculty webpage
https://www.ntnu.edu/iv/master-thesis-regulation

On submission of the thesis the candidate shall submit to the professor in charge a CD/DVD('s) or a link to a net-cloud including the report in digital form as pdf and Word (or other editable form) versions and the underlying material (such as data collection, time series etc.).

Documentation collected during the work, with support from the Department, shall be handed in to the Department together with the report.

According to the current laws and regulations at NTNU, the report is the property of NTNU. The report and associated results can only be used following approval from NTNU (and external cooperation partner if applicable). The Department has the right to make use of the results from the work as

if conducted by a Department employee, as long as other arrangements are not agreed upon beforehand.

Start and submission deadlines
The work on the Master Thesis starts on : 12 February 2018_____

The thesis report as described above shall be submitted digitally in DAIM at the latest: 9 July 2018 at 3pm (revised: 16 July 2018 at 3pm).

Professor in charge: Raed Lubbad
Associate Professor
Department of Civil and Environmental Engineering
NTNU

Other supervisors: _____

Trondheim, dd.mm.yyyy. (revised: dd.mm.yyyy)

_____
Professor in charge (sign)

Citations

FIONA, H. 2013. 1.5C rise in temperature enough to start permafrost melt, scientists warn. *In:* FIONA, H. (ed.).

LANTUIT, H., ATKINSON, D., PAUL OVERDUIN, P., GRIGORIEV, M., RACHOLD, V., GROSSE, G. & HUBBERTEN, H.-W. 2011. Coastal erosion dynamics on the permafrost-dominated Bykovsky Peninsula, north Siberia, 1951–2006. *Polar Research,* 30**,** 7341.

OVEREEM, I., ANDERSON, R. S., WOBUS, C. W., CLOW, G. D., URBAN, F. E. & MATELL, N. 2011. Sea ice loss enhances wave action at the Arctic coast. *Geophysical Research Letters,* 38**,** n/a-n/a.

Dedication

To my son Sayan Bin Akhsan

"you will travel far, my little Goel. My world may be lost, but this is your world now. Take whatever you need from it and make a home…."[1]

[1] Durotan, chieftain of the FrostWolf clan to his new born son; Warcraft (2016)

Abstract

Arctic coasts erode at a rate 3 to 4 times higher than the rates at tropical coasts. Records of Arctic coast erosion are neither comprehensive and nor continuous in time. The number of tools available to predict the shoreline changes in the Arctic is limited. Prone to site-specific issues, these models are only applicable to a limited number of processes. On the other hand, models developed and calibrated for temperate climates do not work properly in the Arctic because of the effect of thermal components.

Erosion process in the Arctic may broadly be classified into two categories: thermoabrasion and thermodenundation processes. Thermodenundation is related to the melting of the frozen coast. The mechanical strength of the frozen soil decreases when the soil undergoes thawing. The weaker mechanical strength of the soil cannot maintain a steeper slope; thus, slopes fail and the crest of the shore retreats. Unlike thermodenundation, thermoabrasion process is rather episodic and it is associated with storm events. During the storm, a coastal bluff in the Arctic faces the storm surge flooding that may lead to the development of a niche at the base of the bluffs. When the niche is deep enough, the frozen bluff becomes unstable and a collapse is triggered. The study completed under this MSc framework is focused only on the thermoabrasion process. A numerical model is developed to predict the shoreline erosion during an extreme event like a storm.

The theoretical model identified the thermoabrasion erosion as a combination of three separate physical processes namely: storm surge, wave-cut niche and bluff collapse. Numerical modules were developed for each physical process. The numerical modules discretise the governing equations and interact with each other dynamically. The three numerical modules were integrated together and calibrated in one model to simulate the thermoabrasion process. A simplified storm surge model was considered for the hydrodynamic inputs. Analytical solutions were used to determine the niche growth during a storm. The numerical model was applied to the field observations of Baydara Bay, Russia. Results are found to be in good agreement with field measurements.

Both deterministic and probabilistic sensitivity analysis was performed to demonstrate the behaviour of the numerical model. For each of the modules relative impacts of the input parameters were determined. Thermoabrasion erosion rate was found to be greatly dependent on wind speed during the storm, inundation depth at the base of the bluff and ice wedge polygon size.

Further field and laboratory works are suggested to improve the understanding of the theoretical model. Higher order accurate numerical schemes can increase the accuracy of the model.

Acknowledgements

Special thanks to Raed Lubbad for allowing me to work on such an interesting project; also, for the enthusiastic support and granting the freedoms. Grateful to Esther, Elakel, David, and Alahyar for the coffee break discussions and potluck parties at the weekends.

Sincere gratitude to Sonja Marie Ekrann Hammer and Øivind Arntsen, and everyone else involved in the CoMEM program.

Contents

List of Figures

List of Tables

Nomenclature

Abbreviation

CoV= coefficient of variation

DHI= Danish Hydraulic Institute

MSL= mean sea level

MSU= Moscow State University

Pdf= probability density function

SINTEFF= Stiftelsen for Industriell og Teknisk Forskning

Symbols

T_r	A resisting moment from a non-hanging portion of the bluff
P_a	Atmospheric pressure
ρ_b	Bluff density
y_{base}	Bottom of the hanging slab; just above niche
x_p	Critical niche depth from the base of the bluff
ρ_i	Density of ice
ρ_s	Density of sediments
ρ_w	Density of water
ε	Diffusivity index
T_d	Driving moment from hanging slab towards bluff collapse
ξ_m	empirical parameter
C_f	Friction factor of the wind-air surface.
h_{id}	Inundation depth at the base of the bluff
L_i	Latent heat of ice
ε_m	Momentum diffusivity at the melting point
S_a	Salinity concentration
C_a	Sediment concentration
c_i	Specific heat of ice
c_w	Specific heat of sea water
c_s	Specific heat of suspended sediment
C	Suspended sediment concentration (initial)

T_a	Temperature of water
m	The empirical constant of *Josberger*
A	The empirical parameters of the longshore current
h_{bluff}	The height of the bluff from the base
x_m	The melting point of the niche from the base of the bluff
β	The opening of niche (empirical)
n	The porosity of the frozen sediments
S_i	The salinity of the ice
S_m	The salinity of the melting point
S	The salinity of the sea water inside niche
U	The velocity of the air
y_{top}	Top of the bluff level
$T_{resisting}$	Total resisting moment acts against bluff collapse
h	Water depth
η_c	Water level increase due to currents
η_b	Water set up due to low pressure
η_w	Water set up due to wind speed
τ_s	Wind stress

1 Introduction

1.1 Background

Almost one-fourth of the land surfaces of the northern hemisphere is permafrost (Fiona, 2013). Thawing of the permafrost releases carbon dioxide and methane in the order of hundreds of gigaton(Anisimov et al., 2006). Permafrost is found in the Arctic, near to it and high altitudes. The exposure of Arctic permafrost bluffs to seawater increased by a factor of 2.5 from 1979 to 2009 for northern Alaska. (Overeem et al., 2011). Worldwide, the annual rate of erosion of the coastline is 0-2meters for 90% of the cases (Lantuit et al., 2011).

Arctic region is responding to climate change more severely than any other regions. Temperature increase is almost twice as the global rate (Serreze et al., 2000). As a result, permafrost is thawing rapidly and the sea ice extent is reducing. Arctic coastal communities are highly affected by the rapid coastline retreats and valuable resources are lost. During episodes of rapid sea-ice loss, the rate of Arctic land warming is 3.5 times greater than the average 21st-century warming rates predicted in global climate models (Lawrence, 2008). While this warming is largest over the ocean, the simulations suggest that it can penetrate as far as 1,400 kilometres inland. The warming acceleration during such events is especially pronounced in autumn. The decade during which a rapid sea-ice loss event occurs could see autumn temperatures warm by as much as 5° Celsius along the Arctic coasts of Russia, Alaska, and Canada (Lawrence, 2008).

Erosion processes of the high Arctic coasts may be broadly divided into two main categories: thermoabrasion and thermodenundation (Are,1988). Thermodenundation is continuous degradation of the frozen coast by thawing and slump failures. Thermoabrasion is episodic; generally triggered by an extreme event such as storm surges. In this thesis, the focus is placed on the thermoabrasion process.

To predict Arctic coastal erosion, understanding of the morphodynamics of the permafrost and seawater is very important. Numerical tools and models that are developed for the temperate climate is not useful here. Arctic coastal erosion is unique in nature; erosion is the result of various coupled physical processes. Unlike soil erosion in low latitudes region, erosion in the high Arctic is caused by both thermal and mechanical processes.

1.2 The objective of the study

The salient objective of the thesis is to develop a numerical model to calculate thermoabrasion erosion rate of the Arctic coast. To elaborate on the objective of the thesis, the following activities and corresponding milestones are planned:

- Development of a conceptual model based on known physical processes (i.e. storm surge, niche growth and bluff collapse).
- Discretization of the governing equations of the conceptual model to seek out a numerical solution where an analytical solution cannot be achieved.
- Calibration and Validation of the numerical model with field data
- Implementation of a sensitivity analysis to demonstrate the behaviour of the numerical model

1.3 Motivation

The aspiration to develop a tool to determine Arctic coastal erosion is to estimate and reduce risk to coastal infrastructures. Industrial infrastructures such as ports, processing plants, and pipelines must all account for coastal flooding and rapid erosion in their designs (Prowse et al., 2009). As the length of the open water season increases (Larsen et al., 2014), so too will the period for shipping which will increase the need for additional marine infrastructure development (Prowse et al., 2009). Arctic ports may face challenges of sea ice loads, rapid erosion by thermoabrasion, permafrost thawing and potentially harbour siltation via the flux of fine sediment from widespread eroding coastlines. More accurate predictions of coastal erosion rates could yield better estimates of carbon flux for the purposes of improving oceanographic and climate models.

1.4 Methodology

A theoretical model was developed based on known physical processes involved in coastal erosion due to thermoabrasion. The governing equations are based on fundamental physics, e.g. conservation of mass, energy, salinity, sediments and not on empirical rules. The governing equations were discretized in time and space. The resulting numerical model can calculate short-term shoreline erosion by thermoabrasion during storms.

Mostly secondary data sources were used to develop the model. To calibrate and validate the model field observations from Baydara Bay, Russia was used. The numerical model was calibrated using field measurements from 2012-2013. Further, the model is validated using field data from 2016-2017.

Deterministic and probabilistic sensitivity analyses were completed to demonstrate the response of the numerical model in different cases. Normal distribution with reasonable CoV (coefficient of variation) was assumed where lack of data did not permit to establish a distribution pattern.

1.5 Limitation

The numerical model developed in the current study was not comprehensive. It is prone to site-specific issues and can be used for a very specific type of erosion (thermoabrasion). Other than these limitations, the following phenomena are not included in the model:

- Sediment types are not considered in the model. The numerical model does not calculate the after-storm profile of the beach. Slope and shape of the beach are highly dependent on the sediments of the eroded blocks. Fine sediments are typically washed away to deeper parts of the coast while coarse sediments may stay nearshore. Coarser sediments thus contribute to raising of the beach and further protects the bluffs.
- Only water is considered as a thermal energy source for the energy balances. Air temperatures and solar radiations are not considered.

2 Literature Review

2.1 Permafrost

A major difference between the Arctic and tropical coasts is the permafrost. If the soil is frozen for more than two years it is called Permafrost. 24% of the land surfaces of the earth consist of permafrost (Fiona, 2013). Most of these areas are in the high Arctic, like Alaska, Greenland and the northern part of Canada.

Typically, water is present in the voids within the soil. Water contained within the pores of particles turned into ice when subjected to temperatures below freezing point. Freezing of waters alters mechanical properties of the soil. Permafrost exhibits higher mechanical strengths due to the presence of ice. Typical characteristic changes are the increment of strength, meanwhile reduction of permeability. These two parameters alter soil properties to great extents. Figure 2-1 shows an exposed permafrost coast open to thawing.

Figure 2-1 Melting permafrost in the northwest territories (knight, 2017).

Soil containing water below the freezing process exhibits volume increase. Another physical process called cryosuction may also occur. Cryosuction is related to water flow in the direction of the freezing front. Water flows through the available pores in the unfrozen portion of the soil which results in ice lenses. Ice lenses grow over time and influence the volume expansion. Uneven volume expansion is a potential danger for the infrastructure and may cause instability.

During thawing, permafrost loses most of the mechanical strength. Frozen water and soil has a close relation as depicted in Figure 2-2.

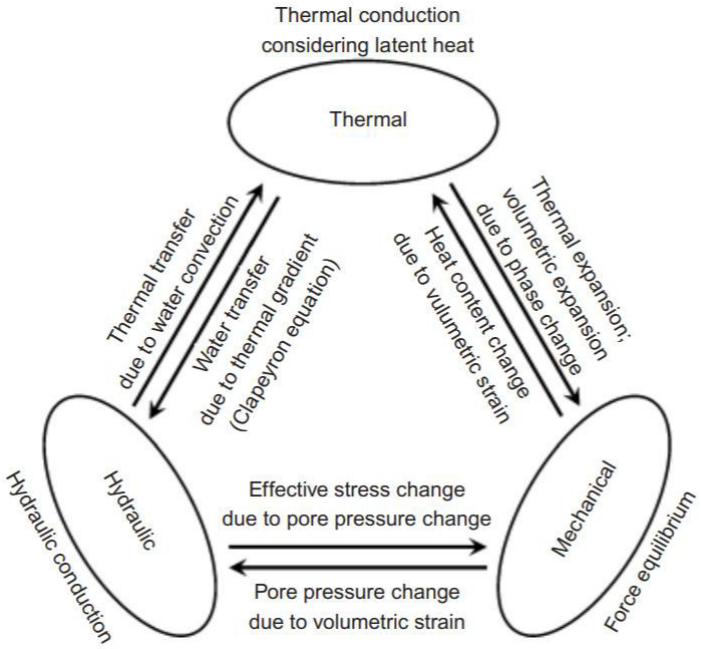

Figure 2-2 Thermal, Mechanical and Hydraulic processes in frozen soil (Thomas et al., 2009).

Permafrost is typically found at high altitudes and close to Arctic circle. Freezing occurs from the surface and downwards, a process called two-sided freezing (Thomas et al., 2009). Naturally, permafrost thaws when exposed to higher temperatures and solar radiations. In case of the open coast or ice-free season in summer; a continuous melting of permafrost occurs along the coast(Pearson et al., 2016).

The extent of permafrost depends on the climatic conditions. Overlaying on top of the permafrost is a thin layer of the active layer. The active layer susceptible to warmer conditions; sometimes thawed during summer. As a result, the thickness of the active layer varies with time and depth. Presence of permafrost in the land has unique effects.

2.2 Ice Wedge

The ice wedge is a crack visible on the surface of the ground (Figure 2-3). Typically formed with ice that penetrates 3 to 4 metres into the soil. During the winter season, water inside the

cracks freezes and expands. Ice acts like solids and expands to form cracks in the surface known as ice wedge. Ice wedges usually connect with each other and form irregular geometric shapes called ice-wedge polygon (Wikipedia, 2018).

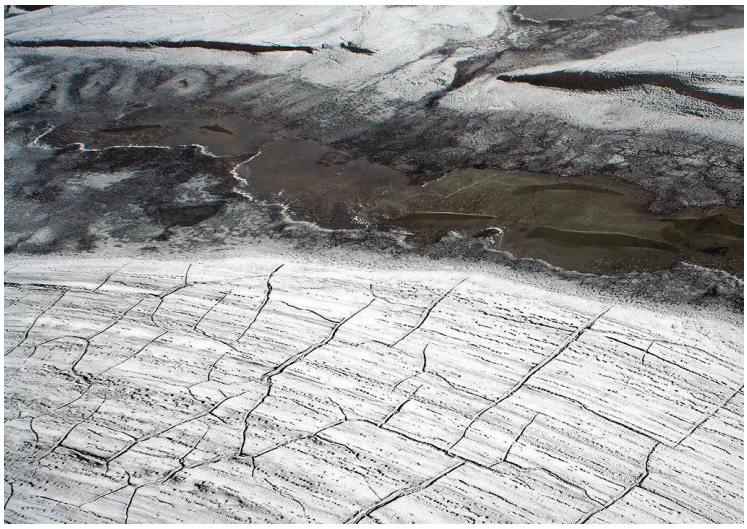

Figure 2-3 Ice wedge polygon on the permafrost [image source: wikipedia.org/wiki/Ice_wedge].

Ice-wedge polygons are a common feature of the permafrost topography. Thermal contraction introduces cracks in the permafrost. Ice wedges begin to grow in the cracks when spring snowmelt infiltrates them and freezes to form near-vertical sheets of ice. Ice-wedge growth deforms the surrounding ground to accommodate the additional volume. The growth of the ice wedges often forces the adjacent ground upwards and laterally, creating a trough above the ice wedge (Osterkamp and Burn, 2015).

2.3 Erosion in the Arctic

There are two unique coastal erosion processes in the Arctic areas: thermodenundation and thermoabrasion. Even though these processes are dominated by both thermal and mechanical actions, we can still distinguish between the two processes.

2.3.1 Thermodenundation

Thermodenundation is a thermal action dominated erosion process. A portion of the frozen bluff is exposed to warm weather that starts to thaw under the actions from hot air, energy from solar

radiation and snowmelt (Guégan 2015). When frozen bluff starts to melt, mechanical strengths are reduced. At one point, the stability of the slope cannot be maintained, a slope slipping occurs(Pearson, 2015). The unfrozen and unconsolidated sediments are prone to wave action and removed by waves and currents (Lantuit et al., 2011).

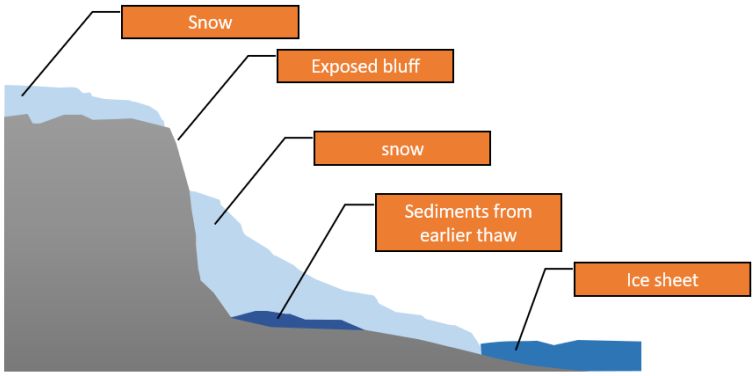

Figure 2-4 A typical coast susceptible to thermodenundation.

Figure 2-4 describes a typical coast in the Arctic during winter to late spring. Most of the coast is covered in snow. Snow itself works as a thermal barrier. It is very common that the whole coast is not covered in snow. Typically, steeper portions are exposed to warmer air. The coast may be protected from wave action. Land-fast ice may prevent the waves to reach the base of the frozen bluffs.

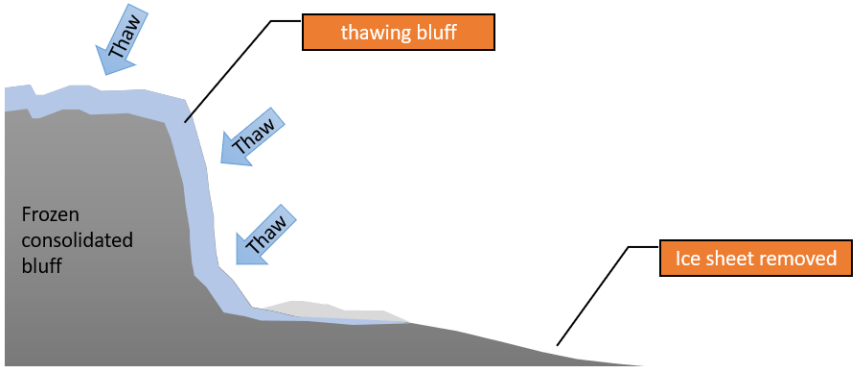

Figure 2-5 Thawing of the frozen bluffs.

Figure 2-5 illustrates the situation of a typical coast in the Arctic during late summer to early fall. In this stage, snowbank and the land fast ice have most likely disappeared. The thawing

process of the bluff progresses inward. The exposed or vulnerable portions of the bluff start to melt(Pearson, 2015).

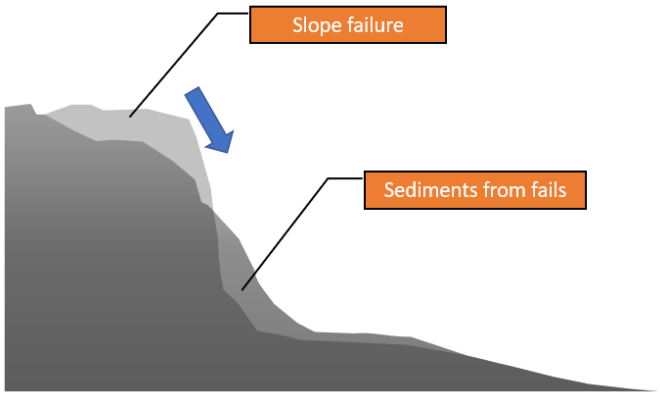

Figure 2-6 Slope fails in the thermodenundation process.

Figure 2-6 describes the second phase of the thermodenundation process where the strength of the material is greatly reduced. The slope becomes physically unstable and the strength of soil ceases to maintain a steeper slope. Due to a reduction in mechanical strength, slope failure will occur at some point and materials will be accumulated at the base.

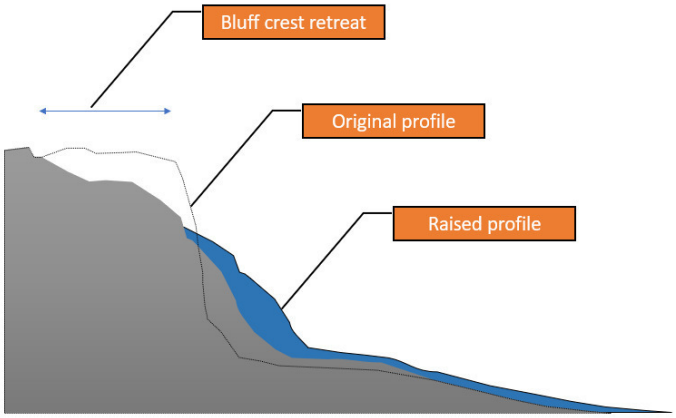

Figure 2-7 Removal of sediments after slope failure.

The after effect of slope failure is described in Figure 2-7. As a result of slope failure, bed profile is raised and the slope is reduced. However, all the collapsed materials do not contribute to bed profile change. Collapsed materials are typically unconsolidated (from the action of thawing and slope failure) and have very little to no-resistance to wave actions. Some of the

failed bluffs are washed away to the deeper parts of the shore by waves and currents. A crest retreat as shown in Figure 2-7 is detected.

2.3.2 Thermoabrasion

Thermodenundation tends to dominate in calm conditions. The rate of removal of thawed sediments may be faster than the rate of melting of the frozen sediment during the storm. This exposes the frozen sediment directly to the mechanical and thermal action of seawater in a different process called thermoabrasion (Günther et al., 2013).

Nairn describes that thawed sediment must be removed from the bluff face and beach prior to thermoabrasion (Nairn et al., 1998). Barnhart (2014) argues that it is not a necessary condition. The time-lapse observation near the coast of Alaska, USA indicated that degrading of the collapsed blocks does little to protect the coast from wave action and thus not a rate-limiting factor for long-term erosion (Barnhart et al., 2014).

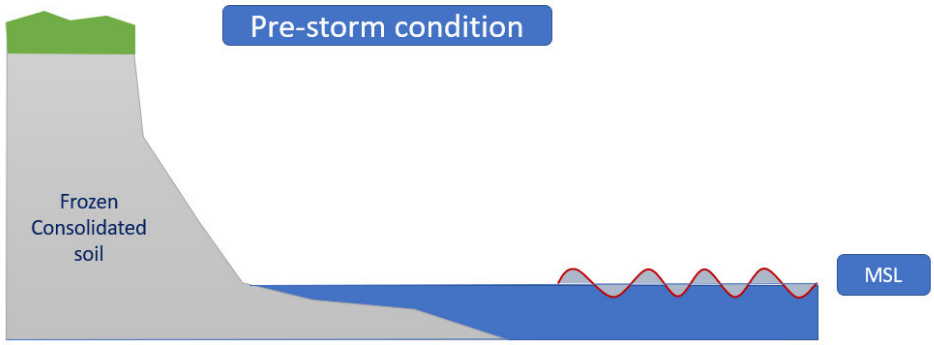

Figure 2-8 A typical beach susceptible to thermoabrasion.

Let's assume a beach on the Arctic coast that can be susceptible to thermoabrasion (Figure 2-8). Waves break in the narrow beach in front of the frozen bluffs. Sediments that are coarse enough to sustain wave actions contributed to the formation of the beach. The beach is above mean sea level so that water cannot reach the base of the bluff. Thawed sediment on the bluff face and on the beach can be assumed to be removed in high tides.

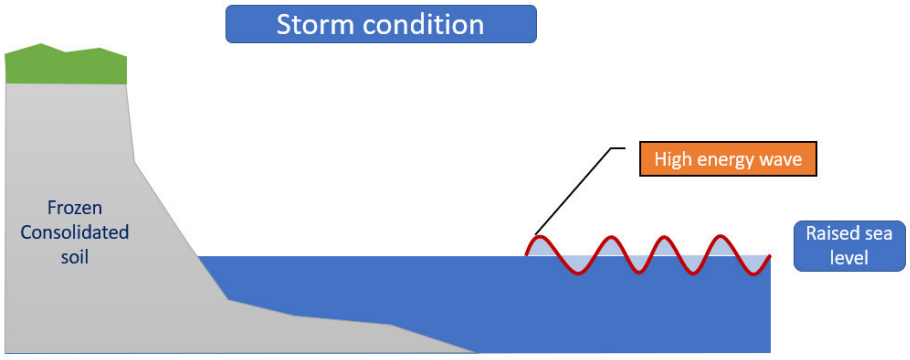

Figure 2-9 Raised water level during a storm.

During a storm (see Figure 2-9), water level starts to rise. The wind blows over the water creates stress on the air-water interface. To counter the force generated by friction, water level near coast raises. Due to water height difference, a force will act towards offshore and balances out the force generated by wind. Wind also creates high energy waves directed towards the coast. As the water level increases, the probability of high wave energy reaching the base of the bluff increases. A wave induced niche will start to grow when water reaches the base of the bluff (Figure 2-10). The eroded sediments from the niche will be carried offshore by return currents. During a storm, the return current can be quite high. Waves will also carry warm water which will further increase the niche growth.

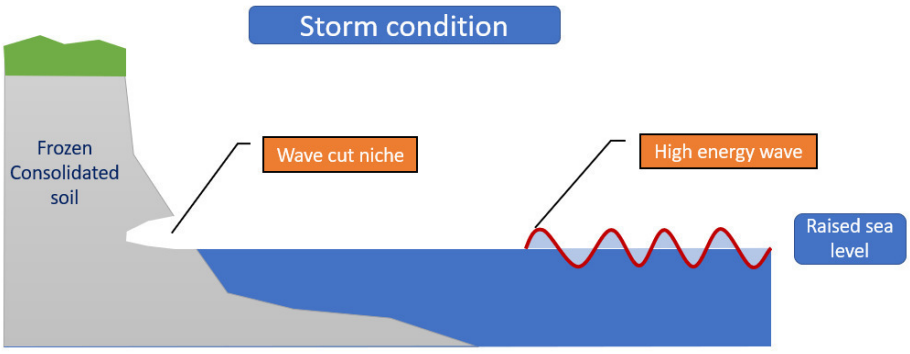

Figure 2-10 Inward niche growth during the storm.

When the niche undergoes considerable growth, the hanging bluff will exert substantial moment as depicted in Figure 2-11. At one point in time, the resisting forces will be smaller than the

failure force and collapse of the bluff will be triggered. The niche depth at which the collapse is initiated is termed *critical niche depth*.

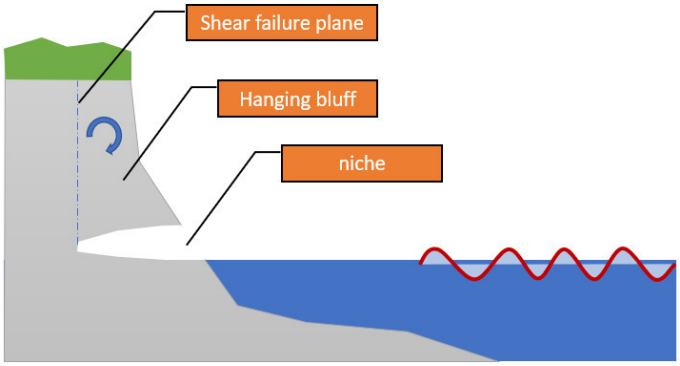

Figure 2-11 Niche growth to a critical depth just before failing.

It is not essential that niche growth will reach critical depth during one storm. It may happen within several storms. When the collapse occurs, the fallen block become exposed to wave action. Over the next few days, the fallen block will be eroded (Figure 2-12). The eroded sediments will be deposited in the bed and may raise the bed. It may raise the beach in front of the bluff face. In this way, the fallen block act as a protective element and reduce the erosion.

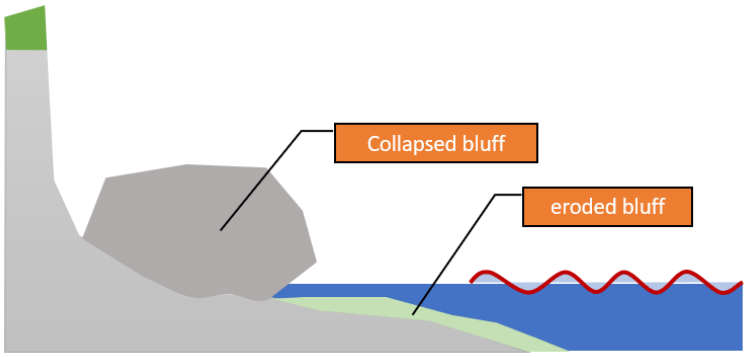

Figure 2-12 Erosion of the collapsed block by waves.

However, warmer turbulent sea water in direct contact with the frozen soil increases thawing rate via convective heat transfer. The temperature difference between seawater and frozen bluff is a key factor determining the rate of cliff retreat (Kobayashi and Aktan, 1986)

As a summary, rapid thawing and removal of sediment result in the formation of horizontal niches in the frozen bluff face (Overeem et al., 2011). Niche grows inwards reducing the stability of the bluff. When the niche reaches critical depth, the stability of the bluff is lost. Collapsed block undergo erosion due to wave and may take days to years to be fully removed from the coast. The bluff which consists of the coarse material may contribute to beach formation. These narrow beach works as a barrier and further reduce the erosion process.

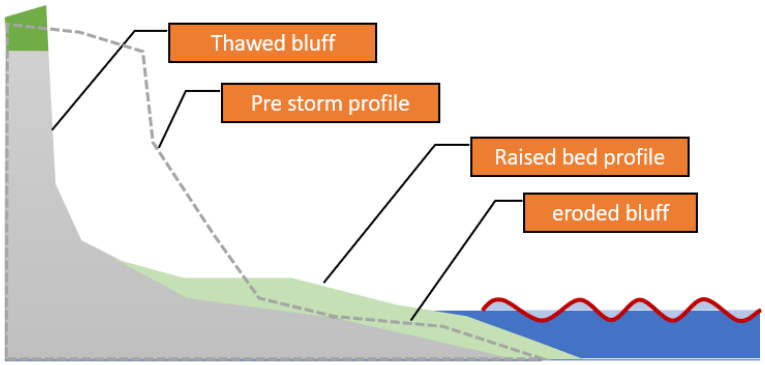

Figure 2-13 After storm condition.

The thermoabrasion is greatly influenced by storm surge since a larger portion of the bluff cliff sediment becomes exposed to seawater (Kobayashi and Aktan, 1986). The increased nearshore depths also enable larger waves to reach bluff which increase the mechanical erosion action. Presence of ice matrix in the soil has two-way action. Firstly, the existence of more ice reduces the erosion as thawing of ice requires a lot of energy; secondly, washing of the sediments are easier if ice content is high.

The rate of erosion is greatly accelerated by the presence of permafrost when the two actions are combined. Thermoabrasion process is episodic; occurring seldom. But erosion rate in this process is very high. This may also expose the infrastructures and communities to sudden risk. Thermoabrasion is also a sequential process, if one condition is not meet, the process will not continue. For example, thermoabrasion requires that water level reach the base of the bluff. Also, a necessary condition that niche reaches critical depth. Then the collapse of the block can be triggered. Because of this nature of the sequential process that triggers one another, the thermoabrasion process becomes remitting and depended on the extreme events.

A summary of the two process, thermodenundation and thermoabrasion is described in Table 2-1.

Table 2-1 Comparison of Thermodenundation and Thermoabrasion

Process	Thermodenundation	Thermoabrasion
Frozen bluff properties	High ice concentration, fine sediments	Fine or Coarse sediments.
Weather	Calm condition	During storm
Ice cover	Open water season is not a necessary condition, energy availability for thawing is sufficient condition	Must be within open water season (summer in the Arctic)
temperate climate models	Sediment transport formulae developed for temperate climate can be used with modification	Temperate climate models are not useful to model this type of erosion as the physics is totally different
Continuity	Can be described as a continuous process	It is highly episodic, that means only occurring when all the preconditioned are achieved

2.3.3 Prediction of the erosion

As discussed in the previous sections (section 2.3.1and 2.3.2), erosion in the Arctic is a combination of various physical processes. Regression of shoreline can be explained from various angles. The dominating physics can be described from the geotechnical point of view considering the bluff strength and finite element analysis of thawing-slope failures. Another way is based on the hydrodynamics of the location. Multi facades of erosion put the scientific community in the dilemma as if "geomorphological roulette for engineers and planner (Brunsden, 2002) ".

Coastal engineers adopted different approached to predict the erosion rate-ranging small to large scale in temporal and spatial aspects. These models can be probabilistic, statistical or deterministic. Since available data to analyse the physics in the Arctic is limited, probabilistic

models are still in innate stage(Frederick et al., 2016). Several software packages are available to model arctic coast. However, most of them are prone to site-specific issues and cannot be applied globally. In practice, the use of the models to realistically predict the stability of a coastal cliff is not possible due to numerous parameters needed and uncertainty in their determination (Brunsden and Lee, 2004).

3 A conceptual Thermoabrasion model

In this chapter, a conceptual model of coastal erosion due to thermoabrasion is formulated. The conceptual model is termed *process based* because the physics related to the real-world erosion are divided into few distinguishable processes. Failure is predetermined and only allowed in very specific ways.

The erosion model described below consists of three major modules. These are:

- Storm surge module
- Niche growth module
- Bluff collapse module

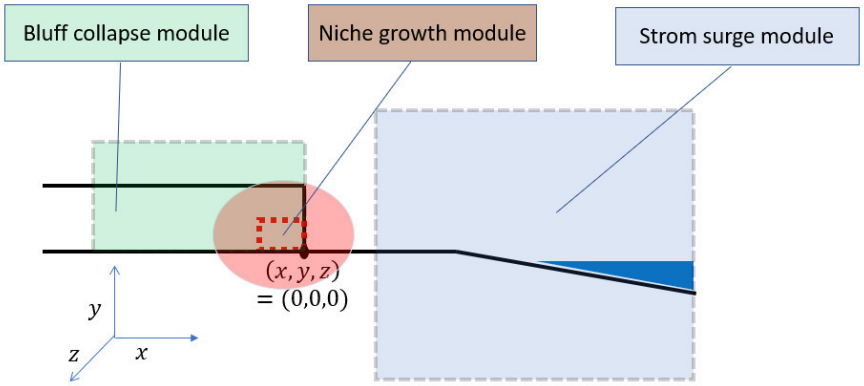

Figure 3-1 Domain of the three modules.

Figure 3-1 depicts the domains of the modules. Centre of the coordinates is placed at the base of the bluffs. Geometric parameters are defined in section 3.1.1.4.

3.1 Simplifying assumptions

Thermoabrasion is a complex process which is very difficult to simulate numerically since the understanding of the process is not complete and thus the process is simplified with reasonable assumptions.

3.1.1 Standardization of the problem

Thermoabrasion is the dominating process in the very particular environment. It requires few specific conditions that must be complied.

3.1.1.1 Episodic event

Thermoabrasion is related to the extreme events. The niche growth does not occur when water stays at Mean Sea Level. In the conceptual model, from the base of the frozen bluff to the shoreline there exist a narrow beach as shown in Figure 3-2. The beach is flat and consists of granular materials which are most probably a remnant of the earlier bluff fails. The beach material is not fine particles and quite resistant to wave action. As the beach is above MSL most of the time, water cannot reach the base of the bluff. Niche growth is not triggered by tide or other small events. Only when warm water reaches the base of the bluff during a storm, niche starts to grow.

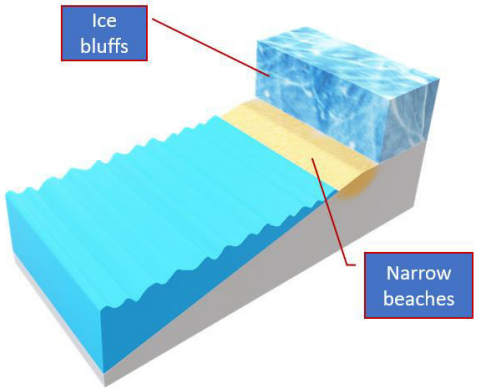

Figure 3-2 Simplified Arctic coast with regular geometry.

3.1.1.2 Regular geometry

The conceptual model assumes the geometry to be regular. The beach is straight with regularly sized bluff standing at the end. The narrow beach will be flooded in case of an extreme event (storms). Figure 2-2 depicts the standardized geometry in pre-storm conditions.

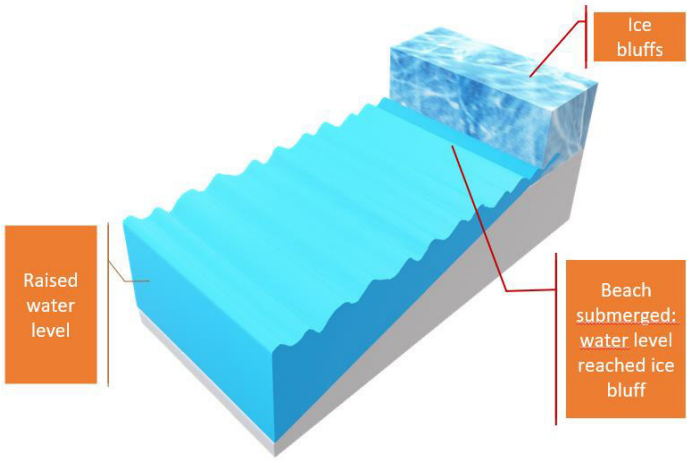

Figure 3-3 Beach is flooded and waves reached the base of the bluff during the storm.

3.1.1.3 Storm condition

One effect of the extreme event is the surge created by the storm. During the storm, wind speed is significantly high. The wind blows over the water surface and generates stress on it. To balance out the force generated from wind speed, the water level rises. During the storm, the beach may be flooded and wave reached the base of the bluff (Figure 3-3). It is only then a wave-cut niche growth is seen at the raised water level. The model assumes the niche is growing uniformly. Figure 3-4 shows one typical niche growth in the conceptual model. Overhanging bluff is of regular geometry and top of the frozen bluff is also assumed to be flat. The niche grows inward and uniformly in the cross direction. The height of the niche is proportional to the water depth in front of the base.

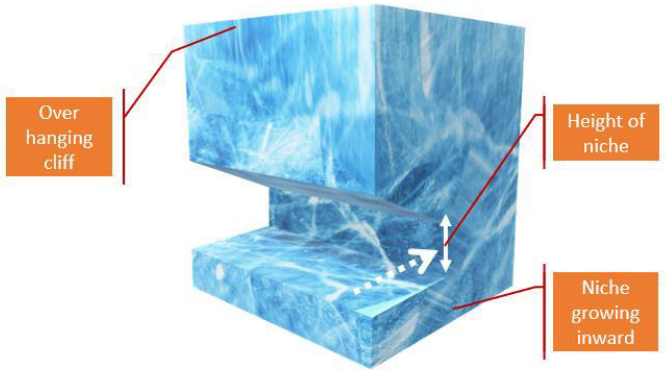

Figure 3-4 standardized inward growing niche: regular geometry and uniform in cross directions.

3.1.1.4 Definition of geometric parameters of niche growth

Few geometric parameters used in the model is standardized first. The base of the bluff (point C) is the centre of the coordinate system. x axis is directed to offshore, y axis vertically above the base of the bluff and z axis in cross shore direction. The face of the bluff is at zy plane at $x = 0$.

Inundation depth (h_{id}) is defined as the water depth at the base of the bluff. Without a storm, the value of h_{id} is zero since it is assumed that the base of the bluff is above MSL. Bottom most point of the hanging bluffs is y_{base} and the highest point of the bluff is y_{top} . The bluff height (h_{bluff}) can be written as $h_{bluff} = \beta h_{id} + (y_{top} - y_{base})$; where β is an empirical parameter. Kobayashi (1985) considered value of β to be 2.

During a storm, the wind blows in the negative x-direction. The niche grows in the negative direction along the x axis. A plane is assumed at the melting point (point M, at $x = -x_m$) of the niche which is continuously growing during a storm. Niche depth is marked as x_m which is dependent on time. Critical niche depth (x_p) is defined as the depth of niche at which the bluff collapse is triggered. A melting plane is assumed at point M of unit width (z direction) and βh_{id} height (y direction). The plane is vertical during niche growth and while growing depth of the niche is kept at βh_{id}.

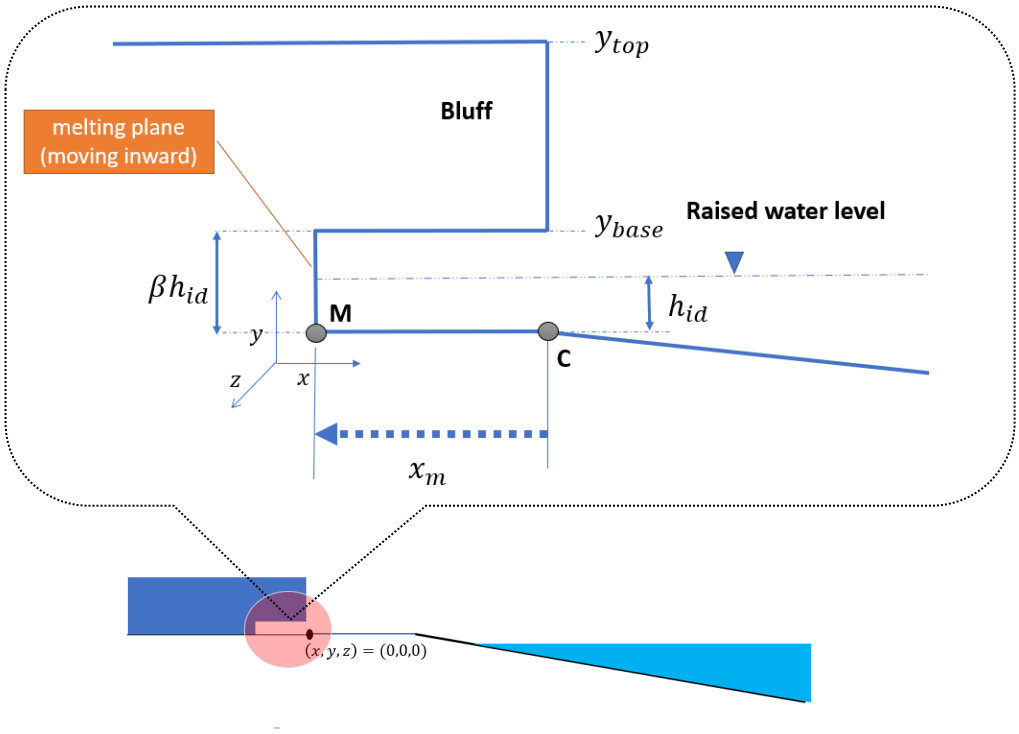

Figure 3-5 Definition of the geometric parameters.

3.2 Strom surge module

Various software packages are available that can calculate storm surges. Some of them account variations in the bed profiles so that diffractions and reflections are properly handled. The conceptual model under the study is based on storm surge model as described by Dean and Dalrymple (2004). Even though the various software is available, a simplistic storm surge module is developed in the current study.

3.2.1 The justifications for adopting a simplified storm surge model

The most important parameter to determine niche growth is the inundation depth (h_{id}) at the base of the bluff. The beach in front of the frozen bluff is either very narrow or non-existing. It can thus be reasonable to assume that maximum wave height in front of the frozen bluff during the storm is depth limited (Kobayashi, 1985). To achieve efficiency, it may be better to calculate the water depth at the point of interest (at base of the bluff) using a simplified storm surge model and assume wave conditions rather than a calculation of wave generations in the deep sea and transform waves to the shore.

Secondly, the niche growth model as described by Kobayashi (1985) does not require wave data of the site during the storm. The important parameters involved in the niche growth are the thermal driving (represented by the ambient seawater) and mechanical driving (represented by the mean water depth in the neighbourhood of the frozen bluff (Kobayashi, 1985)). It will be a great computational effort to accurately calculate wave condition using variable bathymetry. Envisioning that the model would simulate at least 90 days (summer days) and time step would be around 10 minutes, it was decided to go for simplified storm surge model. Simulating wave transformation of a long time with very high precision demands vast computational power which is not justified since the wave conditions are not direct input for the niche growth model.

Subsequent section 3.2.3 describes the storm surge model used for this study.

3.2.2 Definition of storms

Storms are caused by the pressure gradient. Wind flows from high pressure to low pressure. Typically, the centre of the storm is the low-pressure zone. Wind fields are driven along the pressure gradient towards the centre. Storms can generate wind speeds of more than 200 kilometres per hour. While blowing over the ocean surface, wind produces surface waves, surface currents and it blows the ocean coastal waters against the coastline. Shallow bathymetry increases the piling of water. If the coastline is funnel-shaped, flooding can be immense, and lives are threatened.

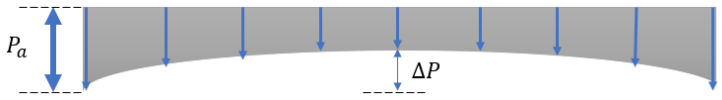

Figure 3-6 Atmospheric Pressure Distribution across a storm.

3.2.3 Storm Surge Components

A storm surge consists of several components, arising from the barometric pressure gradients in the low-pressure storm, the stress coming from wind flows, the Coriolis force induced by earth rotation and the wave set up. The components will be discussed in the following paragraphs.

3.2.4 Barometric water level set up due to low pressure

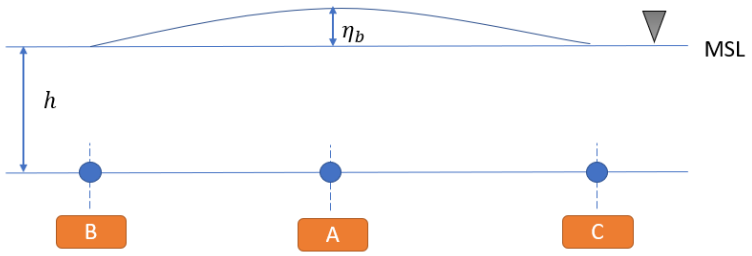

Figure 3-7 Water Level change due to low pressure.

The barometric water level rise is the result of the low-pressure zone at the centre of the storm. The water level is increased in the low-pressure zone. It can be viewed as being pushed up into the low-pressure region by the surrounding high pressure. Figure 3-7 shows such a response of water level due to pressure gradients where point B and C are high-pressure zones and point A is vertically below the centre of low pressure; η_b is the surge due to low pressure. Typical value of such surges is in the order of few centimetres, too small contribution compared with wind stress.

To model this behaviour, hydrostatic pressures must be balanced. Let us assume that water level and storm are stationary. The pressure at the farthest part of water (point B and point C in Figure 3-7) where the pressure gradient is negligible:

$$P(y = -h) = \gamma h + P_a \qquad (1)$$

Where P is the pressure at the bottom of the water column at points B and C, γ is the unit weight of the water, h is the water depth at the point B and C and Pa is the atmospheric pressures.

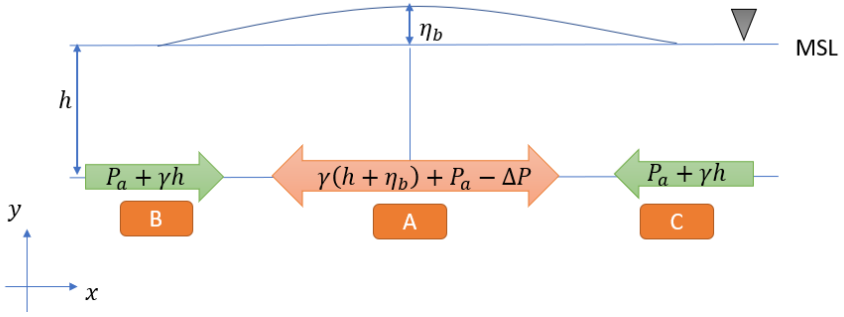

Figure 3-8 Pressure difference due to different water level.

The bottom pressure mentioned in the equation 1 must be equal to the pressure under the centre of the storm. If the pressures are not the same, water will flow due to the difference in forces. Water level must rise to compensate for the pressure difference. Let's ΔP be the pressure difference due to storm (only the pressure difference from the tmosphere). The pressure at the centre of the storm (point A in the Figure 3-8) is:

$$P(y = -(h + \eta_b)) = \gamma(h + \eta_b) + P_a - \Delta P \qquad (2)$$

Balancing the two equations

$$P(at\ point\ A) = P(at\ point\ B\ and\ C)$$

$$\gamma(h + \eta_b) + P_a - \Delta P = \gamma h + P_a \qquad (3)$$

Which leads to the following:

$$\eta_b = \frac{\Delta P}{\gamma} \qquad (4)$$

As a rule of thumb, $\eta_b = 1.04 * \Delta P$ where ΔP is measured in millibars and η_b measured in centimetres (Dean and Dalrymple, 2004). Table 3-1 demonstrated surge level estimated due to pressure difference in storms. Even for Class 5 (Catastrophic) hurricanes, the surge level is only 9.09 cm.

Table 3-1 Estimated surge for pressure drop at different storm class

Storm Class	Pressure (mbar)			ΔP (mbar)	Surge (cm)
	min	max	mean		
1		980	980	33.25	3.24
2	965	979	972	41.25	4.02
3	945	964	954.5	58.75	5.73
4	920	944	932	81.25	7.92
5	920	-	920	93.25	9.09

3.2.5 Water level set up due to Wind Stress

When the wind blows over the water surface, a drag force is created on the interaction surface at speeds of the two fluids are not equal. The direction of that stress is towards velocity of wind since wind speed is significantly higher than water surface. A force is thus generated at the water-air surface, which needs to be countered. A counterforce is generated from pressure difference.

To model the water setup let's consider a control volume as shown in Figure 3-9 which is Δx wide, height is equal to the water column and one unit in the z direction.

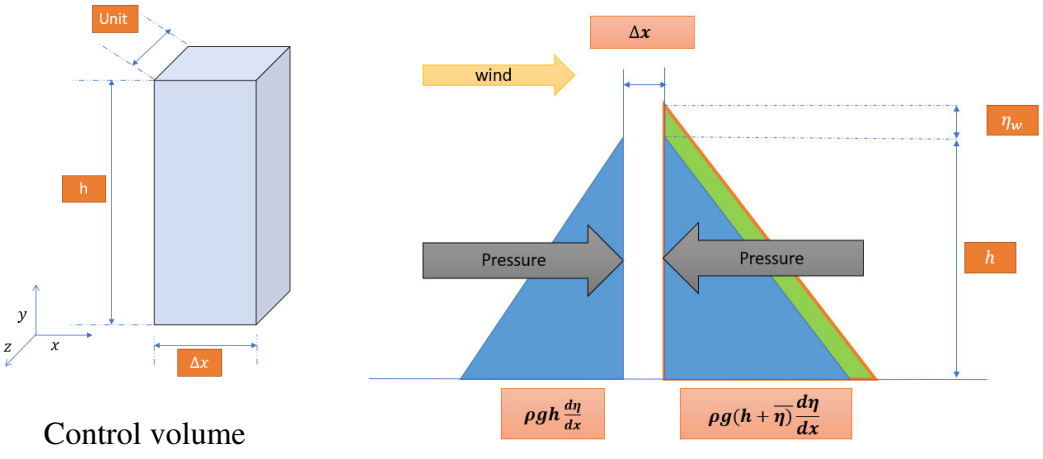

Figure 3-9 Water level difference generating the counter force.

Wind stress cannot be determined theoretically, but numerous experiments established an accepted relation. The empirical formula for wind stress is:

$$\tau_s = \rho_w * C_f * U^2 \qquad (5)$$

where τ_s is the wind stress, ρ_w is the density of water,U is the velocity of the air and C_f is the friction factor of the wind-air surface. Typical values of $C_f$is $1.2x10^{-6}$ to $3.4x10^{-6}$ (Dean and Dalrymple, 2004).

Wind stress(τ_s) working on the surface creates a force $\tau_s * \Delta x$ acting in the wind direction. The water column must rise by η_w (Figure 3-9) to counter the winter force.

3.2.5.1 Force balance equation

The pressure and stresses on the control volume in x direction can be balanced as follows:

$$\frac{1}{2}\rho_w g(h+\eta_w)^2 - \frac{1}{2}\rho_w g(h+\eta_w+\Delta\eta_w)^2 + \tau_{s\Delta x} - \tau_b \Delta x = 0 \qquad (6)$$

where τ_b is the bottom friction acting opposite direction to wind speed. Not considering the higher order terms like $(\Delta\eta_w)^2$ while expanding $(h+\eta_w+\Delta\eta_W)^2$, the following is obtained:

$$\frac{\Delta\eta_w}{\Delta x} = \frac{(\tau_s-\tau_b)}{\rho_w g(h+\eta_w)} \quad (7)$$

As Δx reaches to small values, the above equation can be converted to derivative:

$$\frac{d\eta_w}{dx} = \frac{(\tau_s-\tau_b)}{\rho_w g(h+\eta_w)} \quad (8)$$

The interpretation of the Equation 8 is as follows:

- Water surface slope is related to the stress acting upon it, the larger the stress the steeper the water level slope.
- Shallow water depth has a profound implication. Shallower the water, steeper the water surface. If the coast is shallow the surge will be significantly larger.

3.2.6 Water level Set up due to current

Due to the Coriolis effect, the sea currents may push the water towards the coast depending on the flow direction. For example, in the northern hemisphere, the wind-induced coastal current flows to the south. Coriolis force due to earth's rotation bend the path of the flow and push up the water along the east coast of United States.

Let η_c be the water level increase due to currents. Its magnitude can be calculated as:

$$\frac{d\eta_c}{dx} = \frac{fv}{g} \quad (9)$$

where f is the Coriolis parameter which is equal to $2\Omega \sin\phi$ [Ω=the angular rotation rate of the earth= $7.272x10^{-5} rad/sec$, ϕ=latitude of the considered site and v is the magnitude of the depth averaged currents.

3.2.7 Governing equation of storm surge

Neglecting surge due to pressure and shear stress due to bottom friction, Equations 4, 8 and 9 can be combined to create the governing equation for storm surge (Ravens et al., 2012):

$$g(h+\eta)\frac{d\eta}{dx} = (h+\eta)fv + \frac{\tau_{sx}}{\rho_w} \qquad (10)$$

Where h is the water depth (mean), η is the magnitude of the surge due to a combination of pressure, wind stress and currents, τ_{sx} wind stress normal to the shore ρ= density of the water.

When the slope of the bed (dh/dx) is considered the equation is rewritten as follows:

$$g(h+\eta)\left[\frac{d(h+\eta)}{dx} - \frac{dh}{dx} - \frac{fv}{g}\right] = \frac{\tau_{sx}}{\rho_w} \qquad (11)$$

Equation 11 is the governing equation for the storm surge model. The following physical interpretation can be made:

- The term $(h+\eta)$ influences the solution greatly. When $h \gg \eta$, the solution of η will be very small. As can be seen from the output of the numerical model that in the deep sea, storm surge is negligible.
- The equation is based on force balance in terms of pressure gradients. In deep water, little water depth difference will cause big pressure difference. To create the same pressure difference in the shallow water, water depth difference has to be significantly big.
- Water surface gradient also depends on the stress caused by wind. Higher stress will cause a greater slope.
- Equation 11 has no general analytical solution. It has no time derivative which indicates that the solution is always at a steady state. Input variables such as wind speed, current speed and water depth are time-dependent. These variables are discretized in time and the average values of two adjacent time steps are used.

To calculate storm surge level, the equation 11 is discretized in time and space.

3.3 Niche Growth module

When water reaches the base of the bluff during a storm surge, a wave-cut niche form. The ice present in the bluff starts to melt and some sediments may be extruded. A strong return current generated by the storm washes away the sediments. The conceptual niche growth model presented here is originally proposed by Kobayashi (1985).

3.3.1 Standardization of the problem

Few assumptions are made to standardize the problem. The soil inside the frozen bluff is assumed to be mostly fine sediments. At the melting point, the salinity of the water goes down as fresh water from ice is coming down, but sediments are not deposited rather stays suspended in the water. Moreover, a vertical uniformity is assumed for salinity, sediment concentration and temperature(Kobayashi, 1985).

3.3.2 Governing equation

The time-averaged conservation of mass equation for seawater accounting for the volume of suspended sediment may be expressed as (Kobayashi, 1985) :

$$\frac{\partial}{\partial t}[(1-C)\rho_w h_{id}] + \frac{\partial}{\partial x}[(1-C)\rho_w h_{id} u] = \frac{\partial}{\partial x}\left\{h_{id}\varepsilon_w \frac{\partial}{\partial x}[(1-C)\rho_w]\right\} \quad (12)$$

where ρ_w is the density of sea water, C is the suspended sediment concentration, h_{id} is the inundation depth, u is the shore-normal fluid velocity averaged over a time interval containing an integral number of wave period and a statistically significant number of turbulent eddy cycles (Ostendorf, 1982) and ε_w is the surf zone diffusivity.

It is safe to assume that shallow water equations are valid; at least close to the base of the bluffs (Kobayashi and Aktan, 1986). The melting point of the ice is depended on the salinity, so salinity at the melting point needs to be considered. Time-averaged conservation of salt in the seawater is (Kobayashi, 1985)

$$\frac{\partial}{\partial t}[(1-C)\rho_w S h_{id}] + \frac{\partial}{\partial x}[(1-C)\rho_w S h_{id} u] = \frac{\partial}{\partial x}\left\{h_{id}\varepsilon_s \frac{\partial}{\partial x}[(1-C)\rho_w S]\right\} \quad (13)$$

where S is the salinity of sea water inside the niche, ε_s is the surf zone diffusivity of the salt. Relating between salinity and temperature at the melting interface inside the niche is locked by the curve formulated by Josberger and Martin (1981) and Josberger (1983) as follows:

$$T_m = -m\,S_m \qquad (14)$$

where $m = 0.06\ °C\ per\ ppt\ for\ S_m < 35\%$.

Wave-cut niche is also temperature dependent, so energy balance must be maintained. The following formula is used for energy balance (Kobayashi, 1985):

$$\frac{\partial}{\partial t}\{[(1-C)\rho_w c_w + C\rho_s c_s]Th\} + \frac{\partial}{\partial x}\{[(1-C)\rho_w c_w + C\rho_s c_s]Thu\} = \frac{\partial}{\partial x}\Big\{ h\varepsilon_T \frac{\partial}{\partial x}[(1-C)\rho_w c_w + C\rho_s c_s]T\Big\} \qquad (15)$$

where ρ_s is the density of the sediments, c_w is the specific heat of seawater, c_s is the specific heat of sediments and ε_T is the surf zone thermal diffusivity.

Four diffusivity indices are defined for the wave-surf zone (ε_w), sediment concentration(ε_c), salinity(ε_s) and temperature (ε_T). For simplicity, these are assumed to be equal.

$$\varepsilon_w = \varepsilon_c = \varepsilon_s = \varepsilon_t = \varepsilon$$

Diffusivity index for the numerical model is calculated based on empirical formula (Longuet-Higgins, 1970)

$$\varepsilon = Ah(gh_{id})^{0.5} \qquad (16)$$

where empirical parameter $A = 0.4$ and h_{id} is the inundation depth at the base of the bluff. Figure 3-10 represent the relation. Clearly, as the equation suggest, the relation is parabolic.

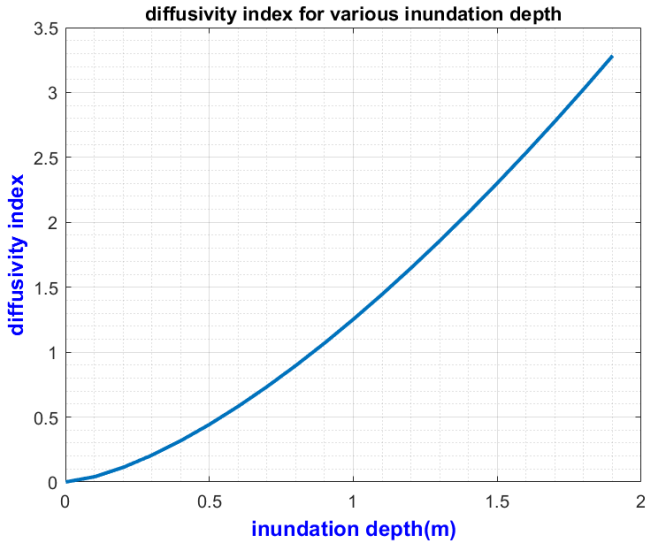

Figure 3-10 diffusivity index for various inundation depth (h).

The combined effect of salinity and temperature is shown in Figure 3-11. The relation is established by Josberger (1981) as follows:

$$T_d = T_a + mS_a \qquad (17)$$

where T_a=temperature of the incoming water/wave and m is a constant. Value of m is 0.06 per ppt of salinity. S_a is the salinity measured in ppt. The term T_d is used for both empirical and analytical solution.

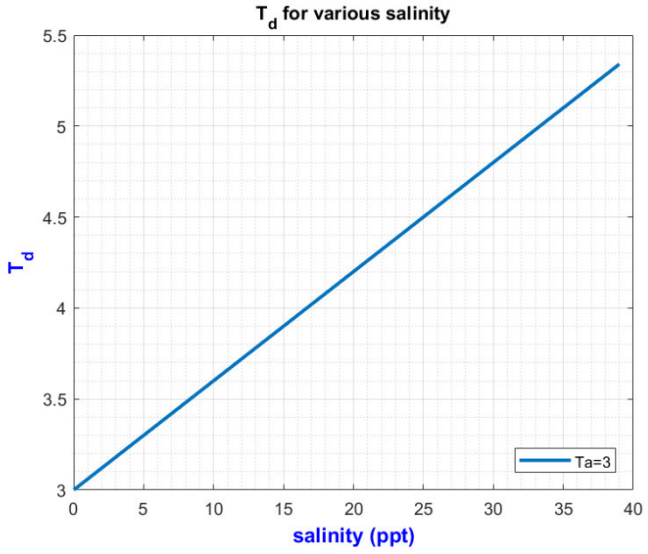

Figure 3-11 Effect of salinity on the melting of ice.

Kobayashi proposed the analytical solution of melting of ice and niche growth are similar to the melting and solidification described by Carslaw and Jaeger (1959). The analytical solution thus becomes:

$$x_m = 2 * \xi_m * (\varepsilon t)^{\frac{1}{2}} \quad (18)$$

where ξ_m is an empirical time dependent dimensionless parameter, it's value changes over space within niche growth. Details of arriving at the analytical solution is described in Appendix B.

Besides the analytical solution Kobayashi established the following empirical formula for niche growth:

$$x_m = 0.0188 T_d * \sqrt{\left(0.4h\sqrt{gh_{id}}\right)t} \quad (19)$$

where T_d is a salinity adjusted thermal driving parameter (Josberger and Martin, 1981) and h_{id} is the inundation depth.

Equation 19 describes the two most important input parameters for the niche growth: salinity adjusted seawater temperature (T_d) and wave height. Wave height is not directly present in the analytical solution. The term h_{id} is a representation of the effects of the waves as the wave-heights are assumed to be depth limited at the base of the bluff. Combined effect of other input parameters was considered constant in the empirical formula. A comparison of the empirical and analytical solution is shown in Figure 3-12 . For a typical case, niche growth over the time calculated from the analytical solution is very close to the empirical equation. However, in the numerical model, the analytical solution was used so that the model can be used for universal cases.

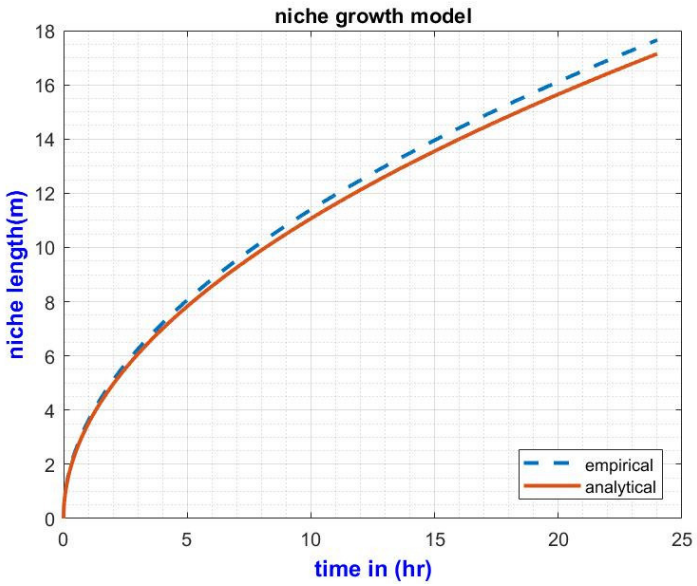

Figure 3-12 Empirical vs analytical solution for niche growth.

3.4 Bluff collapse module

The conceptual model presented here for the collapse of the frozen bluff is adopted from Barnhart (2014) with slight modification. Barnhart developed the model for the coast of Alaska near Dewpoint. The model considers the lower tensile strength at ice wedge boundary. It is not a finite element model and the failure mechanisms are formulated based on field observations.

3.4.1.1 Standardization of the problem

Block collapse is determined by the balance between of the resisting force i.e. the shear strength and driving moment from the weight of the overhanging portion.

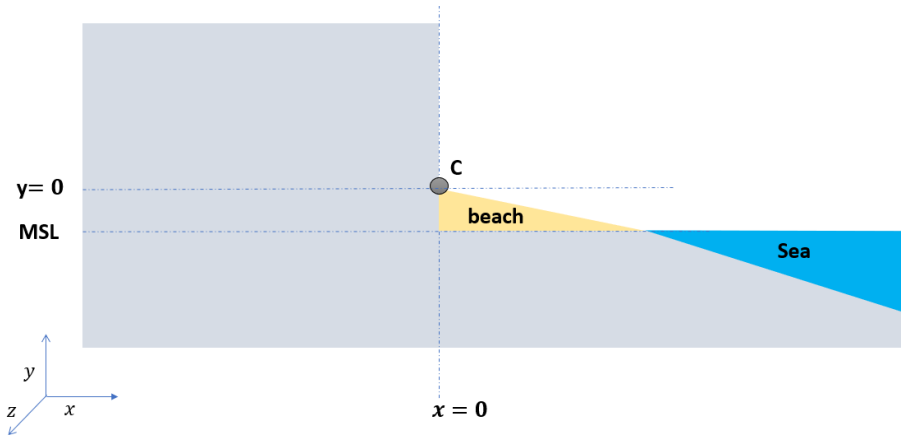

Figure 3-13 Standardized problem of bluff collapse (pre-collapse).

The problem is standardized as shown in Figure 3-13. The origin of the coordinates is placed at the base of the bluff. Origin of the coordinate systems is the point C where $(x, y) = (0,0)$. $y = 0$ line is not at the mean sea level, rather at the same level of niche growth. Mean sea level (MSL) is below the zero line so that the base of the bluff is not flooded in non-storm times. Water level will rise during the storm by the amount of η.

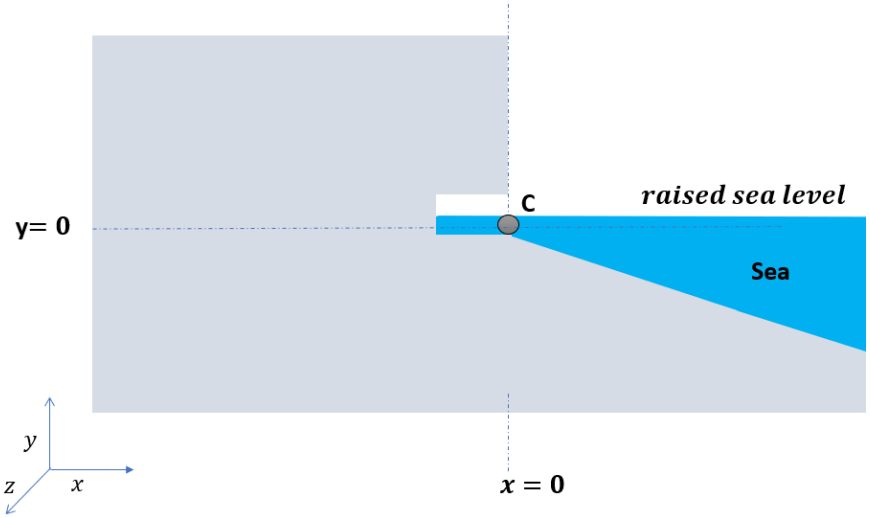

Figure 3-14 Standardized problem of bluff collapse during storm.

The geometry of the bluffs is affected by the storm surge. A niche is developed which is also flooded with sea water and waves penetrate deep into the bluff (Figure 3-14). As a result, an overhanging slab is formed.

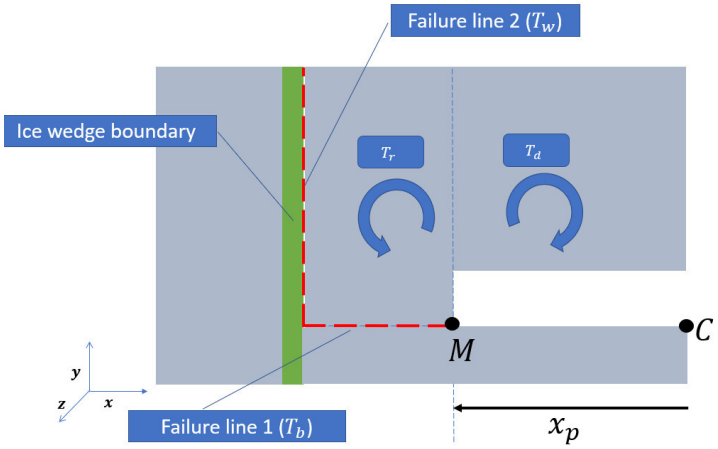

Figure 3-15 details of the hanging bluffs before breaking.

Figure 3-15 shows the details of the hanging bluff before the collapse. At the time t_j just before the bluff collapse, the niche growth is at $x_m = x_p$. The force balance is in breakeven point and

point M ($x = x_p$) will be working as the pivotal point. At point M if the resisting moment is smaller than the driving moment, the collapse will occur. We need to determine when and where the collapse will be triggered.

3.4.1.2 Failure Mechanisms

For simplicity, an assumption was made to have a straight failure plane which expanded uniformly in the z direction (Figure 3-15).

The two failure planes as shown in Figure 3-16 are:

- Failure line 1: horizontal plane at the point of niche extending until the wedge boundary
- Failure line 2: vertical plane at the interaction of ice wedge boundary and frozen bluff

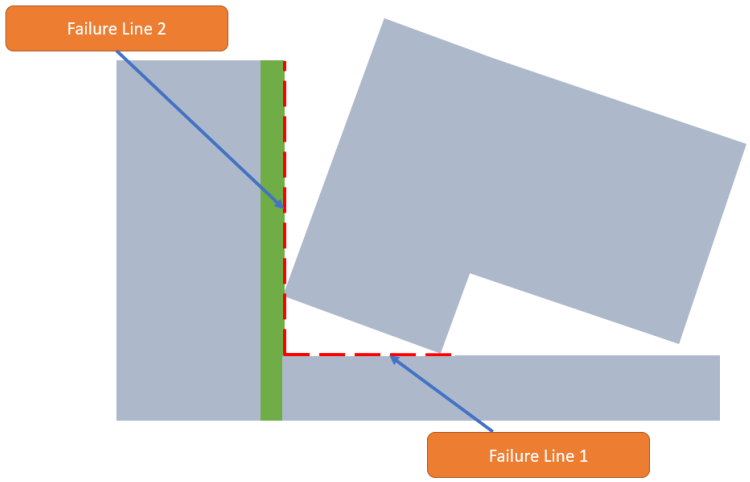

Figure 3-16 Failure mechanism as considered in the conceptual model.

To determine the driving moment (T_d) that acts towards failure, let's assume a finite element of dimension dx and dy . Dimension in z direction is assumed one unit. If the density of the bluff is ρ_b, the weight of the element (dw) becomes:

$$dw = \rho_b * g * dy * dx \qquad (20)$$

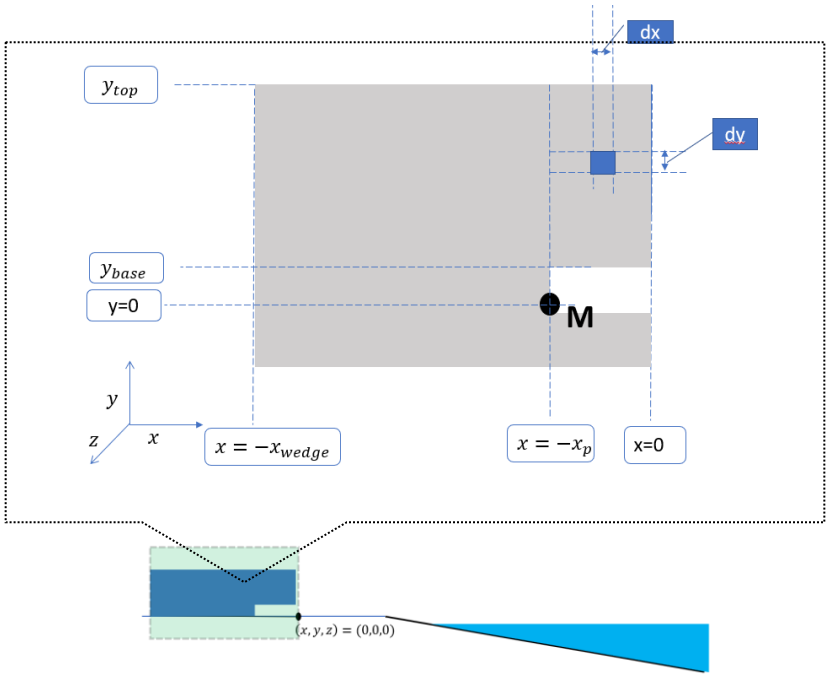

Figure 3-17 Determination of driving moment, T_d

At the time just before the collapse, $t = t_j$, the melting plane of the niche is at $x = x_p$. The element having the weight dw generates a moment T_d with an arm length $(x_p - x)$. To get the total moment of the hanging slab, the limits mentioned in Table 3-2 is considered:

Table 3-2 Limits of the bluff geometry

Vertical limit	Horizontal limit
Lower limit: y= y_{base}	Lower limit: $x = 0$
Upper limit: y= y_{top}	Upper limit: $x = x_p$

The total moment at the point M, at time t_m is:

$$T_d = \rho_b * g * \int_{y_{base}}^{y_{top}} \int_0^x (x_p - x) dx dy \qquad (21)$$

In the failure mechanism, the weight of the non-hanging bluff also creates a moment around the point M and acts against failure. The moment is created by the weight of bluff from melting point $(x = -x_p)$ to the inner edge of the frozen bluff $(x = -x_{edge})$.

As shown in Figure 3-18, another element is considered for resisting forces. It has dimension dx and dz in two directions. Dimension in y direction is assumed unit. If the density of the bluff is ρ_b, the weight of the element (dw) becomes:

$$dw = \rho_b * g * dy * dx \qquad (22)$$

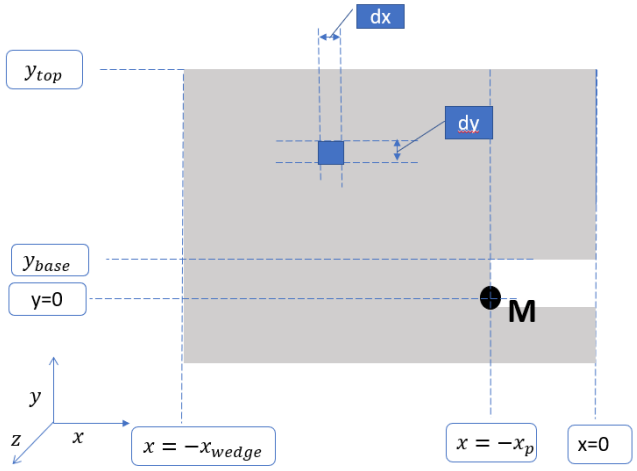

Figure 3-18 Determination of resisting moment (T_r) from non-hanging portion of bluff.

The resisting torque starts after the melting point where $x < -x_p$. For the vertical case, the limit stays the same as previous- from the base of the frozen bluff to the bluff height.

Table 3-3 Geometric limit of the non-hanging bluff

Vertical limit	Horizontal limit
Lower limit: y= 0	Lower limit: $x = x_p$
Upper limit: y= y_{top}	Upper limit: $x = x_{edge}$

where x_{edge} is the distance from the edge of the ice wedge to the base of the bluff.

Using the limit, moment generated by the non-hanging bluff is determined to be:

$$T_r = \rho_b * g * \int_0^{y_{top}} \int_{x_{edge}}^{x_p} (x_p - x_{edge}) dx dy \qquad (23)$$

Two other resisting forces are generated along the failure lines of the bluff (Figure 3-16). Horizontal resisting force is generated from friction between ice surfaces. Let τ_b be the tensile strength of the frozen bluff then the resisting moment, T_f is:

$$T_f = \int_{x_{wedge}}^{x_p} \tau_b * [x - x_p] dx \qquad (24)$$

The vertical resisting moment (T_i) from failure line 2 is at the surface of the ice wedge located at x_{edge}.

$$T_i = \int_{y_{base}}^{y_{top}} \tau_i [x_{edge} - x_p] dy \qquad (25)$$

3.4.2 Governing equation of bluff collapse

Governing equation of the bluff collapse is a balance equation. The driving moment (T_d) acts towards failure while the resisting moments ($T_{resisting} = T_r + T_i + T_f$) act against failure. The governing equation thus is the balance of the two opposite moments.

$$T_d = T_{resisting}$$

$$\rho_b * g * \int_{y_{base}}^{y_{top}} \int_0^x (x_p - x) dx dy = \rho_b * g * \int_0^{y_{top}} \int_{x_{edge}}^{x_p} (x_p - x_{edge}) dx dy + \int_{x_{edge}}^{x_p} \tau_b * [x - x_p] dx + \int_{y_{base}}^{y_{top}} \tau_i [x_{wedge} - x_p] dy \qquad (26)$$

Equation 26 was solved numerically to find the value of x_p. A trial-error approach or "goal seek" is adopted to find the critical niche growth.

4 Numerical Schematization

4.1 Introduction

In the previous chapter (section 3.2 to section 3.4.2) a conceptual model for thermoabrasional bluff erosion is presented. Table 4-1 provides a short description of three modules and most important remarks (Figure 4-1 depicts the interaction between the modules). In this chapter, the governing equations of each module are discretised in time and space to achieve the numerical solutions. The behaviour of the numerical modules is discussed as well.

Table 4-1 Various component of thermo-abrasion model

Module	Description	Output	Adopted from	Remarks
Storm surge module	Calculate storm surge level based on given bathymetry and wind speed	h_{id} for every time step	Dean and Dalrymple (2004)	1D line model, quasi-static equation
Niche growth module	Estimate the depth of the niche inside frozen bluff, required inputs: surge level, temperature etc	x_m for every time step	Kobayashi (1985)	1D, not an empirical formula, based on conservation of mass, energy and salinity
Bluff collapse module	Calculate whether bluff will fail given a certain niche depth	Stability	Barnhart (2014)	2D model, highly dependent on the geometry of frozen bluffs

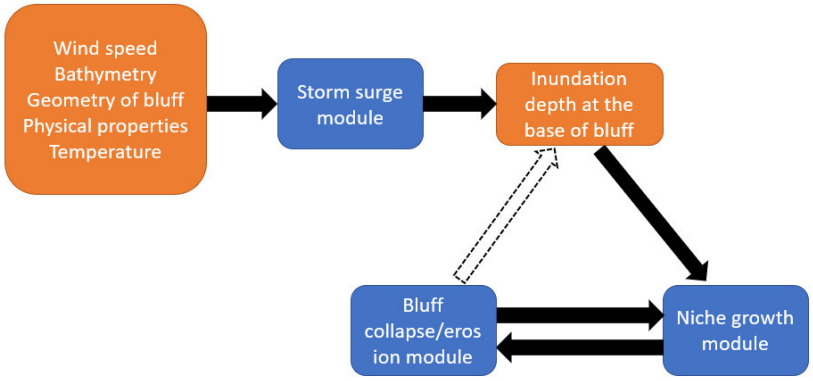

Figure 4-1 Interaction between the modules.

4.2 Numerical schematization of Storm Surge module

Equations 10 and 11, described in section 3.2.7, govern the storm surge module for flat and inclined seabed, respectively. These equations have no analytical solutions but can be solved numerically. The equations have no time-derivatives indicating that the solution is always at the steady state. The equation is discretized in space to achieve the numerical solution. To march the solution in time, it was assumed that the solution in each time step is steady. Input data for wind, current and water depths are updated at every time step.

4.2.1 Numerical Schematization equation

Out of two governing equation, Equation 10 is applicable only to flat seabed. To use the storm surge model for universal cases, Equation 11 was chosen to be discretized. Equation 11 is a first order partial differential equation with no diffusion. Hence the numerical scheme should also be free of numerical diffusion (Zijlema, 2017).

Applying Explicit Euler scheme, governing equation is rewritten as:

$$(h_i + \eta_i)\left[\frac{(h_{i+1}+\eta_{i+1}-h_i-\eta_i)}{\Delta x} - \frac{h_{i+1}-h_i}{\Delta x} - \frac{fv_i}{g}\right] = \frac{\tau_{sx}}{\rho g} \qquad (27)$$

Initial condition

$\eta = 0$ where $x = \infty$ (deep sea condition)

Centre of the coordinates is placed at the base of the bluff. The initial condition for the storm surge model is defined at the deep sea, so the numerical solution starts from deep sea and moves Δx at one step towards the coast in the negative x direction. As shown in Figure 4-2, at a particular time step, the solution is moving in the negative x direction from point A to point B.

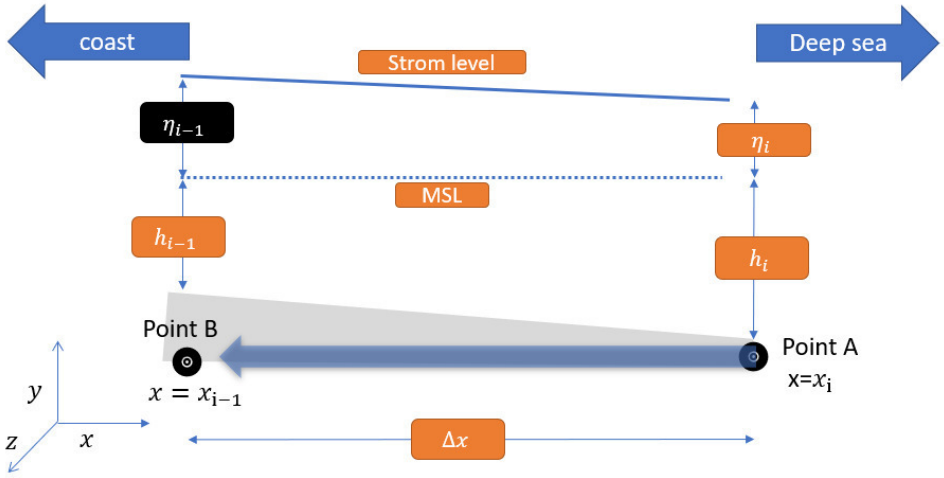

Figure 4-2 Numerical schematizations of the storm surge model.

Since the solution is moving backwards in space, inputs of the discretization are modified as mentioned in the table below.

Table 4-2 Input parameter for numerical schematization (storm surge module)

Parameter	Description	Analytical value	Remarks
η_i	water level above means at point *A*	iΔx	value is known from previous space step
η_{i-1}	water level above means at point *B*	$(i-1)\Delta x$	unknown
h_i	water depth at mean sea level at point *A*	-	value is known from bathymetry data
h_{i-1}	water depth at mean sea level at point B	-	value is known from bathymetry data

It is apparent that only one parameter is unknown which is η_{i-1} . So, the Equation 21 is rewritten as follows:

$$\eta_{i-1} = \eta_i + \frac{f v_i \Delta x}{g} + \Delta x \frac{C_f U_i^2}{g(h_i+\eta_i)} \qquad (28)$$

Where the suffix (i-1) and (i) indicate grid point at (i-1) *Δx and i*Δx distance from the origin. These two points are Δx meter apart.

Equation 28 is solved for every space step as shown in Figure 4-3. For one single time step, the numerical solution is calculated for all grid points of space starting from deep-sea towards the coast. This is repeated for each time steps. Related MATLAB code is provided in Appendix A.

Time and space advancement of the solution is shown in Figure 4-3. At significantly far from the base of the bluff, water is deep and it is reasonable to assume that storm surge is zero. From this initial condition, the numerical model starts to calculate the storm surge for the next point, Δx apart from the initial point. Using Equation 28, it calculates storm surge of the second point given that the bathymetry and other required input values are provided. Sequentially, storm surge level of all the points are calculated for a given time. Then the model starts *time advancement* and at the next time step, module calculates all the points from deep-sea to the coasts.

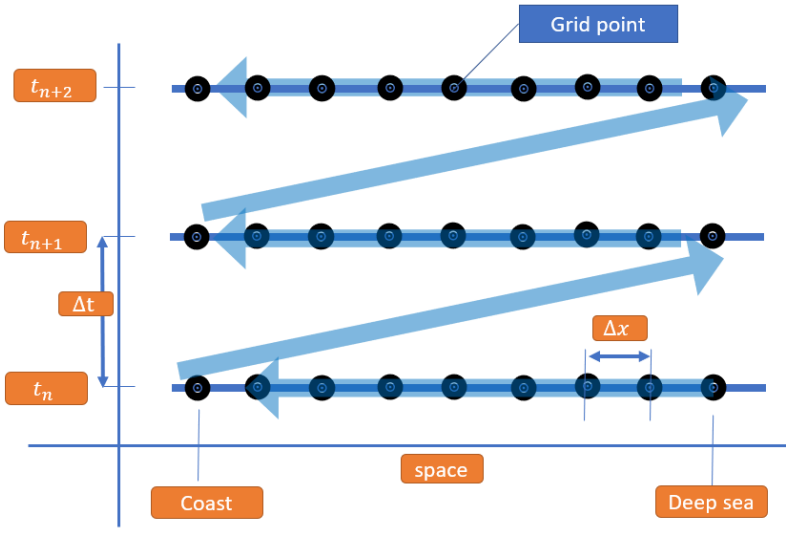

Figure 4-3 Time and Space advancement of numerical model (discretization flow).

4.2.2 The output of the numerical model

Figure 4-5 shows the output result of sample calculations using the code described in Appendix A. Deep sea is assumed to be at 20,000 meters from the coast. The storm surge is generated for a sustained 32 m/s wind speed, 2 m/s longshore currents and latitudes of 68°. Water depth near

shore is 15m or less and slope of the bed is very mild. A random bed profile with smoothening out geometry is shown in Figure 4-4 (only a few hundred meters is shown here). Origin of the coordinate is at the base of the bluff and MSL is at 2m vertically below the bluff base. Bed profile shown in Figure 4-4 is used to evaluate the numerical model.

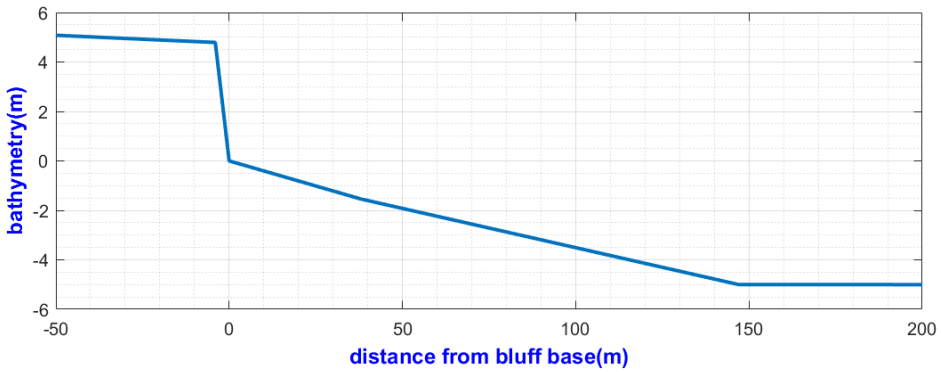

Figure 4-4 a random bed profile used to evaluate numerical storm surge model.

The effect of wind speed on the bed profile is studied by varying the wind speed from 16 m/s to 32 m/s. The results are shown in Figure 4-5. The model predicts that the storm surge at the base of the bluff ($x = 0$) will be 1.5m for a wind speed of 16 m/s. For 32 m/s wind speed, the storm surge level (η) will be close to 3.25m. [note: vertical and horizontal scales are not the same in Figure 4-4 to Figure 4-7.]

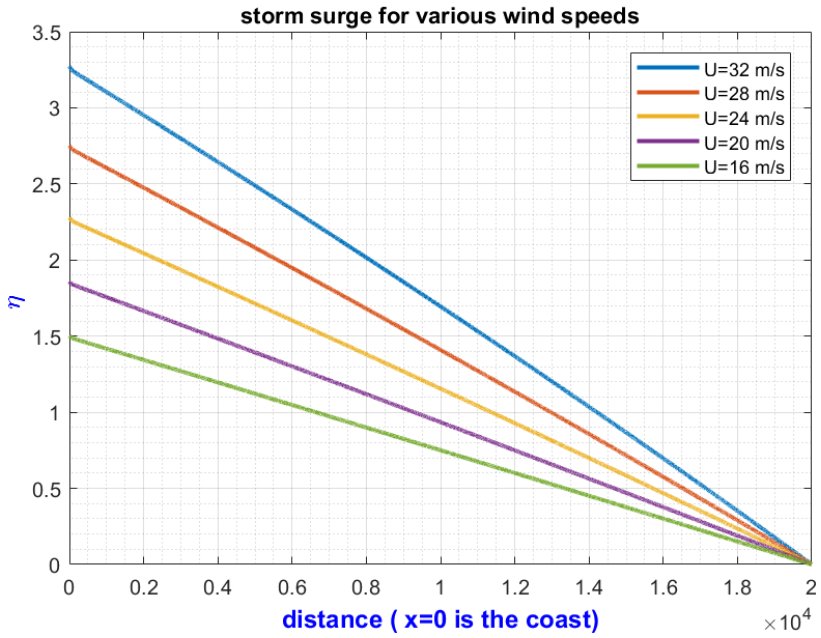

Figure 4-5 Storm surge (η) for various wind speeds.

Figure 4-6 depicts the effect of open water on the storm surge. The model predicts smaller storm surge (η) for shorter open water. It is also interesting to observe the sudden jump in the storm surge near the bluff, see Figure 4-6 and Figure 4-7. This noticeable increase of the storm surge is attributed to the sudden change in bathymetry where water depth close to the bluff is considerably shallow. Another feature is that the jump is higher for smaller open water fetches.

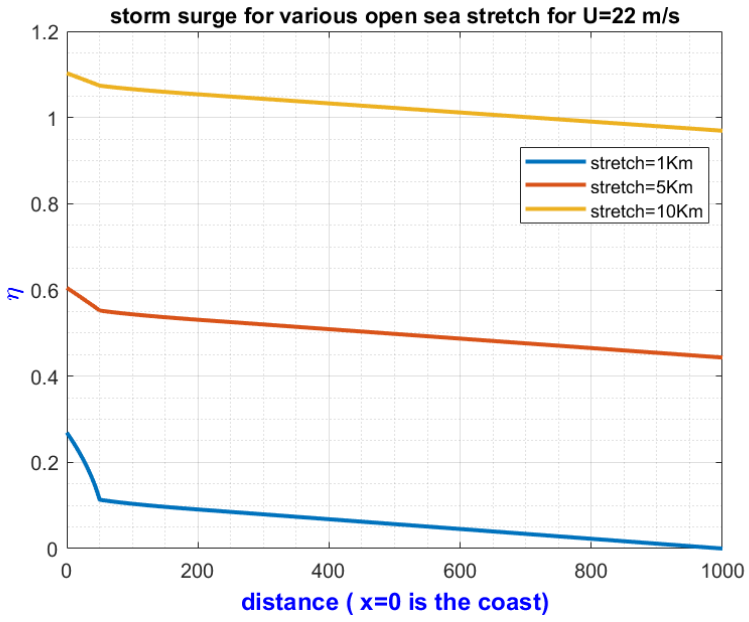

Figure 4-6 Effect of open water on storm surge level.

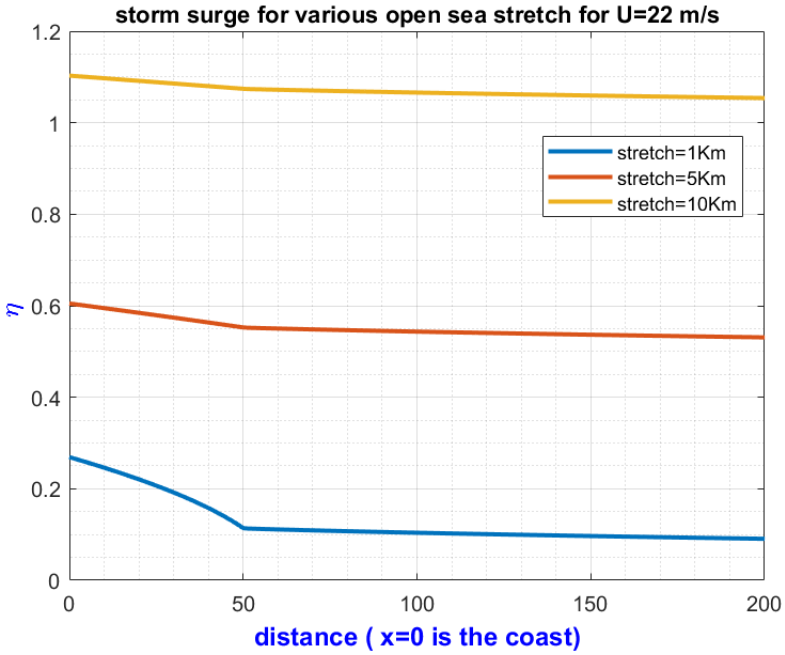

Figure 4-7 Zoomed in first 200 m [Effect of open water on storm surge level].

Recalling the surge level due to wind is only governed by Equation 8 which is repeated here for better readability.

$$\frac{d\eta_w}{dx} = \frac{(\tau_s - \tau_b)}{\rho g(h+\eta_w)} \qquad (29)$$

where η_w is the water level above the mean sea level and h is the water depth.

Equation 29 indicates that storm surge η_w is highly dependent on water depth h. If η_w is smaller than h, the effect of wind stress is countered easily. The physical interpretation is that when in deep water, small pressure ($\rho g h$) difference in the water column is enough to counter force generated by wind stress. But in lower water depths, the height of water column must be significantly different to generate the same amount of the counter-force.

4.2.3 Discussion

The following comments can be made specifically for the numerical model developed for the study:

(1) The model is very sensitive to water depths near the coast. In deep water, water depth does not play a significant role. In other words, it can be concluded that bathymetry of the nearshore determines the accuracy of the model.

(2) Numerical solution considers quasi-static or steady-state solution only. Neither refraction nor diffraction is considered. Moreover, the space discretization is 1D i.e. solution is calculated in a straight line from deep sea to the base of the bluff. If a coast is curved or irregular, this numerical model should be used with caution.

4.3 Numerical schematization of niche growth module

In section 3.3.2 (page 26), the analytical solution derived by Kobayashi is discussed. The analytical solution is as follows:

$$x_m = 2 * \xi_m * (\varepsilon t)^{\frac{1}{2}} \quad (30)$$

Where ξ_m is an empirical parameter and ε is the diffusivity index which is determined by an empirical formula of Longuet-Higgins (1970). Using the analytical solution the numerical module calculates niche growth and melting point at the time and space grid points.

4.3.1 Numerical schematization

All the parameters required for the numerical solution are described in Table 4-3. Estimated or typical values are also provided in the table. Sensitivity analysis was carried and it was found that the numerical model is not highly sensitive to most of the parameters out (see section 6.1.3 for details).

Table 4-3 Input parameters for niche growth

Parameter	symbol	Estimated value
Physical properties		
Mean shore normal fluid velocity	u	1 m/s
Inundation Depth	h_{id}	Calculated by storm surge module
Salinity of the sea water inside niche	S	0.03 ppt
Salinity of the ice	S_i	0.00
Suspended sediment concentration (initial)	C	0
Porosity of the frozen sediments	n	0.4
Density of ice	ρ_i	916 kg/m^3
Density of sediments	ρ_s	2650 kg/m^3
Density of water	ρ_w	1010 kg/m^3

Specific heat of suspended sediment	c_s	0.8374 kJ/kg-K
Specific heat of sea water	c_w	4.187 kJ/kg-K
Specific heat of ice	c_i	2.108 kJ/kg-K
Latent heat of ice	L_i	3340J/kg
Initial Conditions		
Sediment concentration	C_a	0 kg/m^3
Salinity concentration	S_a	30%
Temperature	T_a	$3°C$
Empirical constant *Josberger*	m	$0.06°C$ per ppt
Salinity of the melting point	S_m	To be calculated
Momentum diffusivity at melting point	ε_m	To be calculated
Geometry		
Opening of niche (empirical)	β	2
Empirical parameter of diffusivity index	A	0.4

Using the values mentioned in the table, the analytical equation is solved. A flowchart of a series of equations to reach the analytical solution is mentioned in Figure 4-8. First momentum diffusivity is determined by the empirical formula proposed by Longuet-Higgins (1970). Using the physical parameters three dependent parameter e_1, e_2 and e_3 are calculated which is then converted to parameter d . Parameter d represents the combined effect of waves and other physical parameters like salinity, sediment concentration etc. Using two parameters d and a, the dimensionless variable ξ (Carslaw, 1959) is determined. Thermal parameter T_d is determined from the empirical formula proposed by Josberger and Martin (1981).

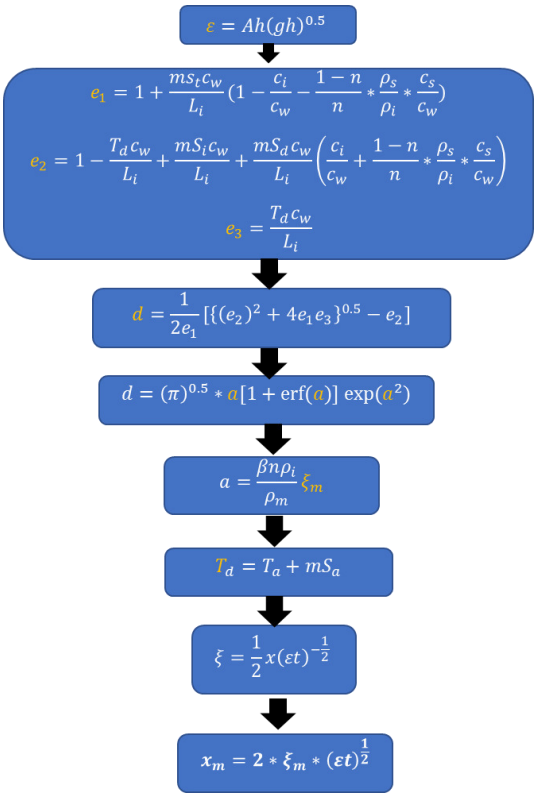

Figure 4-8 Flow chart of niche growth equation.

Lastly, the analytical solution proposed by Kobayashi is used to determine x_m(the distance of the melting point from the base of bluff).

For niche growth module, only time advancement is considered. For every time step, niche growth is calculated. Space advancement of the scheme is not required because the output of the module itself is the space parameter x_m (the distance of melting point). The module calculates the position of the melting point at every time step. A flow of the time and space march of the module is shown Figure 4-9. Suffix $j, j+1, J+2\ etc$ indicate time steps and $i, i+1, i+2\ etc$ means space steps.

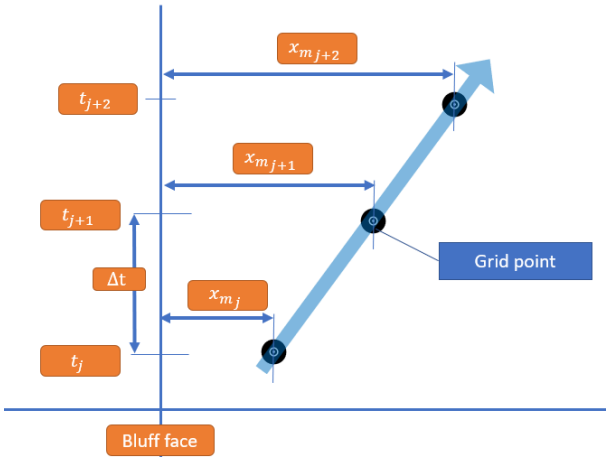

Figure 4-9 time advancement of the niche growth numerical scheme.

4.3.2 The output of the numerical model

Three parameters $e_1, e_2 and\ e_3$ are part of the process of finding the analytical solution (see Figure 4-8). Since these three unknowns are related to the temperature of the incoming water, a short analysis is performed to check the variability of the three unknowns with temperature (Figure 4-10).

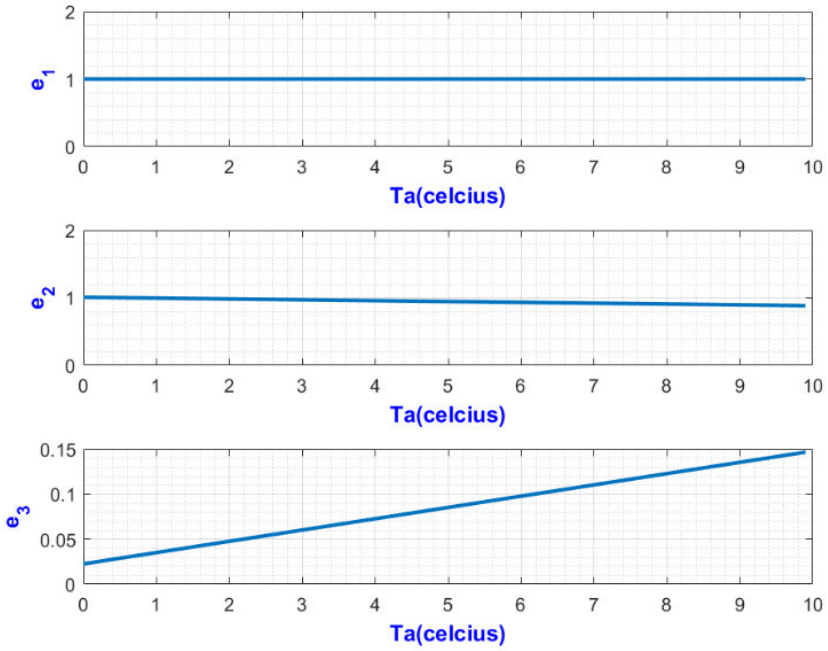

Figure 4-10 e1, e2 and e3 of the analytical solution.

The following observations are made:

- e_1 remains constant even though the equation has temperature as an input. The constant value is 1.
- e_2 shows variability with temperature, but very small.
- e_3 values are very small compared to e_1 and e_2. The variability is also negligible.

Variability of another three unknowns a, d and ξ_m is shown in Figure 4-11. These are also related to the temperature of the incoming wave/water.

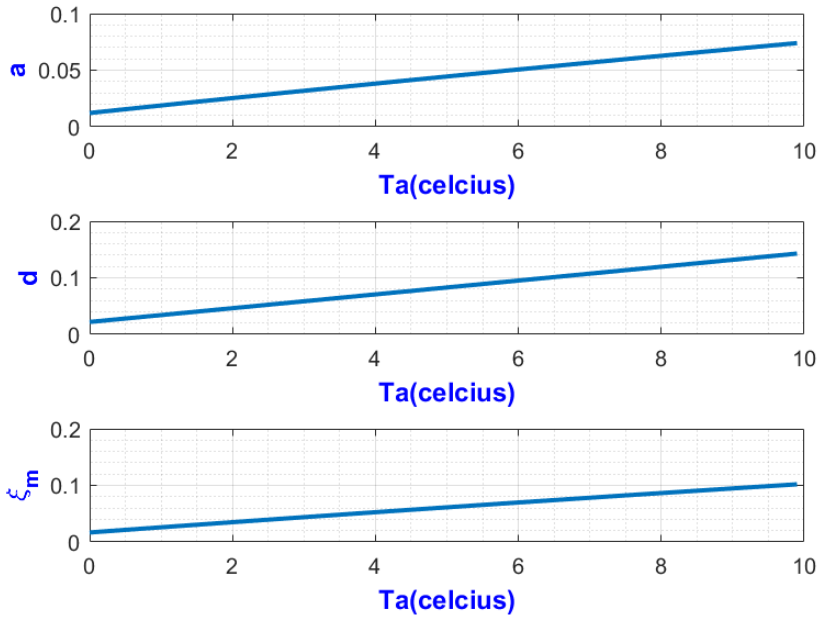

Figure 4-11 a, d and ξ_m variability with temperature.

The following observations are made:

- Unknowns a and d vary with temperature. Difference between the values of d and a are negligible. The relation between a and d is

$$d = (\pi)^{0.5} * a[1 + \text{erf}(a)] \exp(a^2)$$

- The value of ξ_m varies linearly with temperature. ξ_m is used in the analytical solution and directly related to niche growth rate.

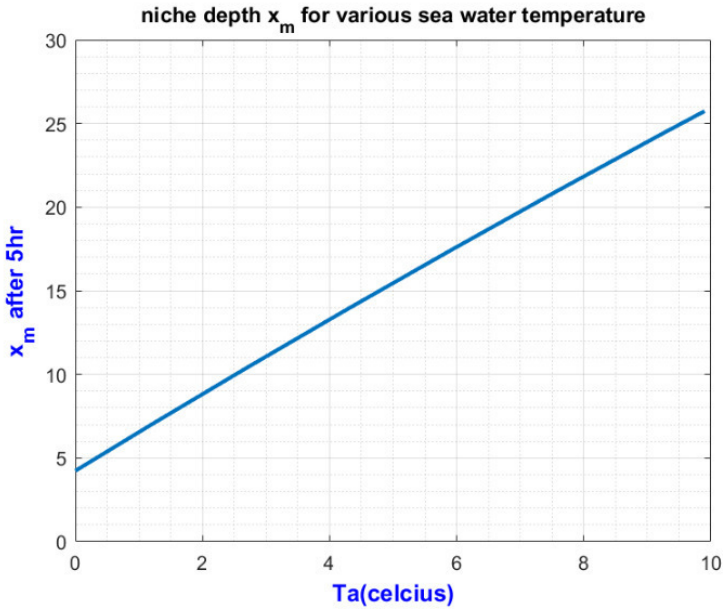

Figure 4-12 Temperature effect on niche growth.

Temperature has a strong linear effect on niche growth rate (Figure 4-12). In the figure, niche growth after 5 hr is plotted against various temperature assuming a constant inundation depth (h_{id}) of 0.5m for all cases. Niche growth for 1°C water temperature was found 6.2m whereas if the temperature is 10°C, niche growth is more than 25m.

4.3.3 Discussion

For the niche growth module, Kobayashi formula is adopted. Schematization of the analytical solution is briefly discussed in section 4.3.1. To understand the behaviour of the numerical model various plots were made and analysed.

The following observations are made specific to the numerical niche growth module developed under the study:

- The numerical schematization uses an analytical solution of Kobayashi formula rather than empirical formula so that the model remains universally applicable. As the empirical formula does not account for salinity, sediment concentration etc, it was omitted from the numerical solution.

- The temperature of the incoming water is very important as a niche growth model is essentially an ice melting mechanism.
- The output of the module is niche growth at every time step. It was assumed that once the niche is developed, ice will not regrow and cover the niche opening. Next storm starts from the wave-cut niche that was developed from the previous storms. Field observation is recommended to further validate this assumption.

4.4 Numerical schematization of Bluff Collapse Model

In section 3.4, bluff collapse mechanism as proposed by Barnhart (2014) is described. The numerical module is developed based on the Equation 26 mentioned in section 3.4.2. The numerical module calculates the stability at every grid point.

4.4.1 Numerical Schematization of the governing equation

Table 4-4 summarizes the destabilizing and resisting moments acting on the bluff.

Table 4-4 Components of bluff collapse

Component	Formula	Remarks
T_d	$\rho_b g \int_{y_{base}}^{y_{top}} \int_{0}^{x} (x_p - x) dx dy$	From an overhanging slab of the bluff
T_r	$\rho_b g \int_{y_{base}}^{y_{top}} \int_{x_{edge}}^{x_p} (x_p - x_{edge}) dx dy$	From a non-hanging portion of the bluff
T_f	$\int_{x_{edge}}^{x_p} \tau_b * [x - x_p] dx$	From horizontal friction
T_i	$\int_{y_{base}}^{y_{top}} \tau_i [x_{wedge} - x_p] dy$	From vertical friction

Figure 4-13 shows the flowchart of the algorithm to simulate a bluff failure. A sample MATLAB script is attached as Appendix C.

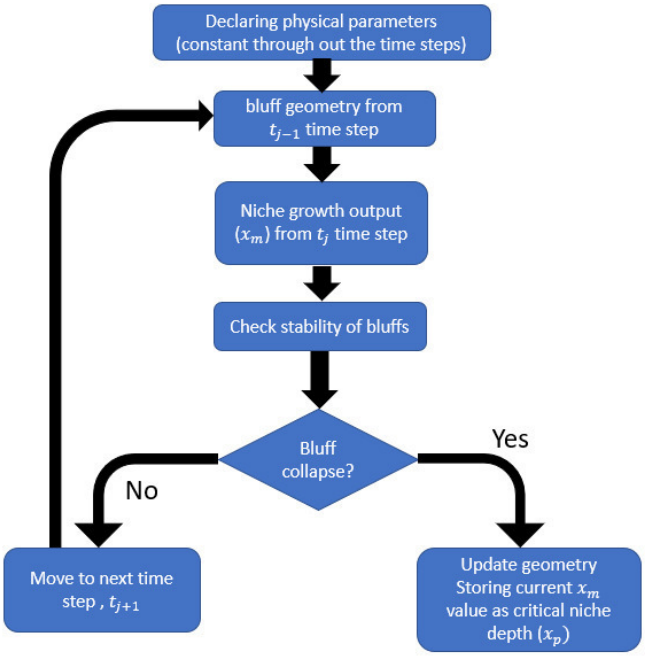

Figure 4-13Flow chart of the numerical schematization.

A direct solution of the stability equation (Equation 26, page 35) cannot be found. Trial and error method is used to determine the critical niche growth. Initially, the numerical model gets a niche growth (x_m), close to zero. Then driving and resisting moments (i.e. T_d and $T_{resisting}$) are calculated. If bluff is stable, that means x_m is smaller than the critical value (x_p). A new trial will be initiated with an incremental value of niche growth. Eventually, bluff will collapse. The x_m value for which collapse mechanism is triggered, is stored as critical niche depth (x_p).

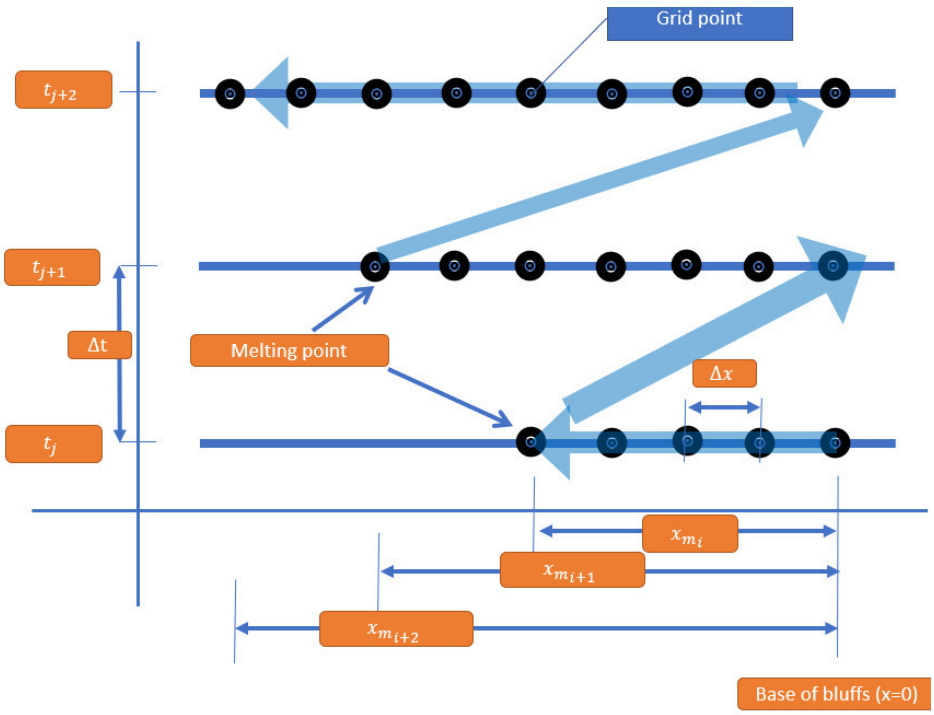

Figure 4-14 space and time advancement of the bluff collapse model during the storm (variable space domain).

Similar to storm surge model, this model also distinguishes between time and space. The numerical solution calculates the stability of each grid points inside the niche for a given time step. If the stability is found to be attained, the model looks into the stability for the next time step.

For a given time step, let's assume the time value is t_j. As equal spaced time step is used, the value of t_j is $j * \Delta t$. For this time value, niche growth module has an output niche depth value (x_m). The niche depth value (x_m) is the cumulative sum from the previous storms. Once the niche depth value (x_m) is calculated for the time t_j, the bluff module checks the stability. The bluff collapse module starts looking for the instability from the base of the bluff. Then it moves forward in to the niche until the melting point of the niche is reached. Unlike the storm surge module, space discretization Δx is kept very small (close to 1cm) to get an accurate result. If there is no stability problem for the given time step t_j, the model will move to next time step t_{j+1}. Figure 4-14 depicts the time and space advancement of the numerical model. Every line is the same space over the different time period. However, numbers of space-steps increase after every time step during the storm. In calm condition, all the space-steps will be the same. See Appendix C for a sample of MATLAB script.

4.4.2 The output of the numerical model

The numerical module for the bluff collapse was applied to various cases to identify its behaviour. Before initializing the calculation, the model requires geometry and strength parameters. A base case representing the Arctic coast of Russia is shown in Table 4-5 and Figure 4-15:

Table 4-5 Typical input values for bluff collapse model

Physical properties		
Parameter	Typical value	Remarks
Density of bluff	1,400 kg/m^3	30% ice content
The tensile strength of ice, τ_i	$1x10^5$ Pa	
The tensile strength of permafrost, τ_b	$2x10^5$ Pa	
Geometry of bluff		
Bluff height ($y_{top} - y_{base}$)	5 m	Typical bluff height (may vary)
x_{edge}	15m	Value suggested by Barnhart (2014)

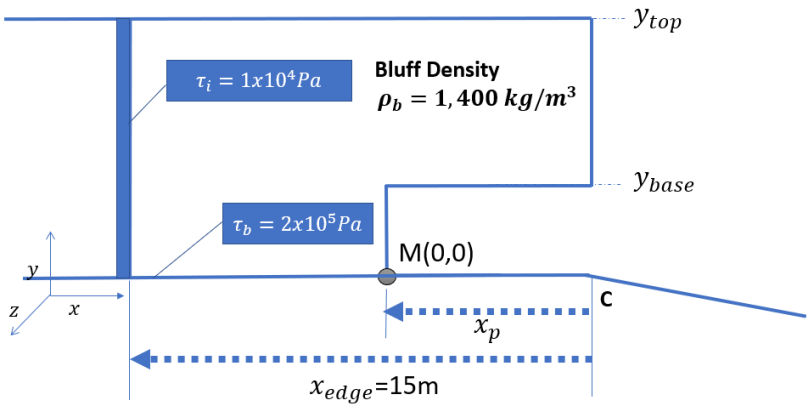

Figure 4-15 Input parameters for bluff collapse module.

The numerical model calculates that at niche depth of 10.326m the stability is lost.

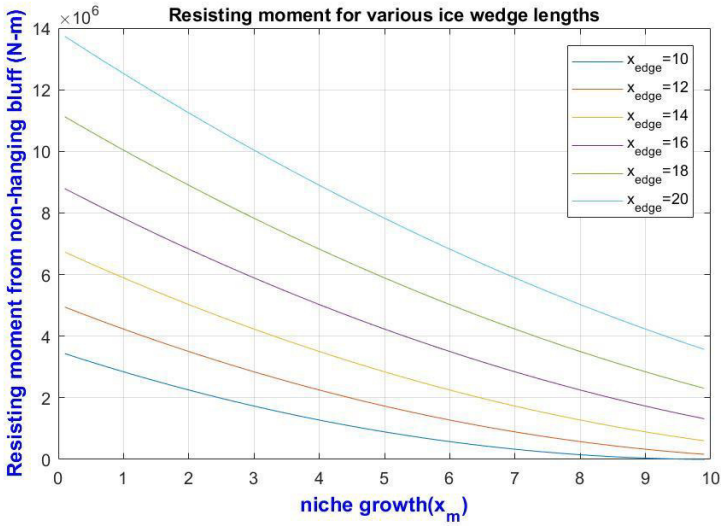

Figure 4-16 Resisting moment for various ice wedge lengths.

Figure 4-16 shows the relation of the niche growth (x_m) with the resisting moment (T_r)for various wedge distances from the bluff face (x_{edge}). For a constant x_{edge}, T_r decreases with niche growth (x_m). When the melting point (x_m) is close to the ice wedge (x_{edge}), the resisting moment is almost zero.

Values of T_f for various x_{edge} is shown in Figure 4-17. T_f decreases when niche growth (x_m) increases. The decrease is not linear; rather it is parabolic. For bigger wedge sizes (x_{edge}), the resisting force is larger.

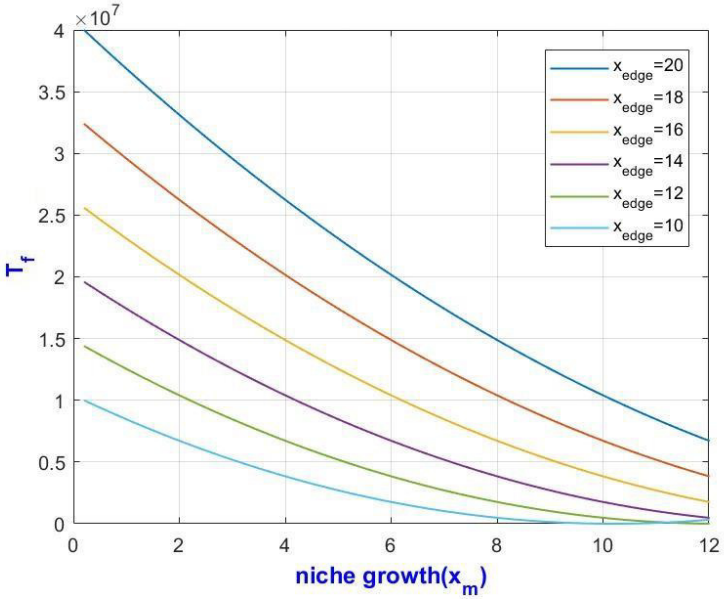

Figure 4-17 T_f for various ice wedge sizes.

Figure 4-18 depicts the values of T_i for x_{edges}. T_i decreases when niche growth (x_m) increases. The decrease is not linear; rather it is parabolic. For bigger wedge sizes, the resisting force is larger.

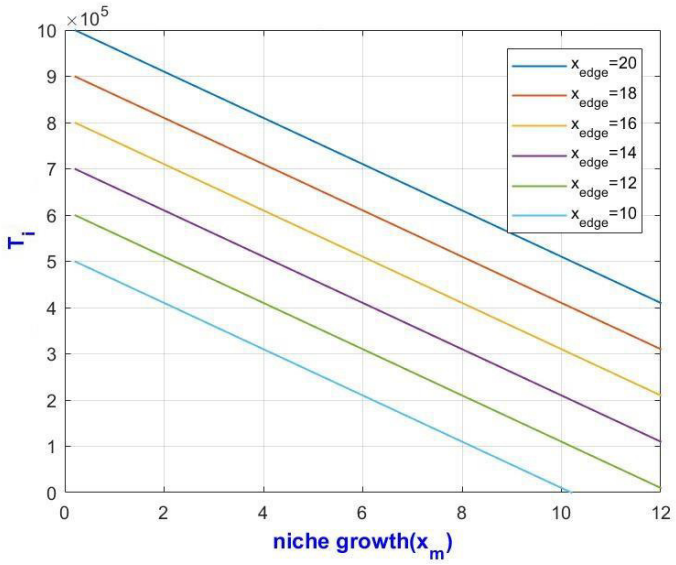

Figure 4-18 T_i for various ice wedge sizes (x_{edge}).

In Figure 4-19 the driving force, T_d is drawn with the thick brown line. The driving moment T_d is independent of bluff geometry. For all sizes of the wedge (x_{edge}) the line is the same. However, the combined resisting moments, $T_{resisting}$ are dependent on bluff geometry.

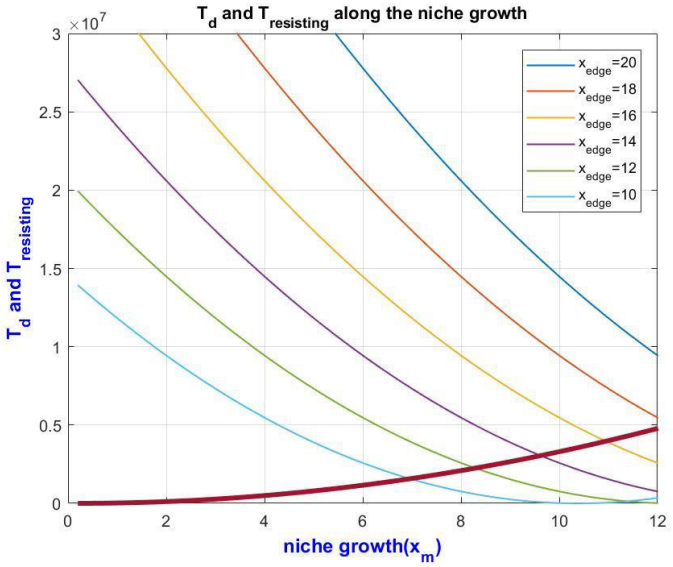

Figure 4-19 Resisting and Driving forces.

Resisting moments ($T_{resisting}$) decreases when the niche is growing inward. But the driving moment (T_d) that works in favour of failure increases with niche growth (x_m). This means there exist a critical niche growth (x_p) for which driving and resisting moments are the same. If the niche growth is more than this critical value, bluff should collapse.

The output of the bluff collapse numerical module is the critical niche depth. Figure 4-20 shows the dependence of the outcome on various input parameters. For each case, the output of the numerical model, i.e. the value of x_p is plotted against a variable input. Wedge size (x_{edge}) and bluff strengths acts against failure, critical niche depth increases when these parameters are increased. On the other hand, bluff density and bluff height act in favour of failure and critical niche depth decrease when density and height of bluff is increased.

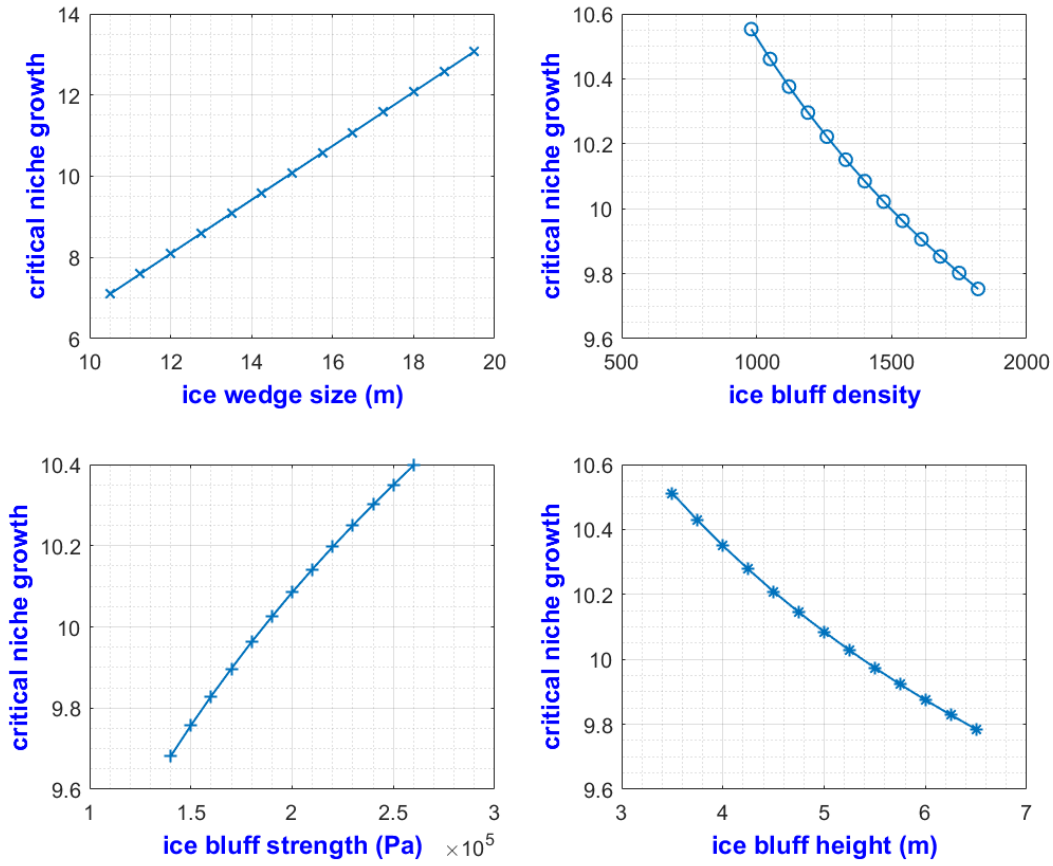

Figure 4-20 Output of bluff collapse model.

4.4.3 Discussion

Discussion of this section is specific to the numerical model, not bluff collapse mechanism as a general process. The following conclusion is made for the numerical model:

(1) Stability has a linear relation with x_{edge}. For bigger wedge size (x_{edge}), the stability is maintained at a greater critical niche depth (x_p). This indicates the importance of the geometry inputs of the model.

(2) It is also noted that bluff height has a negative effect on stability. As the height is increasing, the stability is decreasing.

(3) The mechanical strength of bluff also plays a role. Critical niche depth (x_p) increases with strength increment. However, the relation is not strong since the increase rate is quite small.

(4) If the bluff density increases, critical niche depth decreases. Bluff density parameter is present in both driving and resisting moment equations. Figure 4-20 indicates the bluff density is load parameter i.e. the contribution of bluff density parameter is more on the driving moment and towards failure.

5 Validation of the numerical model

The numerical model described in Chapter 4 is applied to an Arctic coast where the erosion rate is known. Applicable to only thermoabrasion erosion process, the model is not suitable to all Arctic coasts. To calibrate and validate the model, an Arctic coast or part of the Arctic coast is required where thermoabrasion is the dominating process.

5.1 Choice of location

A coast in the Kara sea was chosen where the shore is shallow; a large storm surge is possible and bed profile shows a well-defined bluff face. Two locations were chosen; observation of one site was used to calibrate the model and measurements of the other sites was used to validate. The area was surveyed as part of the work carried out by SAMCoT, Work Package 6, Task 6.1 as a joint study with MSU (Moscow State University) and SINTEF(Kulkarni, 2013).

The bay is situated between the two peninsulas of Yugra and Yamal. It is approximately 350 km long and 250 km wide at the mouth. The study area lies in the northern geo-cryological zone and has practically continuous permafrost. The currents near the area of interest lie in the range of 0.18 – 0.25 m/s with marginally higher velocities during flooding (Odisharia et al., 1997). The sites are located in 3.6 Km on NW direction from the cofferdam of Bovanenkobo-Uhta gas pipeline (coordinates: 68.867459°N;66.741529°E) (Isaev et al., 2017).

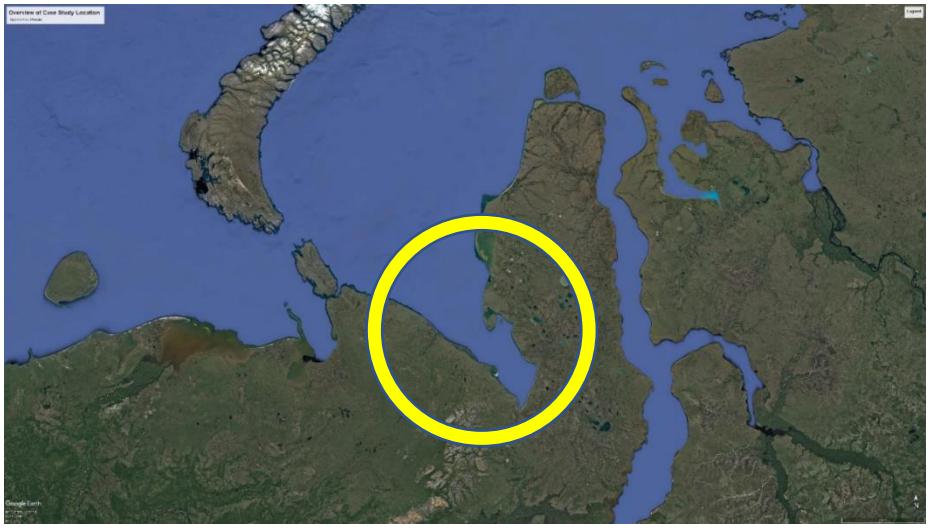

Figure 5-1Overview of the case study location [source: google earth].

Within the case study area, there are three distinctive geomorphological features: beach, laida and marine terrace. Frozen bluffs consist of high clay content. Beach level is smooth, has a very mild slope and no vegetation cover. The surface of the frozen bluffs is covered with ice-wedge polygons (see section 0 for details of ice wedge polygon) (Isaev et al., 2017).

5.1.1 Site-1 location

Site-1 is located close to the mouth of the river Sabryavpenzya (Figure 5-2 and Figure 5-3). In the summer the sea is ice-free. But at the end of winter, some ice are found floating in the sea. However, during a storm in summer, floating ice will not hamper the surge level significantly. Bathymetry and other details are explained in section 5.2.1.1.

Figure 5-2 Satellite image of the site 1 (date: 28 July 2009) [source: google earth].

Figure 5-3 Satellite image of the site 1 (date: 21 May 2016) [source: google earth].

5.1.2 Site-2 location

Site-2 is located left of the Site-1. It is a straight coast. No ice during summer (Figure 5-4). But during winter, land-fast ice may be present. Bathymetry and other physical properties are discussed in section 5.2.

Figure 5-4 Satellite image of the site 2 (date: 28 June 2012) [source: google earth].

Figure 5-5 Satellite image of the site 2 (date: 21 May 2016) [source: google earth].

5.2 Bathymetry

Figure 5-6 Bathymetry overview [source: www.navionics.com].

The gulf is very shallow (less than 10 m) close to the shore (Figure 5-6). The funnel shape of the gulf also increases the possibility of the high surge. Thermoabrasion model developed for this study is 1D and thus cannot capture the effect of the funnel shape.

5.2.1.1 Bed Profiles

For Site-1, bed profile measurements at June 2012 and June 2013 were chosen (Figure 5-7). Bed profiles were measured by Moscow State University (SAMCoT, Work Package 6, Task 6.1) (Isaev et al., 2017).

Table 5-1 Summary of the chosen bed profiles

Case	Timeframe	Erosion (field measurement)	Remarks
Case-1	1 July 2012-30 June 2013	6.9m	Bed profile 1 has lower bluff height. Also, time exposure is different which makes the two cases mutually exclusive.
Case2	1 September 2016-30 August 2017	9.1m	

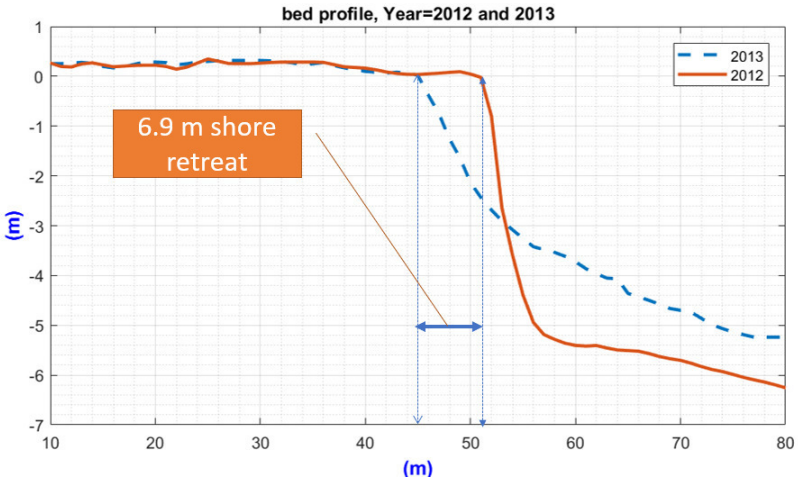

Figure 5-7 Bed profile of site 1, used in Case-1 (2012 and 2013).

For Site-2, bed profiles between September 2016 and September 2017 were chosen (Figure 5-8). These two profiles show well-defined bluff faces with a narrow beach which matches with the assumptions made in the conceptual model. The model can only consider the regular geometry of the bluff, thus to increase accuracy, profiles with lower variations are preferred.

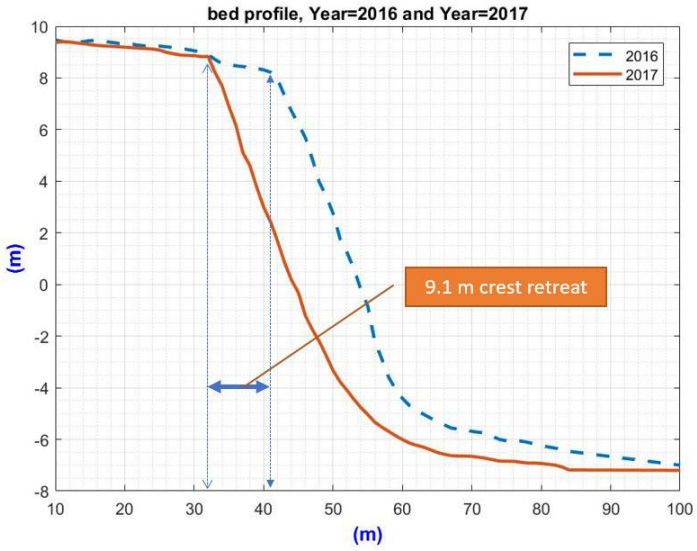

Figure 5-8 bed profile of site2, used for Case-2 (2016 and 2017).

5.3 Wind data

Wind data is collected from the Danish Hydraulic Institute website (waterdata.dhigroup.com/metocean-on-demand) on the location $71°N$ latitudes and $65.5°E$ longitude. Source of the data is the hindcast model of *Climate Forecast System Reanalysis (CSFR), NCEP, NOAA*.

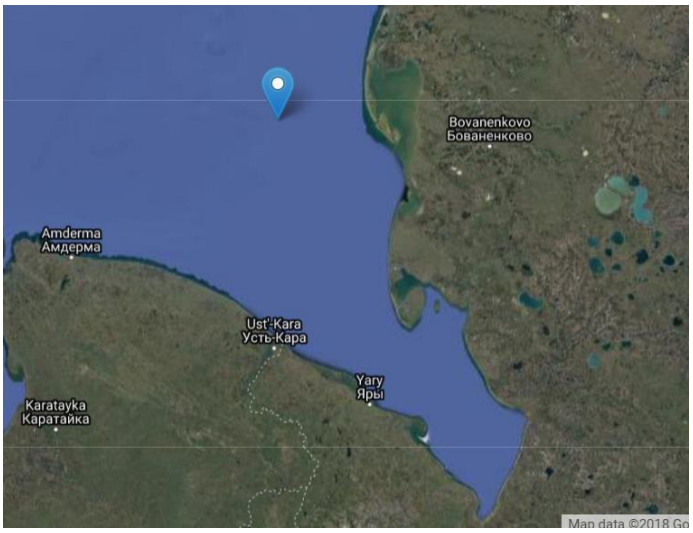

Figure 5-9 position of wind data source.

Two-bed profiles were selected for calibration and validation. Visual inspection of Figure 5-10 and Figure 5-11 reveals that Case-1 bed profile faced fewer extreme events which most probably is the reason of shorter erosion rate than Case-2 (6.9m/yr Vs 9.1/yr).

Table 5-2 Summary of wind speed inputs for the chosen time frames

Profile	Duration	Remarks
Case-1	1 July 2012-30 June 2013 (for site 1)	Wind data inputs are shown graphically in Figure 5-10 and Figure 5-11
Case-2	1 September 2016-31 August 2017 (for site 2)	

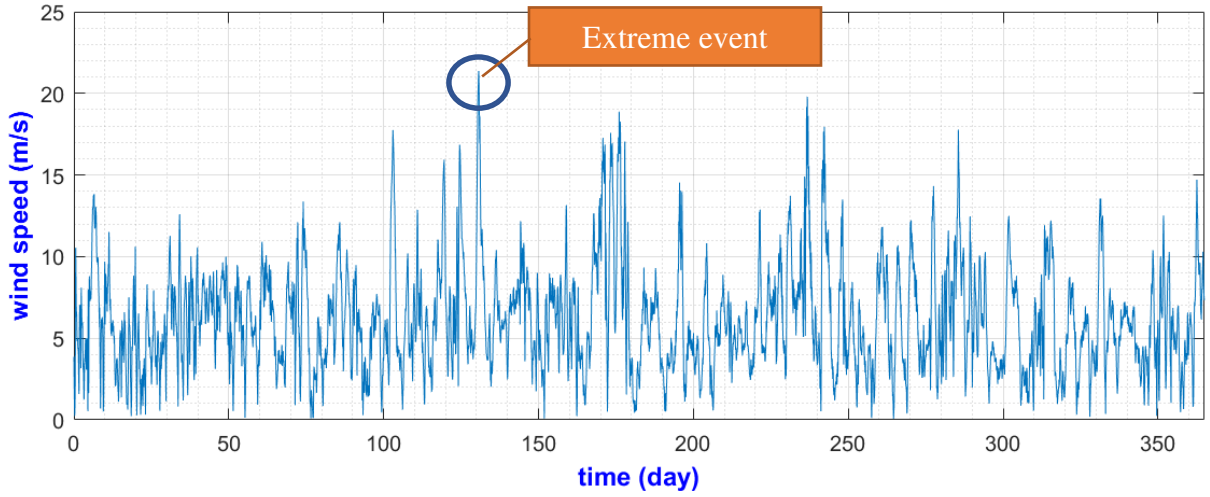

Figure 5-10 Wind speed inputs for the model (Case-1).

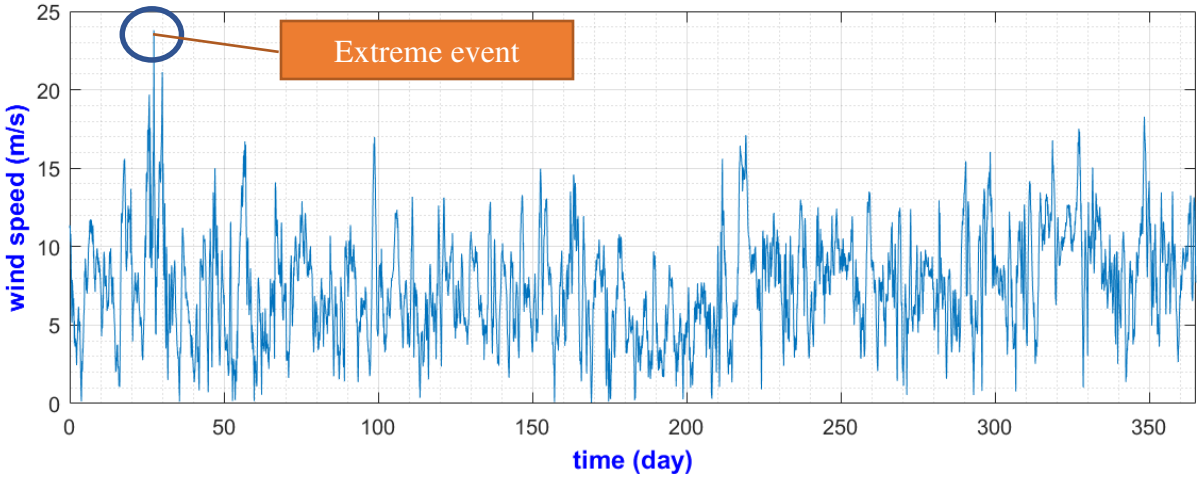

Figure 5-11 Wind speed inputs for the model (Case-2).

A short probabilistic analysis of the wind speed shows the extreme values follow Weibull distribution at the tail. However, in the storm surge module, the probabilistic distribution of wind speed was ignored. Wind speed measurements are of 1hour time interval which was linearly interpolated to fit a 10-minute interval time step.

Table 5-3 Probabilistic analysis of wind speed inputs

Site1	Site2
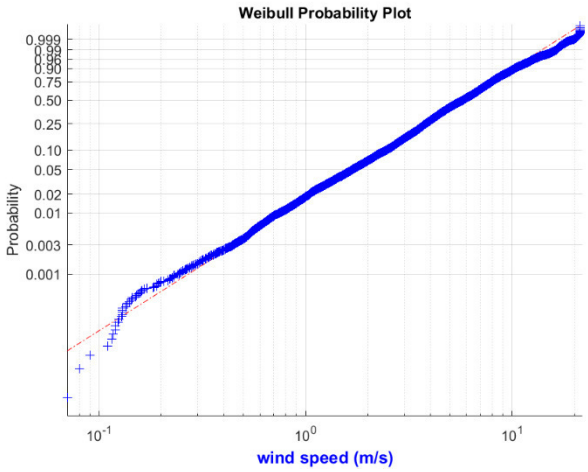	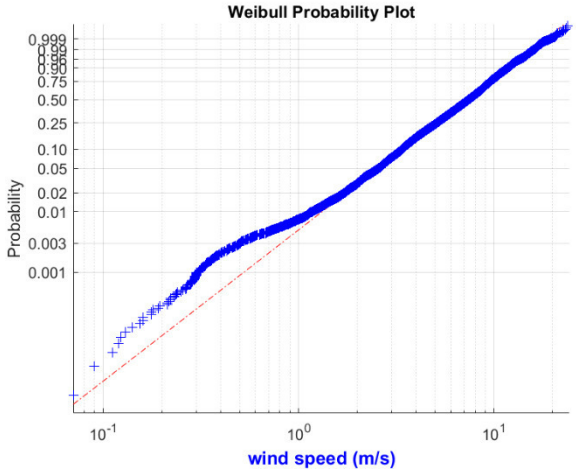

5.4 Case-1 model run

The following inputs were used to calculate numerically the erosion rate by thermoabrasion. Case-1 model run was used to calibrate the model.

Parameters	Values	Remarks
Wind speed	Case-1 (Figure 5-10)	DHI website
Bed profile	Site-1 (Figure 5-7)	Field report (Isaev et al., 2017)
Time duration	1 July 2012-30 June 2013	365 days
Bluff Height	5m (Norm, 5,0.5)	Field report (Isaev et al., 2017)
Time steps	600s	52,555 grid points in the time axis
Space steps	1m/1cm	For storm surge module 1m, for niche growth module 1cm
Salinity	30 ppt (Norm, 30,3)	Assumed
Ice-wedge size	14m (Norm, 14,2)	Assumed based on observation by Ravens (2012)
Number of model run	1,000 different circumstances	For probabilistic analysis, 1,000 different circumstances were considered.

*Norm=normally distributed; followed by mean and standard deviation

The model uses a probabilistic approach and use Monte Carlo simulation technique. Input parameters are randomly drawn from their own distributions (Figure 5-12). The model was executed 1,000 times with varied input parameters. A sample script to run complete model is attached at Appendix D.

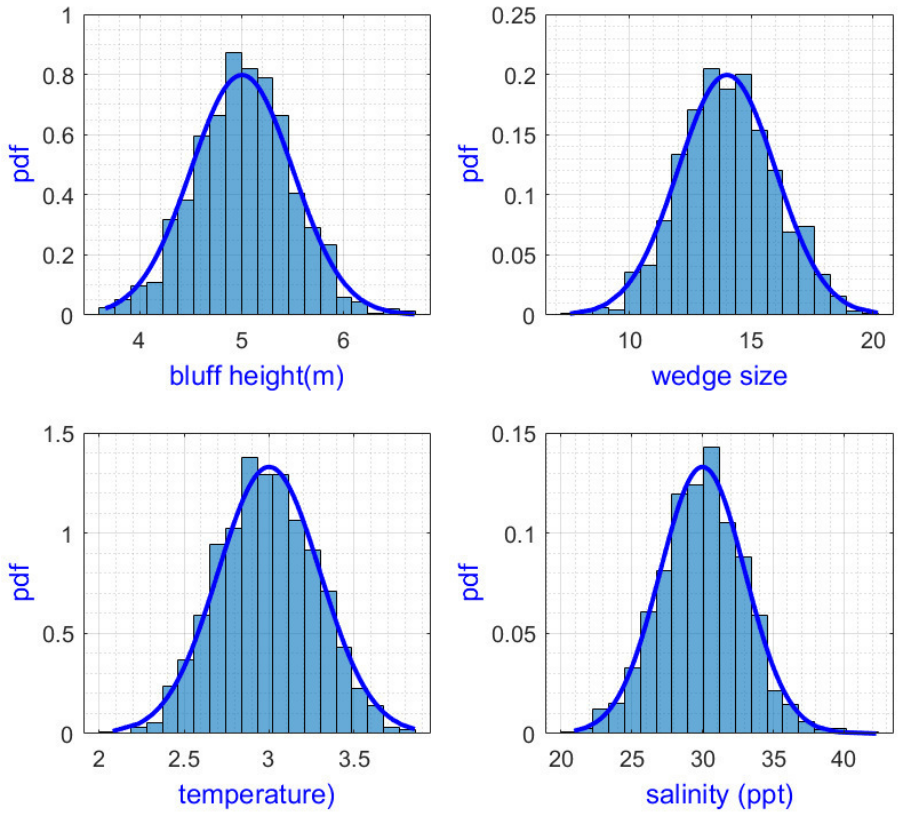

Figure 5-12 Probabilistic Distribution of input parameters.

The bed profile and wind speed data are presented graphically in Figure 5-13 and Figure 5-14.

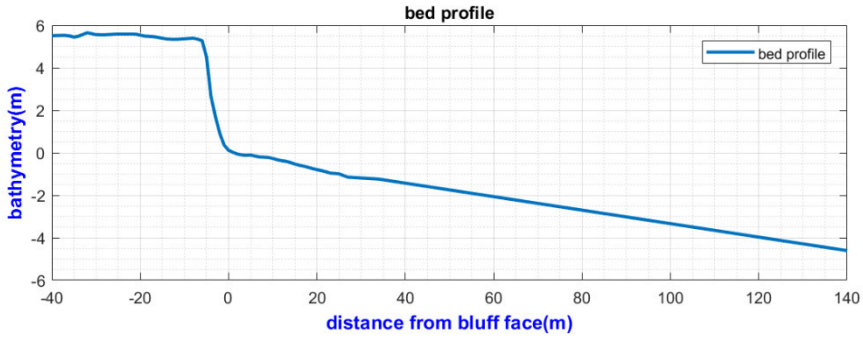

Figure 5-13 Inputs: bathymetry for Case-1.

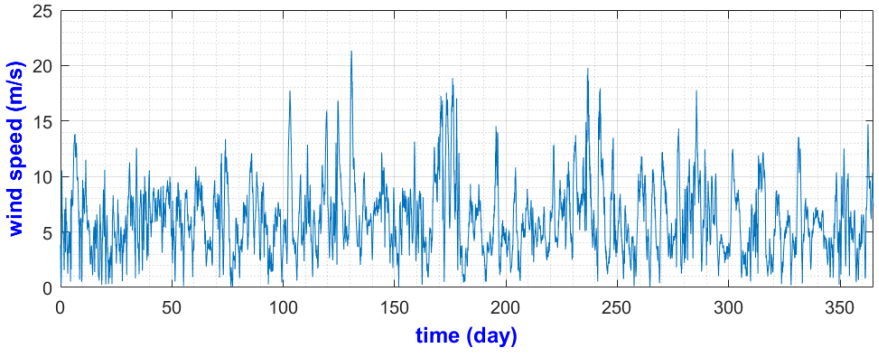

Figure 5-14 Input: wind speed for Case-1.

5.5 The output of Case-1

Using the bed profile-1 (Figure 5-13) and wind speed (Figure 5-14) inputs, storm surge level was calculated. Storm surge peaks coincide with the higher wind speeds. However, not all storms could produce high enough surges that can inundate base of the bluff. *Graph-c* of Figure 5-15 reveals that only fewer times-for higher wind speeds, the water level reached the base of the bluffs. For the most extreme event of the year inundation depth (h_{id}) of the base was found to be around 0.19m (*graph-b*).

Whenever, water level reaches the base of the bluff (inundation depth responses, *graph-c* in Figure 5-15), niche growth starts which in terms contributes to erosion. Erosion rate was calculated to be 6.67m with standard deviation 0.39m for the Case-1.

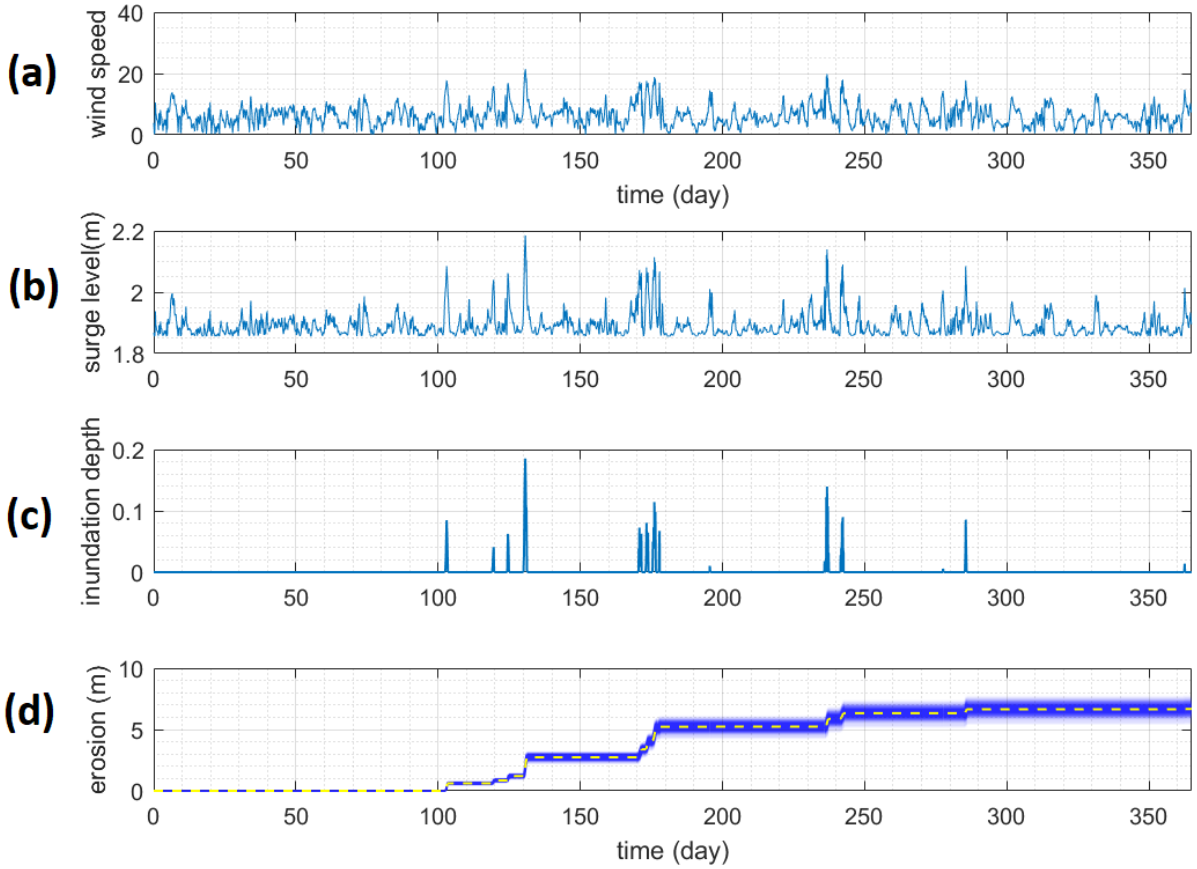

Figure 5-15 outputs of Case-1 (mean erosion shown in dashed line).

The profile faced many storms with wind speeds of more than 15 m/s, but most of those did not trigger thermoabrasion. Only fewer, yet greater storms were able to trigger bluff erosions (*graph-c* of Figure 5-15). The bottom *graph-d* shows the cumulative average erosion rate which reaches more than 5m at the end.

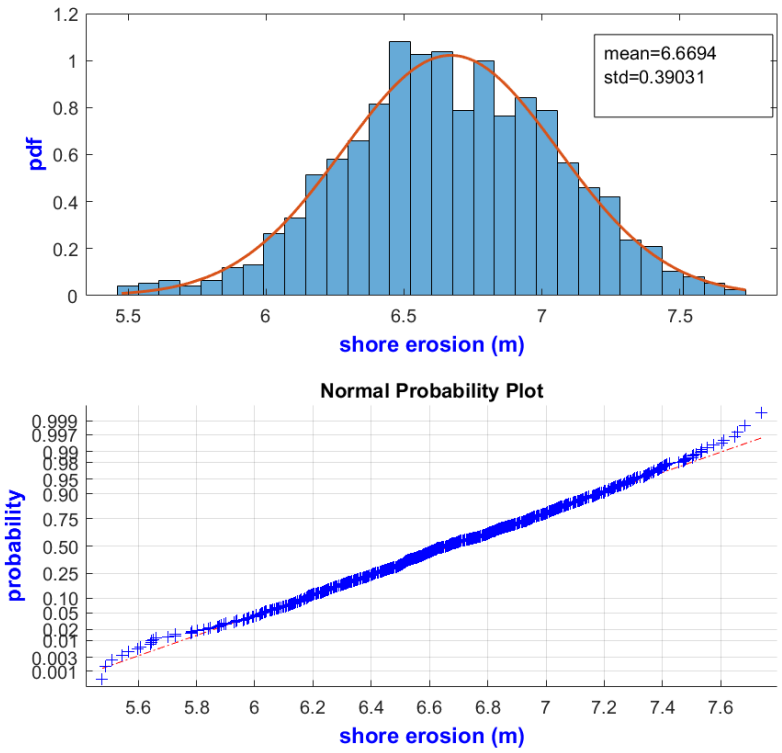

Figure 5-16 Normal distribution of erosion (for the whole year).

Analysis of the cumulative erosion at the end of the year shows a central tendency. When fitted to a normal distribution, deviations are noticeable at both ends. Statistical parameters are shown in the table below:

Table 5-4Output of Case-1

Parameter	Mean	Standard Deviation	Field data
Cumulative erosion (for 365 days)	6.6694m	0.3903m	6.9m erosion is estimated from field report (Figure 5-7)
	6.6452 (95% upper bound) 6.6936 (95% lower bound)	0.3739(95% upper bound) 0.4082(95% lower bound)	

Erosion rate found from the filed measurement for 2012-2013 was 6.9m (Figure 5-7) whereas the numerical model predicts erosion rate would be 6.67m (Table 5-4). Reason for the lower value predicted by the model may be caused by one of the limitations of the model. The model can only calculate thermoabrasion erosion; thermodenundation process is not calculated. This limitation might have contributed to the difference of the calculated and observed erosion rate. Since the difference is small and estimation is of the same order of magnitude, the result was

accepted and calibration was assumed to be completed. With the calibrated numerical model, Case-2 was loaded to validate the numerical model.

5.6 Case-2 model run (Validation)

Case-2 bed profile is different from Case-1 in both time frame and location. The bluff height is higher than the Case-1 (5m Vs 12m). Significant bluff height difference causes the critical niche depth (x_p) to be different.

Table 5-5 Input parameters for the model (Case-2)

Parameters	Values	Remarks
Wind speed	Case2 (Figure 5-11)	For 2016-2017 time period [source: DHI website]
Bed profile	Site-2 (Figure 5-8)	For 2016-2017 time period [source: (Isaev et al., 2017), Figure 5-18
Time duration	1 September 2016-31 August 2017	365 days
Bluff Height	12m (Norm, 12,1.2)	Field observation
Time steps	600s	time step of wind speed data is 1hr, linear interpolation was applied to reach 10-minute time steps
Space steps	1m/1cm	For storm surge module 1m, for niche growth module 1cm
Salinity	30 ppt (Norm, 30,3)	Assumed
Ice-wedge size	14m (Norm, 14,2)	Assumed
Number of runs	1,000 different circumstances	For probabilistic analysis, 1,000 different circumstances were considered.

*Norm=normally distributed followed by mean and standard deviation

Similar to Case-1 model run, one thousand circumstances were considered. The cases were generated from the probabilistic distributions of the inputs as shown in Figure 5-17.

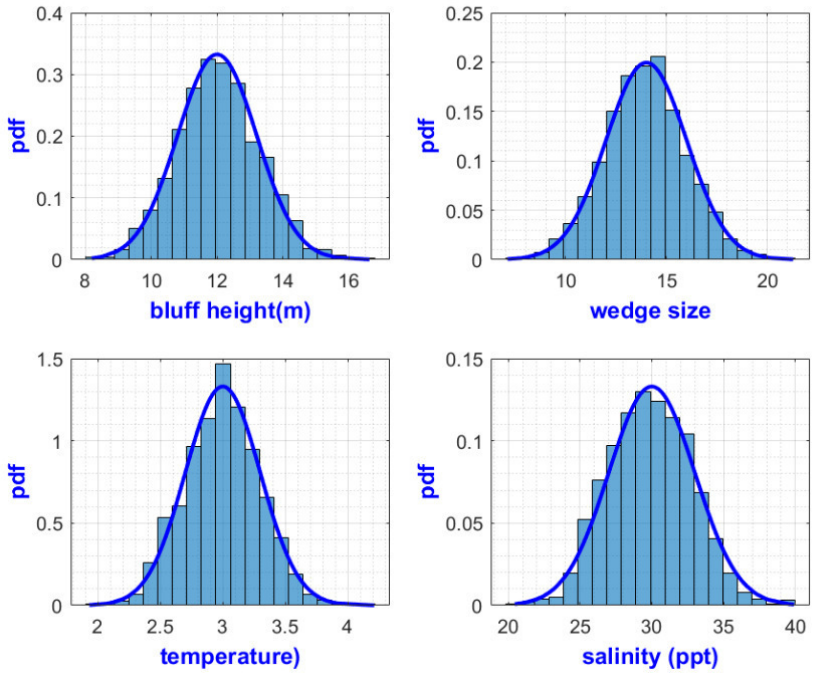

Figure 5-17 Probabilistic distributions of the input parameters.

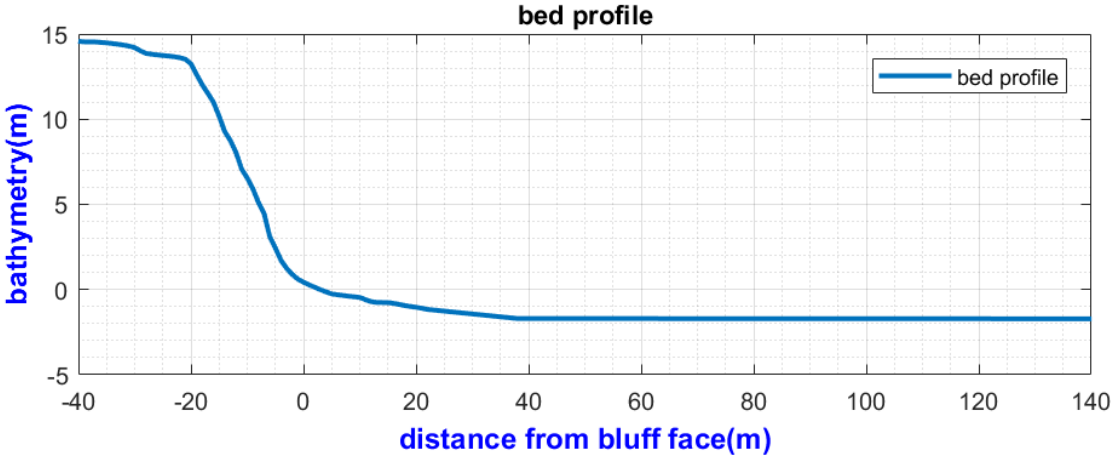

Figure 5-18 Inputs: bed profile for Case-2.

5.7 The output of Case-2

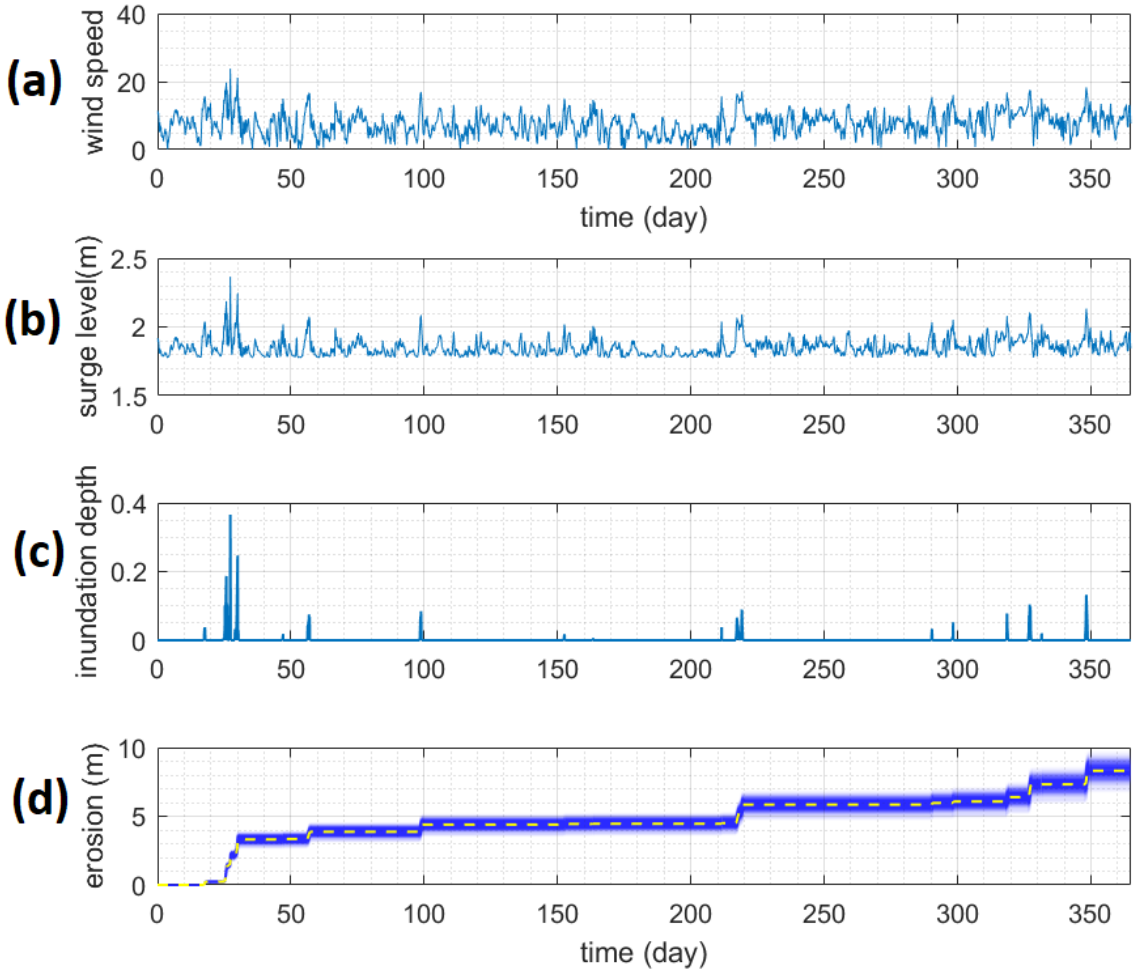

Figure 5-19 outputs of Case-2 (mean erosion shown in dashed line).

One of the major dissimilarities between Case-1 and Case-2 run is the significant difference in maximum inundation depth (h_{id}). Profile-2 faced bigger storms and maximum inundation depth was higher (0.38m vs 0.19m). Much of the erosion is caused by the most extreme event of the year. Other storms also caused erosions and at the end of the time period, cumulative erosion crossed 8m.

Cumulative erosion values at the end of the time period loosely fit to a normal distribution and mean was found to be 8.305m with a standard deviation of 0.488m (Figure 5-20).

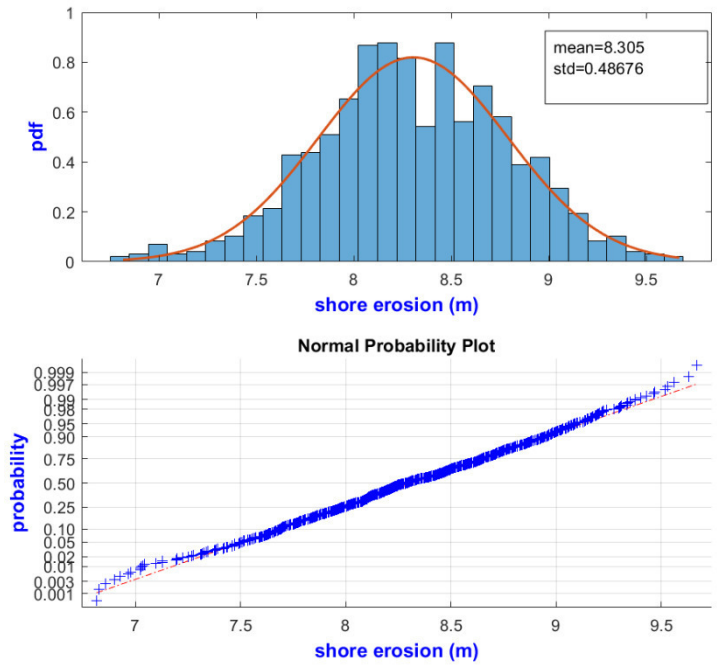

Figure 5-20 Probabilistic analysis of cumulative erosion for Case-2.

5.8 Discussion on validation

Storm surge level was calculated using the bed profiles and wind speed data. Peaks of the storm coincided with the high wind speeds for both the cases. The water level reached the base of the bluff for a limited number of times (11 times) for Case-2 and for the most extreme event of the year inundation depth of the base is around 0.38m.

A central tendency is observed for the 10,000 erosion rates found in Case-2. Erosion rate at the end of the time period was fitted to a normal distribution, deviations are noticed at both of the ends. Statistical parameters are shown in a table below:

Table 5-6Output of Case-2

Parameter	Mean	Standard Deviation	Field data
Erosion (for 365 days)	8.3050 m	0.4868m	9.1m erosion was estimated from field report (Figure 5-8)
	8.2748 (95% upper bound) 8.3352 (95% lower bound)	0.4663 (95% upper bound) 0.5091 (95% lower bound)	

Erosion rate found in the field measurements for 2016-2017 was 9.1m whereas the numerical model predicts erosion rate would be 8.3m.

For the Case-1 (calibration) the accuracy of the prediction was higher because calibrating parameters were open to making adjustments. When validation exercise was performed on the Case-2; the calibrating parameters were locked (see Appendix D on page 110 for the details of the calibration).

Table 5-7 Comparison of field data and model prediction

Cases	**Shore retreat**	
	Estimated from field data	**Predicted by Numerical model**
Case1(calibration)	6.9m	6.67m
Case2 (validation)	9.1m	8.31m

The numerical model is in agreement with the field measurements for two of the cases with reasonable accuracy. However, probabilistic distributions of the input parameters could not be validated. Due to lack of data availability, validation and calibration of the model were not performed on more profiles.

The model was assumed to be calibrated by Case-1 and validated by Case-2 model run, thus used without alteration to perform the sensitivity analysis.

6 Sensitivity Analysis of the modules

Sensitivity analysis was performed to understand the behaviour of the numerical modules. The main objective of the sensitivity analysis was to determine the impact of the independent variables on the dependent variables and outcomes. Both deterministic and probabilistic approaches were adopted for the sensitivity analysis. For the probabilistic analysis, parameters were assumed to be independent; the joint probability of the parameters was not considered. The numerical model is developed for a data-poor environment, i.e. the probabilistic distribution of the majority of the parameters are not known. A normal distribution with 10~20% CoV (coefficient of variation) was assumed for most of the cases.

Concrete is a brittle material with high compressive strength but low tensile strength. Frozen bluff also exhibits the same strength characteristics. Strength parameters of concrete follow a log-normal distribution (Silvestri et al., 2008). Comparing ice with concrete, taken into account both are a brittle material with low tensile strength, log-normal distribution was assumed for strength parameters for bluffs. For the deterministic approach, a base case is used and each parameter was varied separately to investigate the sensitivity of the model to these parameters. The base case is determined by probabilistic analysis and the most probable value with 95% confidence limit is taken as base/mean value.

6.1 Probabilistic Sensitivity Analysis

A probabilistic approach of the sensitivity analysis requires the generation of random values of input parameters following their own distributions. Monte Carlo simulation was performed using the generated random samples. Base cases of the three numerical modules; storm surge, niche growth and bluff collapse were determined before deterministic sensitivity analysis was performed.

The numerical model reads from the two input files: bathymetry and wind. Both of these parameters are site-specific. To make the analysis universal-not prone to site-specific issues; a

hypothetical ideal bathymetry was considered. In case of wind, the mean wind speed of the class 2 storm was considered as the base case.

6.1.1 Bed profile and wind speed for probabilistic sensitivity analysis

The hypothetical bed profile used for the base case is shown in Figure 6-1. It has a very steep slope at the face of the frozen bluff. Thermoabrasion is the dominating erosion process since the narrow near shore is susceptible to larger storm surges.

The extreme value of the wind speed follows a Weibull distribution. For the sensitivity analysis, extreme value generation is not required, rather a normal distribution around the extreme value better serves the purpose.

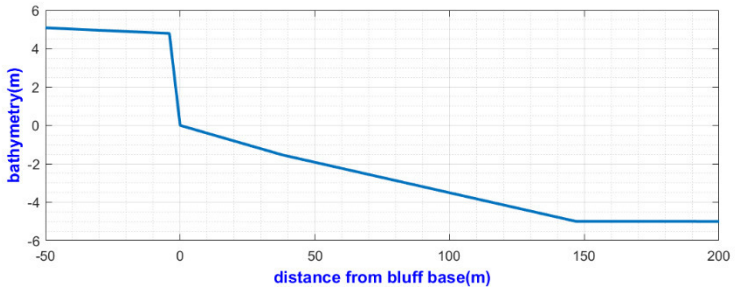

Figure 6-1 Hypothetical bed profile (first 100m).

6.1.2 Probabilistic sensitivity analysis of the storm surge module

The input parameters and their distributions for the storm surge numerical module are given in Table 6-1.

Table 6-1 Input parameters for storm surge module for sensitivity analysis.

Parameter	Distribution	Mean	Std Dev.	CoV	Remarks
Wind speed	Normal	22	2	10%	Not Weibull distribution
Bed profile	deterministic	variable			Hypothetical profile
Friction factor	Deterministic	$1x10^{-6}$			Standard value
Water density	Deterministic	1025			Saline water
Mean sea level	Normal	-3	0.3	10%	The base of the bluff is at level zero
Latitudes	Deterministic	68°			High altitudes for Arctic cases
Longshore current	Normal	2	0.3	15%	
Fetch length	Deterministic	5,000			(see section 4.2.2 for the effect of fetch length)

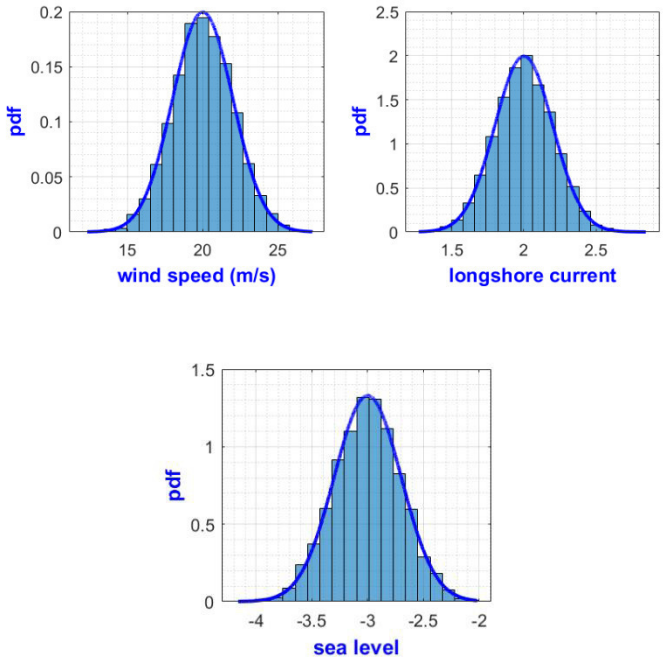

Figure 6-2 Input parameter distributions for storm surge module.

Figure 6-2 demonstrate distribution patterns of the input parameters. For the Monte Carlo simulation, 10,000 random samples were generated to determine the distribution of the outcome with reasonable accuracy. The output of the storm surge module is the storm surge level across the given bed profile. The following outcome of the Monte Carlo simulation was observed, see Figure 6-3.

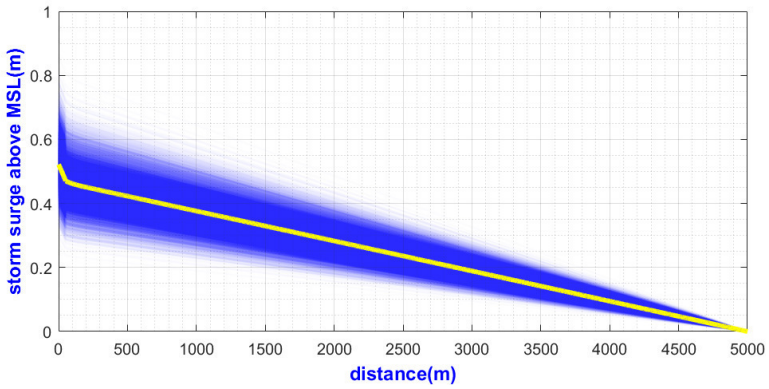

Figure 6-3 Output of storm surge model (mean value is shown in yellow line).

A high variability in the surge level was observed for a 20 m/s mean wind speed. Surge level varies between 0.38 to 0.8m at the base of the bluff. Surge level at 10, 25, 75 and 300m offshore from the base of the bluff are shown in Figure 6-4. Observed surge levels deviated from the normal distribution line at both ends of the tails. However, the deviance can be ignored because the most probable values are sought out, not the extreme cases.

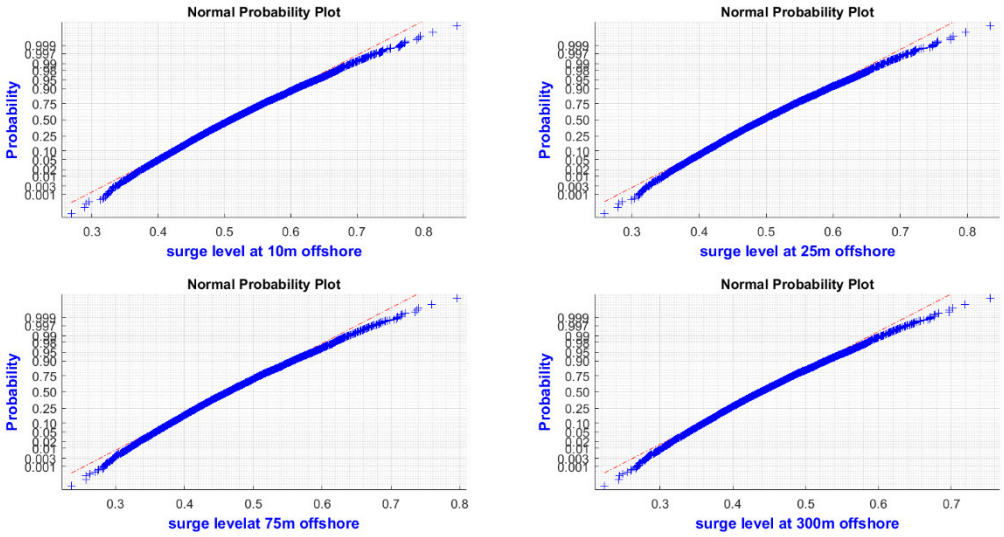

Figure 6-4 Storm surge level distribution fit (normal) at the various offshore location.

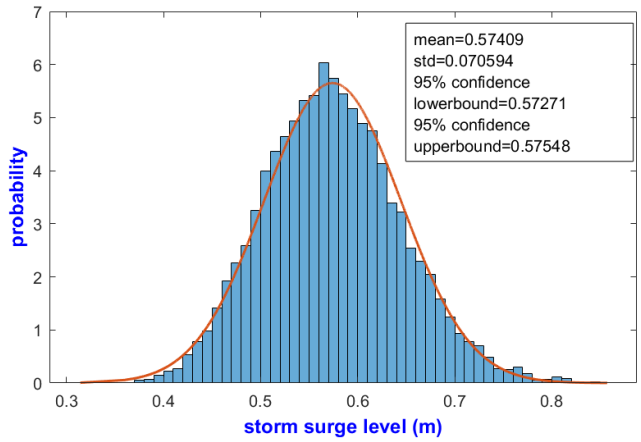

Figure 6-5 storm surge distribution at the base of the bluff (x=0 m).

Point of interest for the storm surge module is the water level near the shoreline. Inundation depth (h_{id}) at the base of the bluff is the input parameter for the niche growth module. Figure 6-5 depicts the distribution of the storm surge level at the base of the bluff. Mean value of the inundation depth for 10,000 samples was found to be 0.574m. This value is taken as a base case for deterministic sensitivity analysis.

6.1.3 Probabilistic sensitivity analysis of Niche growth module

The output of the niche growth module is the estimation of the depth of the niche. The relation between time and niche growth is parabolic, after several hours, niche growth rate decreases considerably.

Niche growth module requires some physical properties and geometric parameters as inputs. Geometric and strength parameters which are deterministic is mentioned in Table 4-3. Table 6-2 describes the input parameters with probabilistic distributions only and Figure 6-6 represents the distribution patterns of the generated samples.

Table 6-2 Input parameters for niche growth module

Parameter	Distribution	Mean	Std Dev.	CoV	Remarks
Inundation depth, h_{id}	Normal	0.5m	0.1	20%	CoV is taken higher since highly variable
Temperature (water), T_a	Normal	3°	0.3	10%	

Salinity	Lognormal	m=30 ppt	V=5		Lognormal distribution since the variation of salinity is very unlikely
Beta (β)	Normal	2	0.2	10%	β empirical constant as proposed by Kobayashi (1985); distribution is assumed

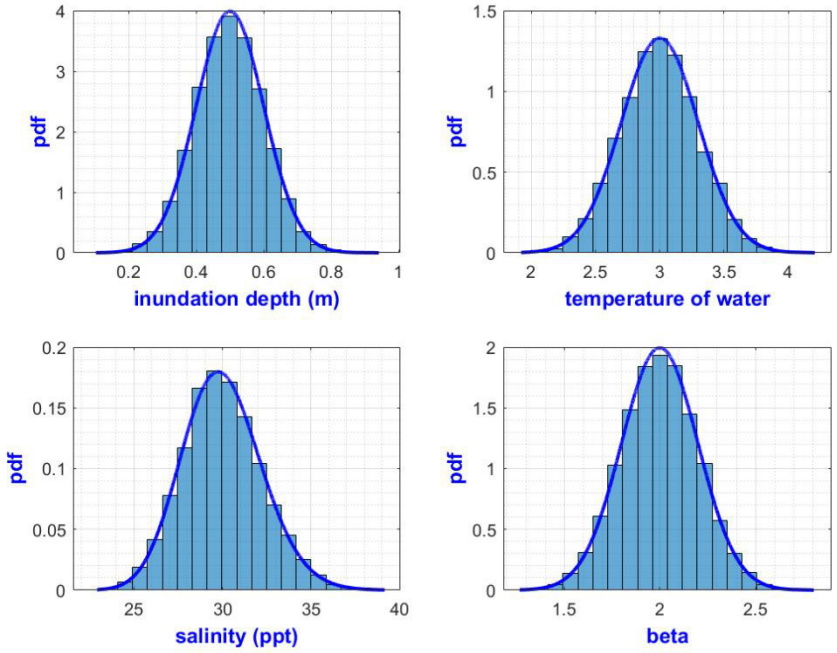

Figure 6-6 Distribution of the input parameters for niche growth module.

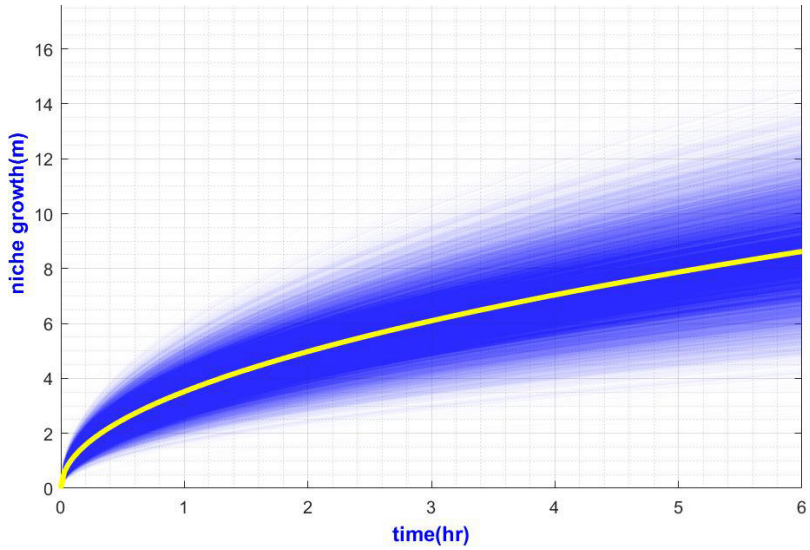

Figure 6-7 Probabilistic output of the niche growth module (mean is shown in yellow line).

The output of the 10,000 sample cases is shown in Figure 6-7. One semi-transparent blue line is one case of niche growth over the time, the yellow line is the mean. The central tendency is examined and niche depth at every hour is compared in Figure 6-8. After 4hr, depending on the input conditions, niche depth can be in between 2.8m to 13m which is a quite wide range (statistical analysis of niche depth after 4hr is shown in Figure 6-10). This also indicates how big the impacts of the four input parameters on the module (a deterministic sensitivity analysis indicates the relative importance of the four parameters in section 6.2.3 at page 91).

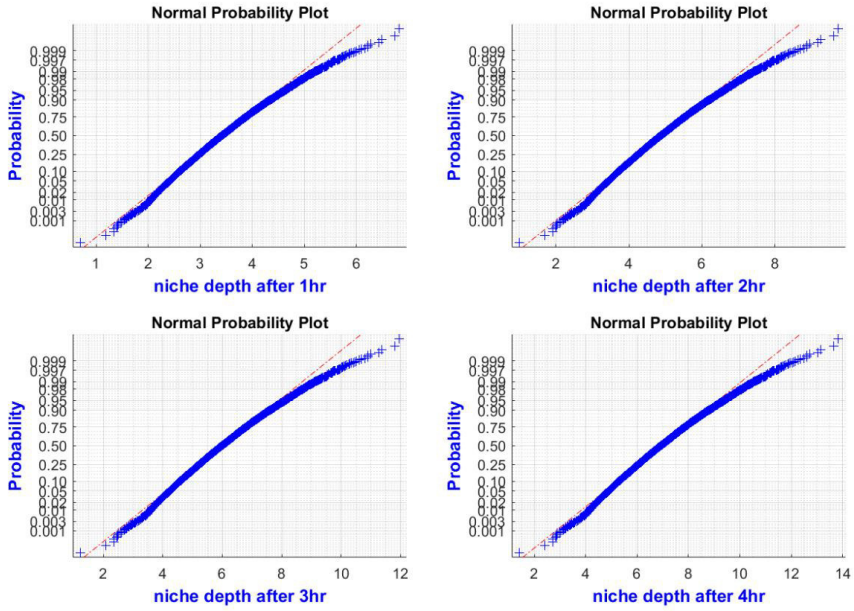

Figure 6-8 Probabilistic distribution of the niche depth after a certain time.

Normal probability plot of the niche depths (x_m) reveals that at the tail, the samples deviates from a normal distribution. Since, most probable niche depth is sought out rather than the extreme values, those points are not considered. Probability density functions of these four cases are depicted in Figure 6-9.

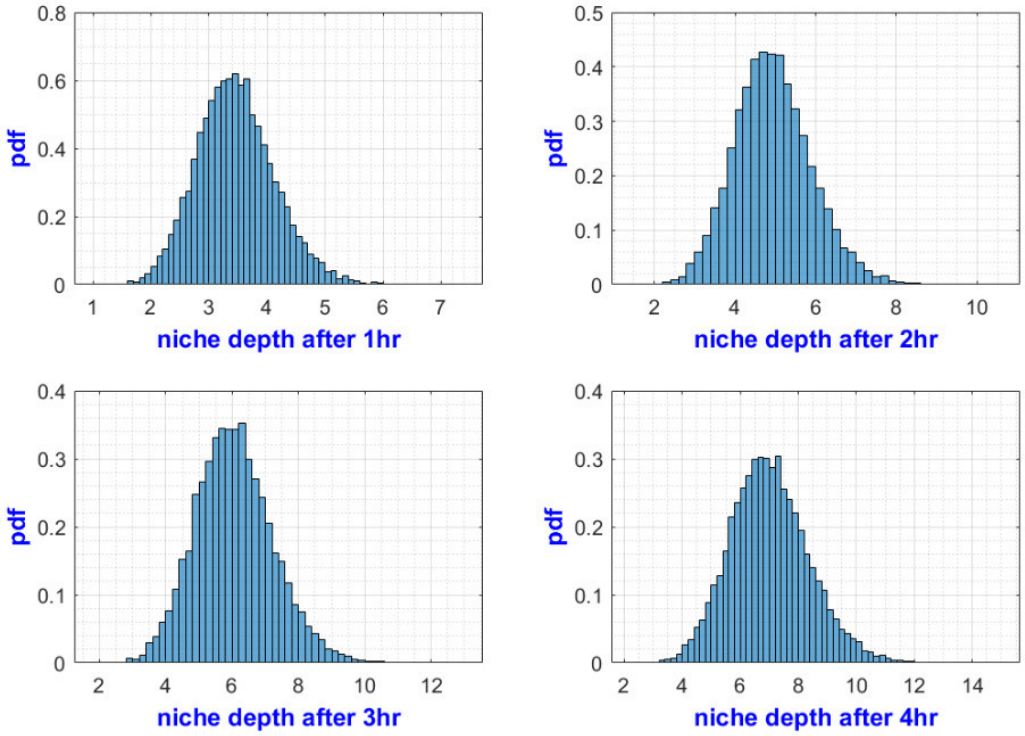

Figure 6-9 Distribution of the niche depth after 1,2,3 and 4 hrs.

Detailed statistical analysis of niche depth after 4hr indicates that mean value of the x_m is 6.9m with a standard deviation of 1.37m. Since the CoV value is quite high (19.8%), it can be concluded that the accuracy of the input parameters is of high importance.

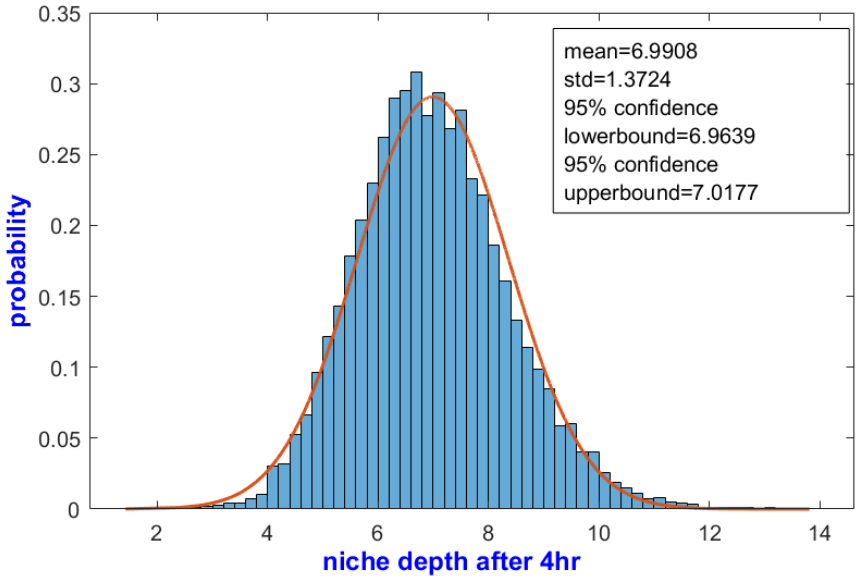

Figure 6-10 Probabilistic analysis of niche depth after 4 hr (fitted to normal distribution).

6.1.4 Probabilistic sensitivity analysis of Bluff Collapse module

Bluff collapse module requires geometric properties as core inputs and tensile strengths of the frozen bluff to determine the critical niche depth. When the output of the niche growth module is bigger than the critical niche depth determined by the bluff collapse module, a shoreline retreat is estimated. Probabilistic distribution of the geometric and mechanical strength parameter inputs are presented in Table 6-3 and probabilistic density functions of the generated samples are presented in Figure 6-11.

Table 6-3 Input parameters for bluff collapse

Parameter	Distribution	Mean	Std Dev.	CoV
wedge size, x_{edge}	Normal	16m	1.6	10%
Bluff density,ρ_b	Normal	1400 kg/m^3	140	10%
Tensile strength (ice)	Log normal	$1x10^4$ Pa	V=100	
Tensile strength (bluff)	Lognormal	$2x10^5$ Pa	V=200	
Bluff height, $y_{top} - y_{base}$	Normal	5m	0.5	10%

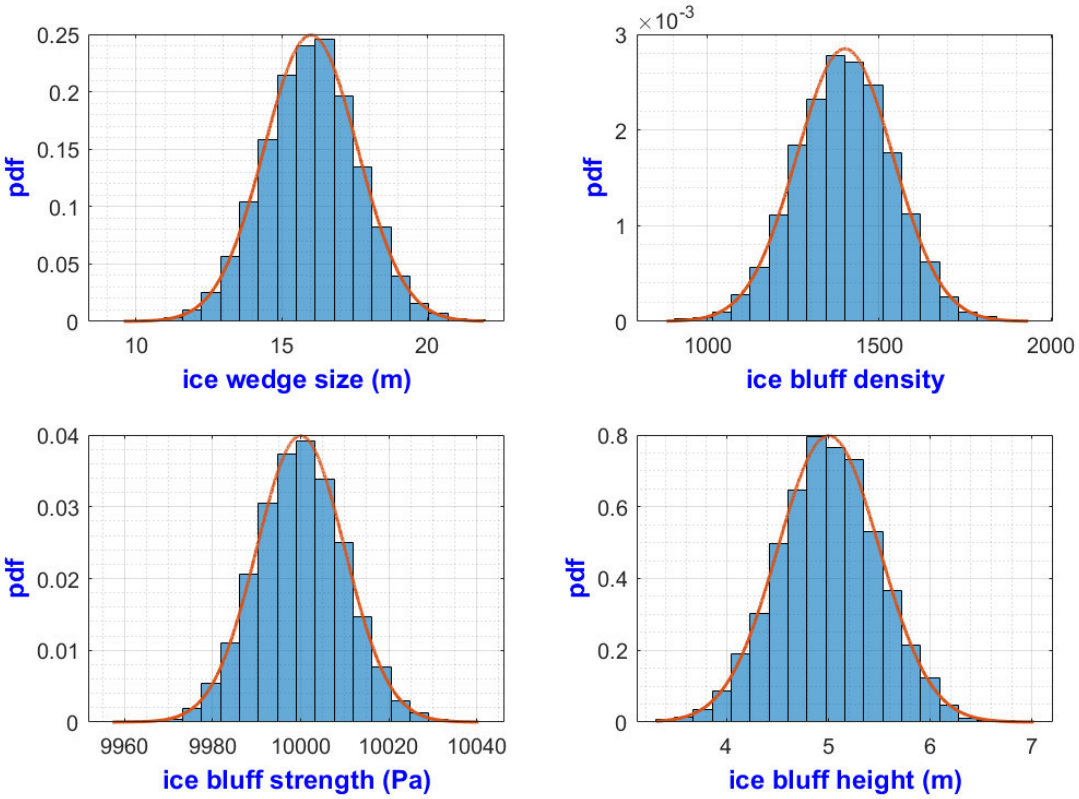

Figure 6-11 Input parameter distribution of the bluff collapse module.

Using the distributions of the parameters, 10,000 sample cases were generated to perform a Monte Carlo simulation. The outcome of the numerical module is the critical niche growth (x_p) which is time independent.

When normal distribution was fitted on the ten thousand output values a mean of critical niche depth was found to be 10.728m. Thomas Ravens used 10m critical niche growth which was obtained from observation in the coast of Alaska, USA (Ravens et al., 2012).

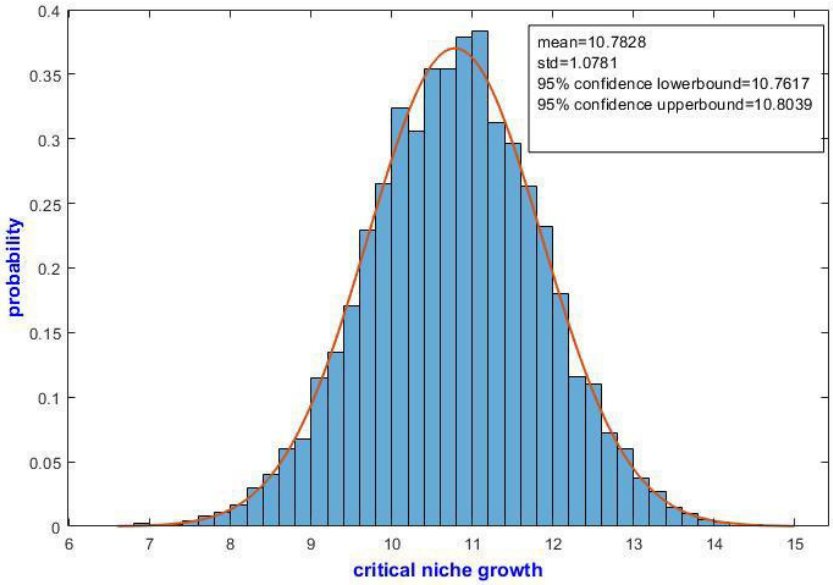

Figure 6-12 Distribution of critical niche growth after 4hr (10,000 cases).

6.1.5 The probability of the bluff collapse

The output of the bluff collapse module is a probabilistic distribution of the critical niche depth (x_p) and output of the niche growth module is a probabilistic distribution of niche growth (x_m). Figure 6-13 demonstrate the progress of x_m and its distribution in hourly intervals. Critical niche depth (x_p) depends on the geometry and physical parameters, hence time independent in Figure 6-13. But distribution of x_m progress towards the right and at one point in time coincides with the distribution of x_p. In a deterministic approach, bluff collapse response is binary; either bluff is stable (0) or collapsed (1). But in probabilistic analysis, failure probability can be estimated as shown in Figure 6-14. It was found that bluff collapse probability (P_f) was close to zero at initial hours of the storm. It is only after 3hour, the probability of collapse starts to increase and after 6 hours from the starting of the storm, the relation became linear.

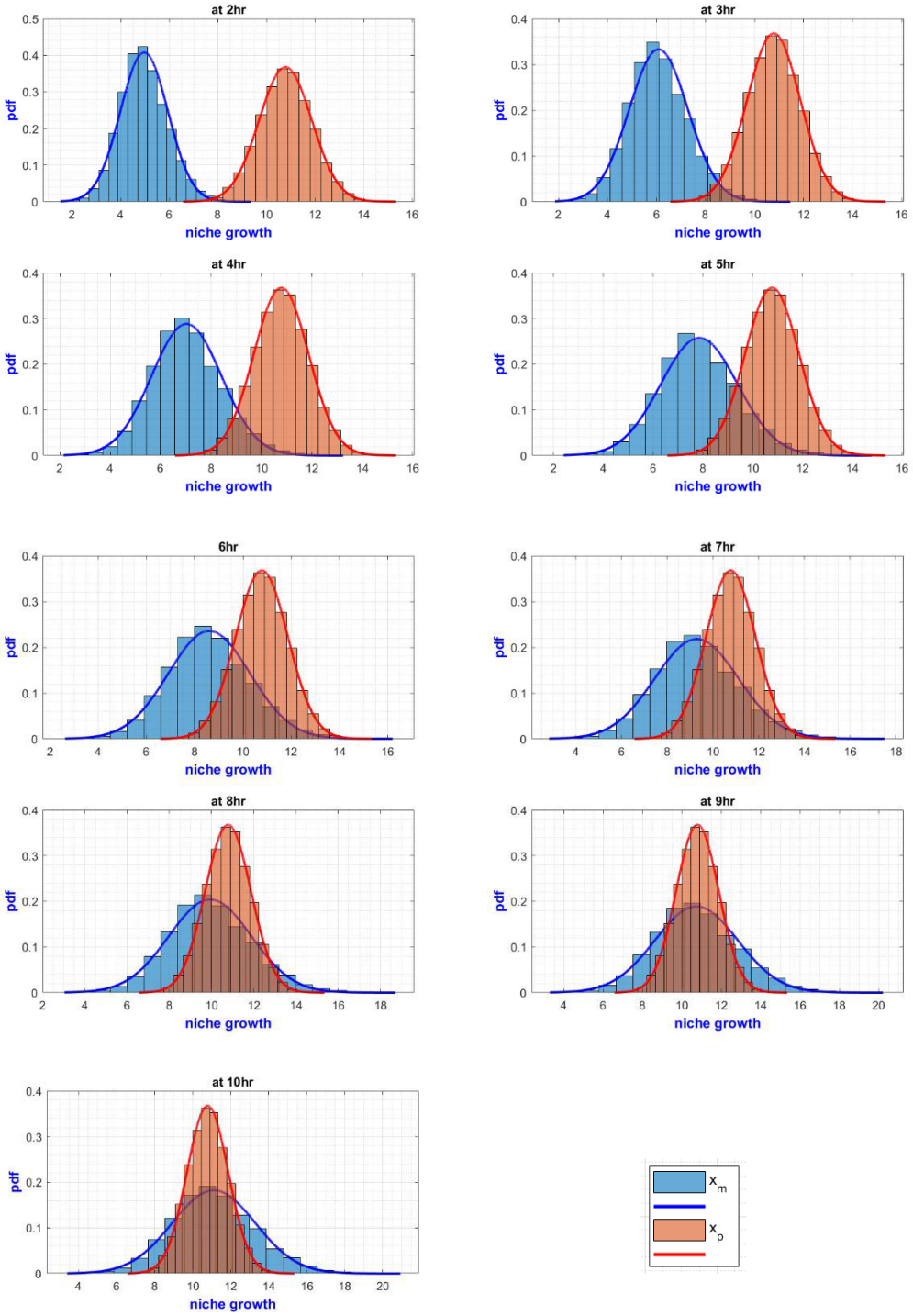

Figure 6-13 Distribution of x_m and x_p at one-hour intervals.

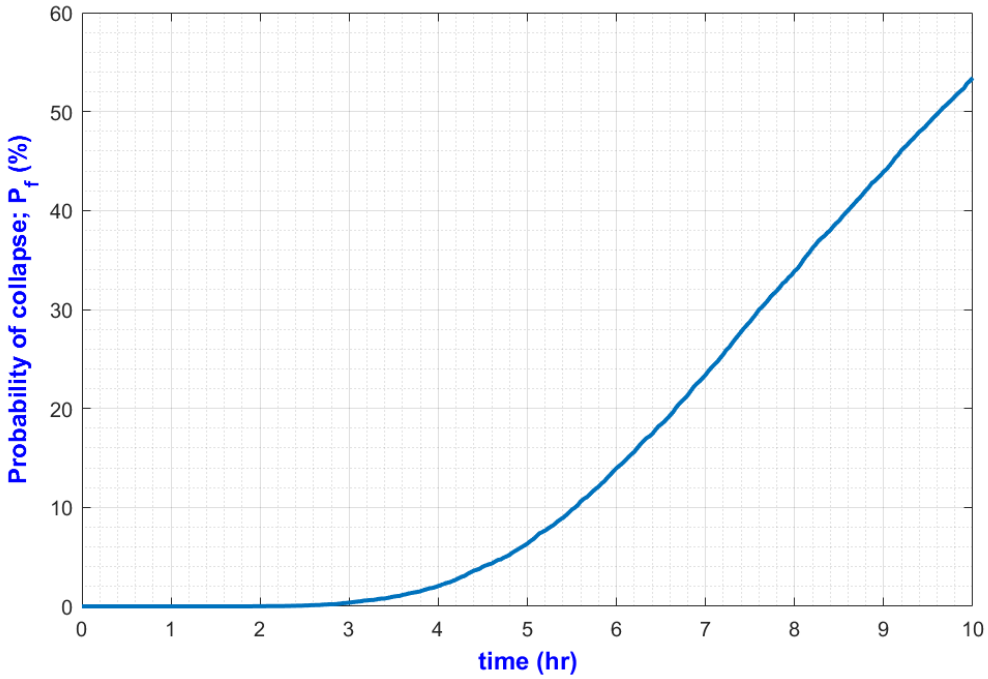

Figure 6-14 Collapse probability during a storm.

The probability of the bluff collapse reached more than 50% after around 9.7 hours. At 10th hour mean value of x_m was found to be 10.82m which is slightly more than mean critical niche depth (x_p) of 10.78m. In the deterministic analysis, it would be considered as collapsed. But probabilistic analysis reveals that collapse probability is only 53.4%.

6.1.6 Summary of the probabilistic sensitivity analysis

Outputs of the probabilistic sensitivity analysis are shown in Table 6-4 which were used as a base case for the deterministic sensitivity analysis.

Table 6-4 Summary of outputs of probabilistic sensitivity analysis

Module	Output	Mean value	Std. Dev.	CoV
Storm surge	h_{id} , inundation depth at the base	0.5352	0.068	12.72%
Niche growth	x_m , niche depth after 4hr time	6.99	1.372	19.63%
Bluff collapse	x_p , critical niche depth	10.78	1.07	9.93%

6.2 Deterministic sensitivity analysis

To understand the behaviour of the model, a deterministic sensitivity analysis was performed. The change of each model outputs is calculated by changing the values of the few important parameters. The procedures adopted for deterministic sensitivity analysis is as follows:

- Mean values determined in the probabilistic analysis was used as a base case; the standard deviation was ignored. Each parameter was varied in the range of ±30% (upper and lower bound). It is highly possible that the temperature of seawater can be 30% more or less from a typical $3°C$ value. But it is highly unlikely, the salinity of the water will change 30% from the typical value of 30 ppt. While performing the sensitivity analysis such probability was not taken into consideration.
- Inter-relation of the parameters was not considered. For example, when the bluff density was changed, all other parameters were kept constant at typical values even though bluff density is related to tensile strength. Since the interaction of the parameters are not known or well established, it was ignored.
- Percentage of change from a typical value was considered. The typical values were chosen based on the area of interest Arctic coast of Russia (see section 5.1.1 on page 59 for details of the location). The change of the parameter was introduced as a percentage of the typical value. The motivation behind to show changes as "percentage" was to place all the cases on the same axis.

6.2.1 The methodology of Sensitivity Analysis

Amid the unknown distributions of the parameters, a deterministic approach can be useful to provide indications of the relative importance of the parameters. The steps followed for sensitivity analysis are as follows:

Step 1: a *base* value of the parameter was determined. If the values were zero (for some cases as initial conditions), the model was transferred to another time and space frame so that percentage of change could be applied. Mean values found in the probabilistic analysis were taken as the base values.

Step 2: Percentage-change for a parameter was considered ±30% from its base value. The following formula was used to record the change as a percentage of the typical value.

$$x(\%) = \frac{Changed\ value - base\ value}{base\ \ value} * 100 \qquad (31)$$

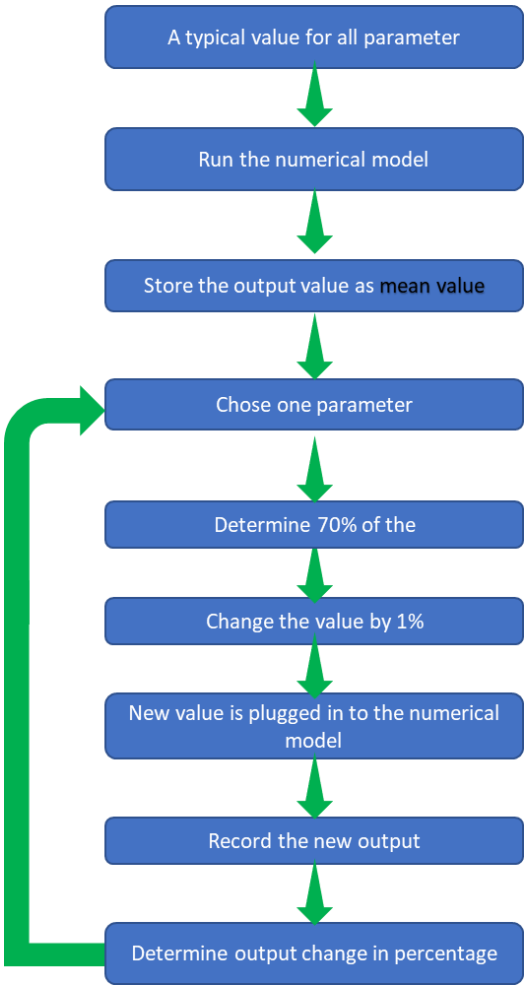

Figure 6-15 Flow chart of deterministic sensitivity analysis.

Step 3: Keeping all the other parameters at the same value, only one parameter at a time was changed and plugged into the numerical model.

Step 4: Each numerical module has one specific output, for example, storm surge module calculates water level at the base of the bluff (h_{id}). For the base case, the response of the module was recorded as *base output*. Then for the y axis, the percentage of change in output was recorded using the following formula:

$$y(\%) = \frac{\text{new response from model} - \text{base output}}{\text{base output}} * 100 \qquad (32)$$

Step 5: Step 4 is repeated in both the directions until a positive 30% change and negative 30% change for one parameter was achieved. Then another parameter was chosen.

A sample MATLAB script is also attached in Appendix E.

6.2.2 Sensitivity Analysis of Storm Surge model

Lower and upper bound of the parameters are shown in Table 6-5. Number of cases considered were 26 and compared with the base values.

Table 6-5 Input parameters for sensitivity analysis of storm surge module

Parameters	Minimum values	Maximum values	Typical values
Wind speed	14	26	20 m/s
Longshore current	1.4	2.6	2m/s
Mean sea level	-1.4	-2.6	-2m

Figure 6-16 depicts the result of a deterministic sensitivity analysis. The following conclusions can be drawn:

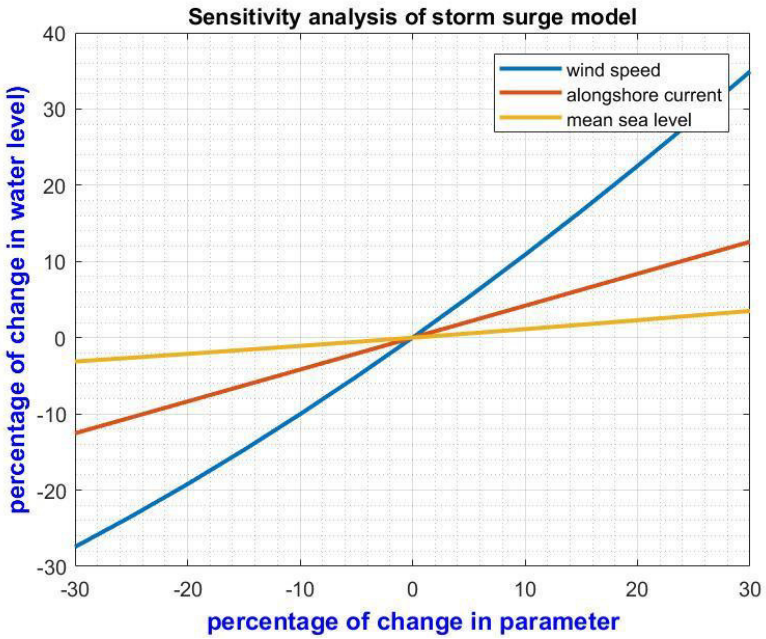

Figure 6-16 Sensitivity analysis (deterministic) of storm surge model.

1) The model is most sensitive to wind speed which indicates the impact of the storm on the thermoabrasion process. The relation between output-input; changes in wind speed and inundation depth (h_{id}) is almost linear. Since the wind speed data is recorded with high accuracy, the storm surge level was determined with reasonable precision.
2) The model is least sensitive to mean sea level. In the storm surge module, the tide was not considered. Most of the high-altitude Arctic coasts exhibits very small tidal range. Since it was found from the sensitivity analysis that numerical module was not responding much to changes in sea levels, ignoring the input of tide is justified.
3) Longshore current, if flowing in opposite direction, may reduce the surge level even further. From the graph, it is clear that the response of the model was not high enough to justify a separate longshore current module or inputs from a global ocean current model.

6.2.3 Sensitivity Analysis of Niche Growth module

Lower and upper bound of the parameter values is shown in Table 6-5. Several numbers of cases were generated and compared with the base values to determine the sensitivity of the module.

Table 6-6 Input parameters for sensitivity analysis of niche growth

Parameters	Minimum values	Maximum values	Typical values
Inundation depth	0.35	0.65	0.5m
Temperature (water)	2.1	3.9	3°C
Sediment concentration (suspended)	0.07	0.13	0.1
Salinity	21	39	30ppt

Figure 6-16 depicts the result of a deterministic analysis. The following conclusions can be drawn:

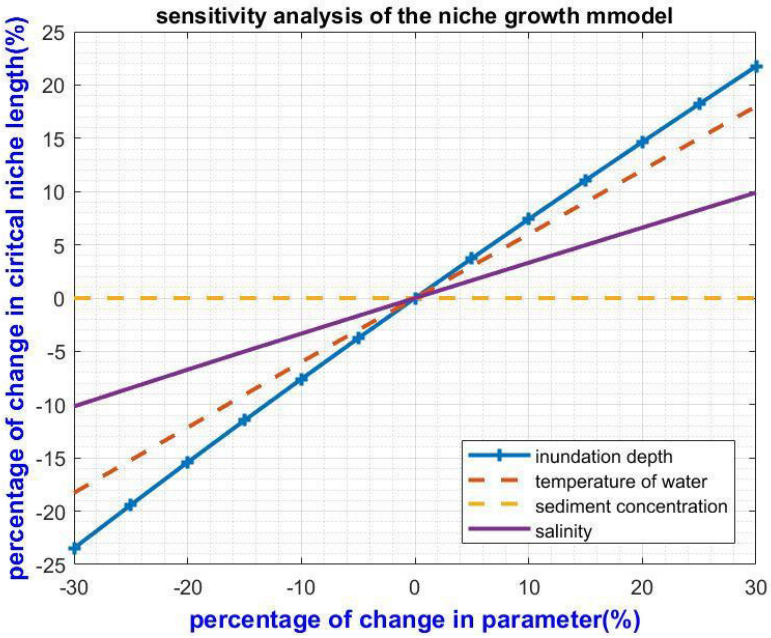

Figure 6-17 Sensitivity analysis of niche growth.

1) Kobayashi formula does not have wave conditions as input for the niche growth. Rather it is assumed that waves are depth limited; inundation depth can represent wave conditions. Sensitivity analysis also confirms that assumption. The numerical model is most sensitive to inundation depth at the base of the bluff.
2) Interestingly, the numerical module was mostly insensitive to sediment concentration at the melting point. Whereas, the salinity at the melting point had an impact on the niche growth.
3) The second most important parameter for the niche growth module is the temperature of the water. Inundation depth indirectly represents mechanical abrasion and temperature of the water represents the thermal activities. Out of the two parameters, inundation depth had a higher impact on the module.

6.2.4 Sensitivity Analysis of Collapse model

Parameters that were considered for the sensitivity analysis of bluff collapse module is given below:

Table 6-7: Inputs of the sensitivity analysis bluff collapse model

Parameters	Minimum values	Maximum values	Typical values
Geometry			
Bluff height	3.5m	6.5m	5m
Ice-wedge size	10.5m	19.7m	15m
Physical properties			
The tensile strength of ice	$7x10^3$	$1.3x10^4$	$1x10^4$
The tensile strength of bluff	$1.4x10^5$	$2.6x10^5$	$2.0x10^5$
Density of bluff	980 (close to pure ice)	1,820(almost ice free)	1,400

65 cases were considered, Figure 6-18 shows the result of the sensitivity analysis. The following observations can be made:

- x_{edge} is the most sensitive parameter. Length of critical niche depth (x_p) responds almost linearly with the change in wedge size (x_{edge}). As expected, as the wedge size increases critical niche depth also increases.
- Critical niche depth is almost insensitive to the tensile strength of bluff. The components of the resisting moments that act against bluff failure are not dependent on tensile strength; rather it depends mostly on bluff height and wedge length (x_{edge}).
- Parameters linked with the geometry of the frozen bluffs are most important. When improving the accuracy of the model, greater effort should be placed on the proper accounts of variation of bluff geometry.

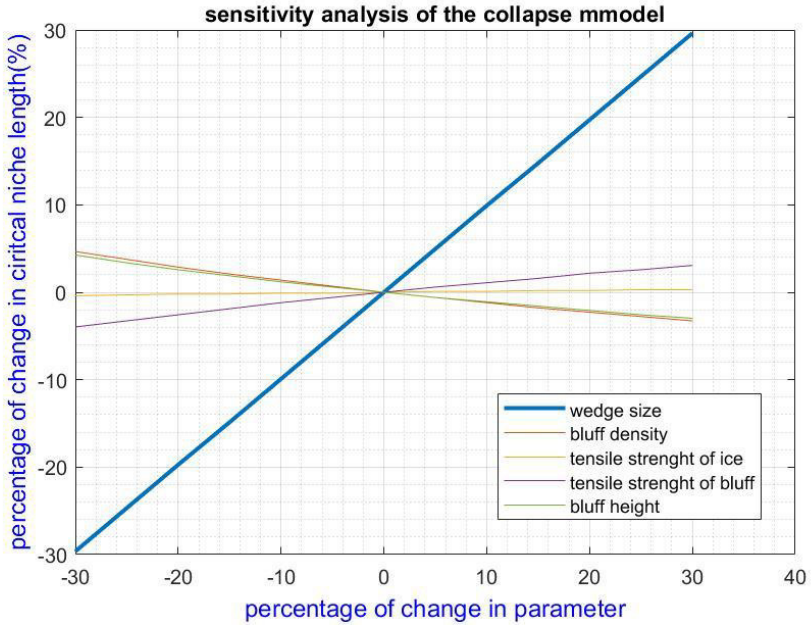

Figure 6-18 Sensitivity analysis of the bluff collapse.

A comparison between wedge size (x_{edge}) with critical niche depth (x_p) is shown in Figure 6-19. The relation is close to linear. As x_{edge} decreases, the critical niche depth (x_p) length also decreases. In this graph, the height of the bluff was kept constant.

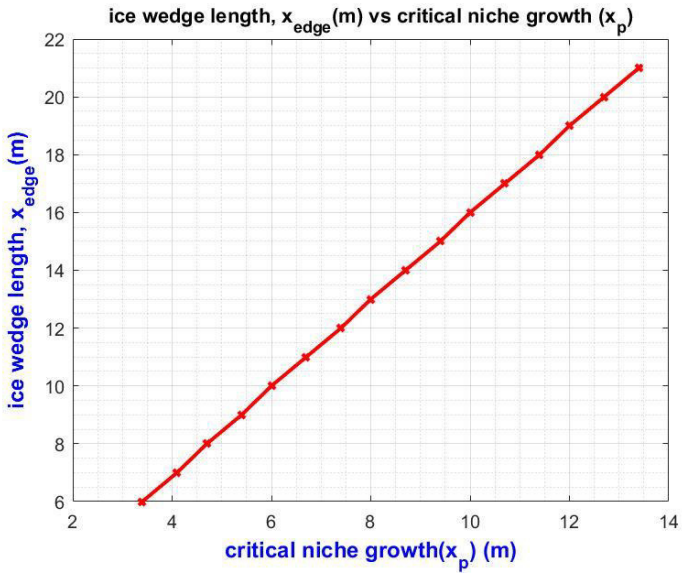

Figure 6-19 x_p and x_{edge} has a linear relation.

7 Conclusion and Recommendation

7.1 Summary

The numerical model developed under the study is an initial tool to predict shoreline erosion. Thermoabrasion erosion was divided into three separate distinguishable processes (storm surge, niche growth and bluff collapse) and separate numerical solutions were prepared for each process. The modules were combined to simulate erosion caused by extreme events like storms.

The model was applied to the Arctic coast of Baydara, Russia and simulation results were found to be in good agreement with field observations. Since the model works in a data poor environment, a proper understanding of the responses of the numerical solutions to varied conditions is important. A sensitivity analysis was performed by changing input parameters to investigate the behaviour of each module.

The findings of the study are summarised below:

- The model performed satisfactorily as a proof of concept. The behaviour of the model is analysed and found to be agreeing with real-world physics.
- Thermoabrasion erosion rate was found to be greatly dependent on wind speed during the storm, inundation depth at the base of the bluff from storm surge and ice wedge polygon size.
- Bluff collapse probability is found dependent more on the geometry than the mechanical strength parameters. The probability of bluff collapse increases linearly during the storm after the initial six hours.
- Water depth at the base of the bluff has the high impact on the rate of niche growth, so a preventive measure for thermoabrasional coastal erosion would be increasing beach level.
- The most extreme event of the year (storm) was found to be contributing most to the thermoabrasional erosion.

7.2 Recommendation for further studies

The numerical model is prone to several limitations (see section1.5), some of which can be solved with greater efforts. Conversion from the 1D model to the 2D model can be the first step. Most of the parameters are considered uniform in the cross direction (z axis) and thus the model cannot capture the variability of the input parameters in a curved shore. The 2D analysis will be able to predict erosion with more certainty.

Numerical scheme used in the study is mostly Explicit Euler which is first order accurate scheme. To attain more accuracy and better stability, numerical schemes should be modified to a higher order scheme. To develop a comprehensive model to predict long-term shoreline changes, both thermodenundation and thermoabrasion processes should be included.

8 Reference

ANISIMOV, O. & RENEVA, S. 2006. Permafrost and changing climate: The Russian perspective.

ARE , F. E. 1988. Thermal Abrasion of Sea Coasts. *Polar Geography and Geology,* 12.

BARNHART, K. R., ANDERSON, R. S., OVEREEM, I., WOBUS, C., CLOW, G. D. & URBAN, F. E. 2014. Modeling erosion of ice-rich permafrost bluffs along the Alaskan Beaufort Sea coast. *Journal of Geophysical Research: Earth Surface,* 119**,** 1155-1179.

BRUNSDEN, D. 2002. Geomorphological roulette for engineers and planners: some insights into an old game. *Quarterly Journal of Engineering Geology and Hydrogeology,* 35(2): 101-142.

BRUNSDEN, D. & LEE, E. M. 2004. Behaviour of Coastal landslide systems: an interdisciplinary view. *Zeitschrift für Geomorphologie N.F.,* 134.

CARSLAW, H. S. 1959. *Conduction of heat in solids,* Oxford, Clarendon Press.

DEAN, R. G. & DALRYMPLE, R. A. 2004. *COASTAL PROCESSES with Engineering Applications*.

FIONA, H. 2013. 1.5C rise in temperature enough to start permafrost melt, scientists warn. *In:* FIONA, H. (ed.).

FREDERICK, J., THOMAS, M., L. BULL, D., JONES, C. & ROBERTS, J. 2016. *The Arctic coastal erosion problem*.

GUÉGAN , E. 2015. *Erosion of permafrost affected coasts: rates, mechanisms and modelling* PhD Thesis.

GÜNTHER, F., OVERDUIN, P., SANDAKOV, A., GROSSE, G. & GRIGORIEV, M. 2013. Short- and long-term thermo-erosion of ice-rich permafrost coasts in the Laptev Sea region. *Biogeosciences,* 10**,** 4297.

ISAEV, V., POGORELOV, A., AMANGUROV, R., KOMAROV, O., GORSHKOV, E., BELOVA, N., ALEKSYUTINA, D. & KOKIN, O. 2017. *Field investigation and laboratory analyses; Baydaratskaya bay 2017*.

JOSBERGER, E. G. & MARTIN, S. 1981. A laboratory and theoretical study of the boundary layer adjacent to a vertical melting ice wall in salt water. *J. Fluid Mech.,* 111**,** 439-473.

KNIGHT, N. 2017. *Study Shows Massive Global Permafrost Melt Underway While Trump Mentions Climate Not Once* [Online]. Available: https://www.commondreams.org/news/2017/03/01/study-shows-massive-global-permafrost-melt-underway-while-trump-mentions-climate-not [Accessed 3 July 2018].

KOBAYASHI, N. 1985. Formation of thermoerosional niches into frozen bluffs due to storm surges on the Beaufort Sea coast. *Journal of Geophysical Research: Oceans,* 90**,** 11983-11988.

KOBAYASHI, N. & AKTAN, D. 1986. Thermoerosion of Frozen Sediment Under Wave Action. *Journal of Waterway, Port, Coastal, and Ocean Engineering,* 112**,** 140-158.

KULKARNI, R. R. 2013. *Numerical Modelling of Coastal Erosion using MIKE21.* MS, Norwegian University of Science and Technology.

LANTUIT, H., ATKINSON, D., PAUL OVERDUIN, P., GRIGORIEV, M., RACHOLD, V., GROSSE, G. & HUBBERTEN, H.-W. 2011. Coastal erosion dynamics on the permafrost-dominated Bykovsky Peninsula, north Siberia, 1951–2006. *Polar Research,* 30**,** 7341.

LARSEN, J. N., ANISIMOV, O., FEDERATION, R. & HODGSON, D. 2014. Climate Change 2014: Impacts, Adaptation, and Vulnerability. Part A: Global and Sectoral Aspects. Contribution of Working Group II to the Fifth Assessment Report of the Intergovernmental Panel on Climate Change Cambridge, UK: Cambridge University Press. .

LAWRENCE, D. 2008. Permafrost threatened by rapid retreat of arctic sea ice.

LONGUET-HIGGINS 1970. Longshore currents generated by obliquely incident sea waves: 1. *Journal of Geophysical Research,* 75**,** 6778-6789.

NAIRN, R. B., SOLOMON, S. M., KOBAYASHI, N. & VIDRINE, J. 1998. Development and Testing of a Thermal-Mechanical Numerical Model for Predicting Arctic Shore Erosion Processes. *PERMAFROST - Seventh International Conference.*

ODISHARIA, G. E., TSVETSINSKY, A. S., MIKHAILOV, N. N. & & DUBIKOV, G. I. 1997. Specialized information system on environment of Yamal Peninsula and Baydaratskaya Bay. *Proceedings of Inrernational Offshore and Polar Engineering Conferense (ISOPE-97)***,** 574-581.

OSTENDORF, D. W. 1982. Longshore dispersion over a flat beach. *Journal of Geophysical Research: Oceans,* 87**,** 4241-4248.

OSTERKAMP, T. E. & BURN, C. R. 2015. CRYOSPHERE | Permafrost. *In:* NORTH, G. R., PYLE, J. & ZHANG, F. (eds.) *Encyclopedia of Atmospheric Sciences (Second Edition).* Oxford: Academic Press.

OVEREEM, I., ANDERSON, R. S., WOBUS, C. W., CLOW, G. D., URBAN, F. E. & MATELL, N. 2011. Sea ice loss enhances wave action at the Arctic coast. *Geophysical Research Letters,* 38**,** n/a-n/a.

PEARSON, S. G. 2015. Erosion in the Arctic: A Coastal Engineering Perspective. Norwegian University of Science and Technology.

PEARSON, S. G., LUBBAD, R., LE, T. M. H. & NAIRN, R. B. 2016. Thermomechanical erosion modelling of Baydaratskaya Bay, Russia with COSMOS. *Scour and Erosion.* CRC Press.

PROWSE, T., FURGAL, C., CHOUINARD, R., MELLING, H., MILBURN, D. & SMITH, S. L. 2009. Implications of climate change for economic development in northern Canada: energy, resource, and transportation sectors. *Ambio,* 38(5)**,** 272–281.

RAVENS, T., JONES, B., ZHANG, J., ARP, C. & SCHMUTZ, J. 2012. Process-Based Coastal Erosion Modeling for Drew Point, North Slope, Alaska. *Journal of Waterway, Port, Coastal, and Ocean Engineering,* 138**,** 122-130.

SILVESTRI, S., GASPARINI, G., TROMBETTI, T. & CECCOLI, C. 2008. Statistical analysis towards the identification of accurate probability distribution models for the compressive strength of concrete. *14th World Conference on Earthquake Engineering.* Beijing, China.

THOMAS, H. R., CLEALL, P., LI, Y. C., HARRIS, C. & KERN-LUETSCHG, M. 2009. Modelling of cryogenic processes in permafrost and seasonally frozen soils. *Géotechnique,* 59**,** 173-184.

WIKIPEDIA. 2018. *Permafrost* [Online]. Available: https://en.wikipedia.org/wiki/Permafrost [Accessed 15 May 2018].

ZIJLEMA, M. 2017. lecture notes for the Course CIE4340 Computational Modelling of Flow and Transport, TU delft. Netherlands. TU Delft.

Appendix

Appendix A. Storm Surge Module scripts

Required inputs

The script reads from the 'bath.dat' file. The file has to be in the same directory. 'bath.dat' file is generated from a 'csv' or comma separated value format file. Origin of the co-ordinates for the bathymetry can be referenced to section 5.2.
Note that some line of the scripts is 'commented out'. All the units are in meter-kg-N format.

Some parameters are declared within script rather than asked as inputs. The values of such parameters are taken as standard value.

```
%this script will read the bathymetry txt file
clear all;
%global parameters
g=9.81;

%read from bath.dat file
filename = 'bath.dat';
M=csvread(filename,1,0);%this will read from row 2
% plot(M(:,1),M(:,2))
% hold on;
%this will print first column ( in x axis) vs the second column of
the matrix
% now we need to interpolate between the values so that PDE can work
deep_sea=20000; % this will
dx=10;
xq=0:dx:deep_sea;


%this will be my grid points
vq1 = interp1(M(:,1),M(:,2),xq); %vq1 id the bathmetric values, xq
is the x axis

% we need water depth at every points
sealevel=-8;%water level at MSL, pre-storm condition
g_points=numel(vq1);

for j=1:1:g_points
    MSL(j)=sealevel;
    if abs(vq1(j))<abs(sealevel)
        h(j)=0;
```

```
    else
        h(j)=-vq1(j)+sealevel;
        MSL(j)=sealevel;
    end
end



% inputs for wind shear stress

k=1.2e-6; % this is the drag coefficient
pw=1025; % density of water
U=32; % wind speed [ may be we can read it from input file]
Twx=pw*g*k*U^2;
termA=Twx/(g*pw);
%inputs for long shore
omega=7.29e-5;
latitude=68;
f=2*omega*sin(latitude*3.14/180);% we need to change the degree to
radian
V=3; % this is the longshore current
termB=f*V/g;
n(g_points)=0;
start=100;
test(1)=0;
test2(g_points)=0;

% now we use the numerical solution of the storm surge equation


for i=g_points:-1:2

        n(i-1)=termA*dx/(h(i)+n(i))+termB*dx+n(i);

end

storm_level=sealevel+n;
figure


ax1=subplot(1,1,1)
plot(ax1,xq,MSL,'b--','linewidth',1)
hold on;

plot(ax1,xq,storm_level,'r-','linewidth',1)
hold on;

grid minor;
```

```
y_target='meter';
title('Storm surge level')
xlabel('meter','FontSize',12,'FontWeight','bold','Color','b')
ylabel(y_target,'FontSize',12,'FontWeight','bold','Color','b')
legend({'MSL','Bed Profile','storm surge
level'},'Location','northeast')

ylim([-11 1])
```

Appendix B. Niche growth module

Below is the flow chart showing how to calculate the niche growth depth (x_m):

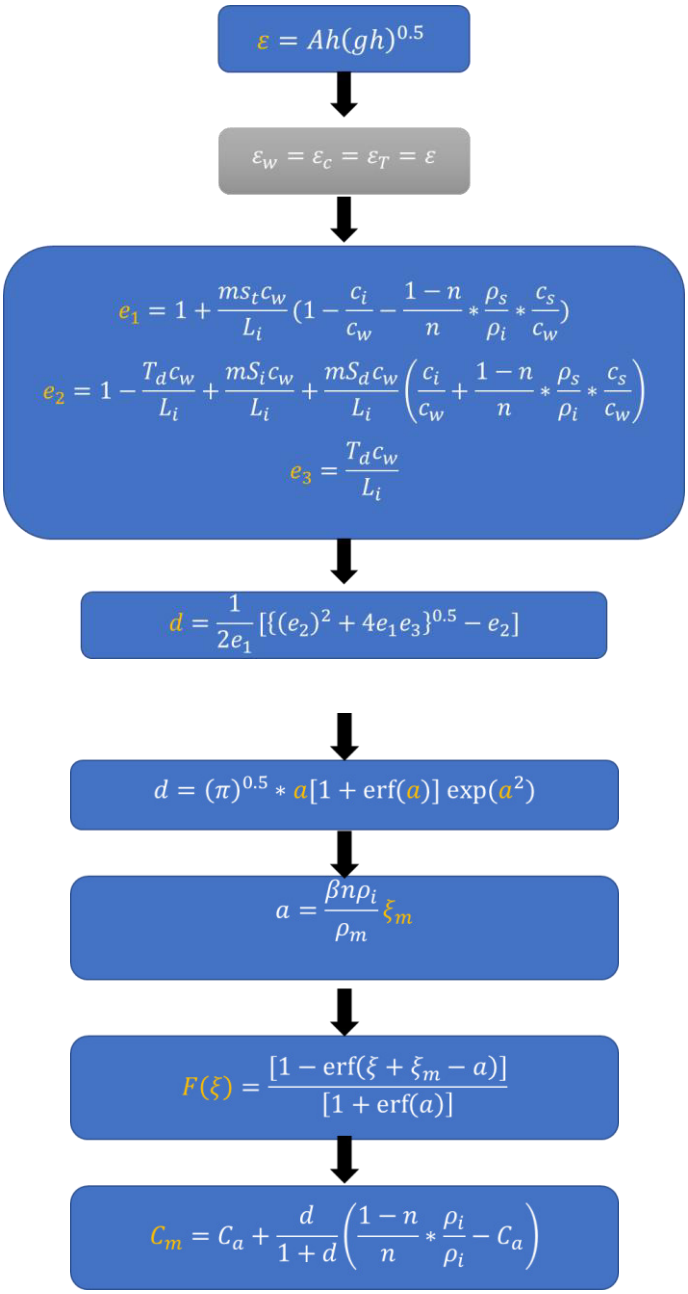

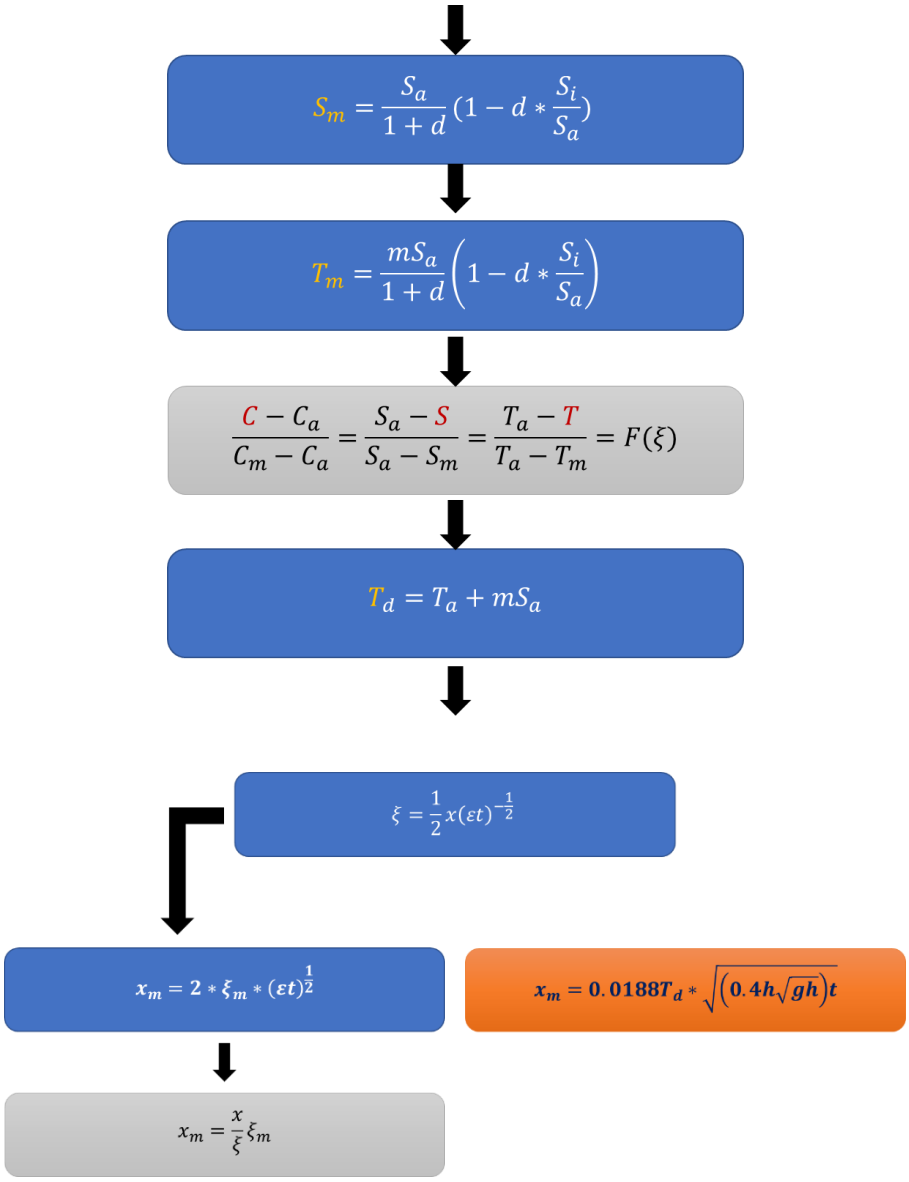

A sample MATLAB script is provided below

```
function [x,y,z]=niche_growth(T_a)

%global parameter
g=9.81;

t_in=0;
t_out=10*3600;
```

```
%initial condition
S_i=0.00; %ice salinity
n=0.4; % porosity
p_i=916; %density of ice
p_s=2650; %desnity of sediments
p_w=1010; %desnity of water
c_s=837.4; %specific heat of suspended sediments
c_w=4187; %specific heat of water in jkg/k
c_i=2108; %specific heat of ice jkg/k
L_i=334000; %latent heat of ice
% this will be constants. physical properties will be same for all
location

%assumption for initial conditions
C_a=0; %initial suspended sediment concentration
S_a=30/1000; %salinity of the incoming sea water ; unit per PPT
m=0.06*1000; % Josberger constant

%assumption related to geometry
beta=2;
% T_a=3; % this is also assumed
h=0.5; % this is kept constant for now. h should vary along x
A=0.4; % given by Inman

epsilon=A*h*(g*h)^0.5;
T_d=T_a+m*S_a;

%determining value of d
E1=1+m*S_i*c_w/L_i*(1-c_i/c_w-(1-n)/n*p_s/p_i*c_s/c_i);
%E1 value should be close to 1
E2=1-T_d*c_w/L_i+m*S_i*c_w/L_i+m*S_a*c_w/L_i*(c_i/c_w+(1-
n)/n*p_s/p_i*c_s/c_w);
% E2 value should be close to 1
E3=T_d*c_w/L_i; %E3 should be significantly smaller than 1

d=1/2/E1*((E2^2+4*E1*E3)^0.5-E2); %d values should be close to E3

a_all=0:0.01:0.3;
d_all=pi^0.5*a_all.*(1+erf(a_all)).*exp(a_all.^2);
a=interp1(d_all,a_all,d);


%solver is not working
% syms a;
% eqn=pi^0.5*a.*(1+erf(a)).*exp(a.^2)==d;
%  a_s=solve(eqn,a)


xi_m=a*p_w/beta/n/p_i;
```

```
%time will start from 0 to 20 hour
t=t_in:30:t_out;

%calculated x_m
xm_real=2*xi_m*sqrt(epsilon*t);
% y=E1;
% x=t/3600;
x=t/3600;
y=d;
z=xm_real;
end
```

Appendix C. Bluff Collapse Numerical Schematization

The script below is a function. Inputs parameter are:

X_edge= wedge size. Standard values is 15m.

p_b= density of the bluff. With 30% sediment concentration, typical value is 1400 kg/m^3

T_ice=tensile strength of ice. Typical values of the strength are $1x10^4 N/m^2$

T_b= tensile strength of bluff. Typical values are close to $2x10^5 N/m^2$

Z_top=bluff height. Typical values ranging from 3.5~5 meter. In the site Baydara Russia; typical value is 5m.

The function will return critical niche growth in meter.

```
=====================================================
function y=collapse(x_edge,p_b,T_ice,T_b,z_top)

%global parameter
g=9.81;
%
% % physical properties of the system if unsure of the parameter
values
% p_b=1400; % density of frozen bluffs. in kg/m3
% T_ice=1e4;
% T_b=2e5;

%geomtry
% z_top=5; %height of the frozen bluff
z_p=0; % niche point
i=0;
counter=0;
func1=@(x)x_p-x;
i=0;

for x_p=0:.01:x_edge
```

```
    i=i+1;
    counter(i)=i+1;
    func1=@(x)x_p-x;
    z=integral(func1,0,x_p);
    T_d(i)=p_b*g*(z_top-z_p)*z;
    T_r(i)=0.5*p_b*g*(z_top-z_p)*((x_p-x_edge)).^2;
    T_i(i)=T_ice*(x_edge-x_p)*(z_top-z_p);
    T_f(i)=T_b*integral(func1,x_edge,x_p);
    Result(i)=T_r(i)+T_i(i)+T_f(i)-T_d(i);
    if Result(i)<0
        break;
    end
end

y=x_p;
end
```

Appendix D. Model Run

Calibration parameters

Two calibration parameters were introduced to fit the progress of erosion with field measurements. Three numerical modules exchange inputs in between them and these calibration parameters influence the interactions. As shown in the Figure 8-1, two calibration parameters *alpha* (α) and *beta* (β) are introduced between the interaction of the modules.

Calibration parameter *alpha* works between the interaction of storm surge module and inundation depth at the base of the bluff. Another parameter *beta* determines the erosion rate from niche growth rate and critical niche depth.

Table 8-1 calibration parameters

Calibration parameter	Target	Physical interpretation
Alpha (α)	Control parameter for storm surge and niche growth module interaction	Controls when and where niche growth module will be triggered.
Beta (β)	Interaction between Bluff collapse-niche growth modules	Converts critical niche depth and niche growth module to erosion rate

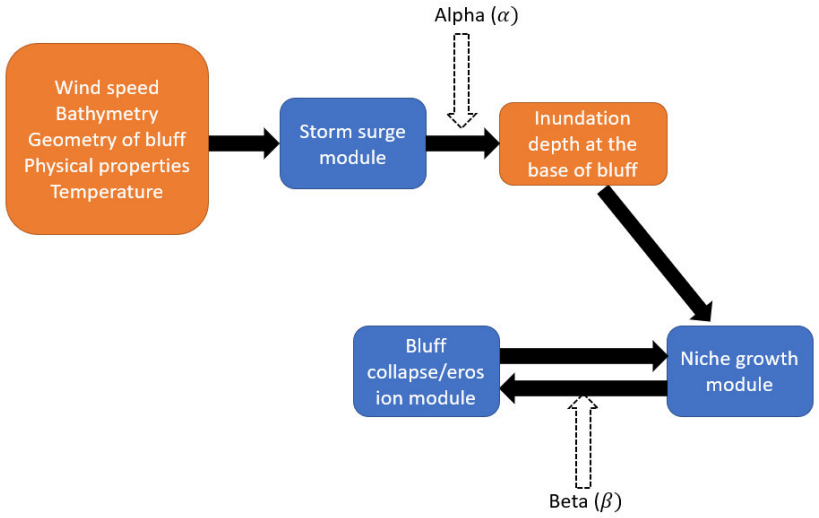

Figure 8-1 Introduction of the calibration parameters at the interaction between modules.

The following formula is used for the *beta* parameter:

$$beta\ (\beta) = \frac{3}{mean\ critical\ niche\ growth\ x\ mean\ bluff\ wedge\ size\ (x_{edge})}$$

where the mean is the mean of the parameter fitted to normal distribution (not algebraic mean).

Matlab script

```
%required inputs
%geomtry
sample=1000;
z_top=(randn(sample,1) * 0.5 ) + 5; %height of the ice bluff
x_edge=(randn(sample,1) * 2 ) + 14; % width of typical ice wedge
dt=600; % time step , by default it is 10 min
beach_level=0;
%temperature of the wave
T_a=(randn(sample,1) * 0.3 ) + 3;

%calibration parameter

MSL=-.28;

z_p=0;

% physical properties of the system
p_b=1400; % density of ice bluffs. in kg/m3
T_ice=1e4;% tensile strenght of ice
T_b=2e5;% tensile strength of bluff
%wind speed
% U will be a time series

[tq Uq]=f_wind(dt);
%now wind data is gathered- time in tq and values in Uq

tq_timer=numel(tq);% we take number of time the program should run
%for every tq values we need storm surge level
n=1:1:tq_timer;%declaring variable
h=n;%initial condition
for i=1:1:tq_timer
    n(i)=MSL+f_storm(Uq(i));
end


%%

%at this point we have time step values (tq), corresponding wind
speed(Uq)
%and storm surge level(n)

% we need to decide whether storm surge level is critical or not
% we only run niche growth model if the water level is positive
```

```
% that means n values has to be greater than 0, otherwise niche
growth
% model will not triggered

%we need to convert n values to water depth at base h

for i=1:1:tq_timer
    if n(i)<0
        h(i)=0;
    else
        h(i)=n(i);
    end
end
figure

ax1=subplot(3,1,1)
plot(tq/3600/24 ,Uq)
grid on;
grid minor;
xlabel('time (day)','FontSize',12,'FontWeight','bold','Color','b')
ylabel('wind speed
(m/s)','FontSize',12,'FontWeight','bold','Color','b')
xlim([0 365])

ax2=subplot(3,1,2)
plot(tq/3600/24 ,n+2)
grid on;
grid minor;
xlabel('time (day)','FontSize',12,'FontWeight','bold','Color','b')
ylabel('surge
level(m)','FontSize',12,'FontWeight','bold','Color','b')
xlim([0 365])

ax3=subplot(3,1,3)
plot(tq/3600/24 ,h)
grid on;
grid minor;
xlabel('time (day)','FontSize',12,'FontWeight','bold','Color','b')
ylabel('inundation depth
(m)','FontSize',12,'FontWeight','bold','Color','b')
xlim([0 365])

%%

i=1;
x_m(1)=0;
x_critical=1:1:sample;
for i=1:1:sample
    x_critical(i)=critical_niche(x_edge(i),p_b,T_ice,T_b,z_top(i));
end
```

```
x_critical_mean=normfit(x_critical);

%%
beta=3/(x_critical_mean*x_edge);
x_m(tq_timer,sample)=0.00;
y(sample)=0;
for j=1:1:sample
    y(1,j)=0;

    for i=1:1:(tq_timer-1)
           x_m(i+1,j)=f_niche_growth(T_a(j),h(i),tq(i),tq(i+1));
        x_m(2,j)=0;

    end
x_m(2,j)=0;
y=cumsum(x_m);

end
%%

t_day=tq/3600/24;



%%

figure
h1=subplot(4,1,4)

for i=1:1:sample

   h2a=plot(t_day,y(:,i),'-b', 'LineWidth',1);
   h2a.Color(4)=0.01;
   hold on,
      end

for i=1:1:52555
    [value sigma]=normfit(y(i,:));
   mean_1(i)=value;
end
plot(t_day,mean_1, '--y','linewidth',1)


grid on;
grid minor;
xlabel('time (day)')
ylabel('erosion (m)')
xlim([0 365])
```

```
ax2=subplot(4,1,1)
plot(t_day,Uq,'linewidth',0.5)
grid on;
grid minor;

xlabel('time (day)')
ylabel('wind speed')
xlim([0 365])

ax3=subplot(4,1,3)
plot(t_day,h,'linewidth',1)
grid on;
grid minor;
ylabel('inundation depth')
xlim([0 365])


ax2=subplot(4,1,2)
plot(tq/3600/24 ,n+2)
grid on;
grid minor;
ylabel('surge level(m)')
xlim([0 365])


%%

figure
ax1=subplot(2,1,1)
result_B=sort(y(52500,:));
histogram(result_B,30,'Normalization','pdf')
hold on,
[mean, std,mean95,std95]=normfit(result_B,0.05);
dim=[0.7,.8,0.2,0.1];
str={strcat('mean=', num2str(mean)),strcat('std=', num2str(std))};
annotation('textbox',dim,'String',str)
f = exp(-(result_B-mean).^2./(2*std^2))./(std*sqrt(2*pi));
plot(result_B,f,'LineWidth',1.5)
xlabel('shore erosion
(m)','FontSize',12,'FontWeight','bold','Color','b')
ylabel('pdf','FontSize',12,'FontWeight','bold','Color','b')

ax1=subplot(2,1,2)
normplot(result_B)
xlabel('shore erosion
(m)','FontSize',12,'FontWeight','bold','Color','b')
ylabel('probability','FontSize',12,'FontWeight','bold','Color','b')
```

Appendix E. Sensitivity Analysis

This script returns the sensitivity analysis of the bluff collapse model. It requires another function to determine the stability. The function is also provided below. The output is the sensitivity analysis based on output parameter critical niche growth.

Typical value of the numerical model is provided as comments. Explanation of the parameters are same as mentioned in the appendix Appendix C.

Deterministic sensitivity analysis

```
clear all;
critical=sens_col(15,1400,1e4,2e5,5);

alpha=0.7:0.05:1.3;
counter=size(alpha);
i=0;
%x_edge
for i=0:1:(counter(2)-1)
    i=i+1;
    x_axis(i)=(alpha(i)-alpha(7))*100;
    critical2(i)=sens_col(15*alpha(i),1400,1e4,2e5,5);
    percent(i)=(critical2(i)-critical)/critical*100;
    target(i)=i;
end
plot(x_axis,percent,'linewidth',2)
hold on;
%p_b
for i=0:1:(counter(2)-1)
    i=i+1;
    critical2(i)=sens_col(15,1400*alpha(i),1e4,2e5,5);
    percent(i)=(critical2(i)-critical)/critical*100;
    target(i)=i;
end
plot(x_axis,percent,'bo')
hold on;
% T_ice
for i=0:1:(counter(2)-1)
    i=i+1;
    x_axis(i)=(alpha(i)-alpha(7))*100;
    critical2(i)=sens_col(15,1400,1e4*alpha(i),2e5,5);
    percent(i)=(critical2(i)-critical)/critical*100;
    target(i)=i;
end
plot(x_axis,percent,'-')
hold on;
```

```
%T_b
for i=0:1:(counter(2)-1)
    i=i+1;
    x_axis(i)=(alpha(i)-alpha(7))*100;
    critical2(i)=sens_col(15,1400,1e4,2e5*alpha(i),5);
    percent(i)=(critical2(i)-critical)/critical*100;
    target(i)=i;
end
plot(x_axis,percent)
hold on;
%bluff height
for i=0:1:(counter(2)-1)
    i=i+1;
    x_axis(i)=(alpha(i)-alpha(7))*100;
    critical2(i)=sens_col(15,1400,1e4,2e5,5*alpha(i));
    percent(i)=(critical2(i)-critical)/critical*100;
    target(i)=i;
end
plot(x_axis,percent)
hold on;
grid on;
grid minor;
y_target='percentage of change in ciritcal niche length(%)';
title('sensitivity analysis of the collapse mmodel')
xlabel('percentage of change in
parameter','FontSize',12,'FontWeight','bold','Color','b')
ylabel(y_target,'FontSize',12,'FontWeight','bold','Color','b')
legend({'wedge size','bluff density','tensile strenght of
ice','tensile strenght of bluff','bluff
height'},'Location','northeast')
xlim([-30 30])
```

this script is calling a function for few hundred times. The function "*sense_col*" is as follows:

```
%this function returns the critical niche depth
function y=collapse(x_edge,p_b,T_ice,T_b,z_top)

%global parameter
g=9.81;
% typical values of the required inputs are given below
% % physical properties of the system
% p_b=1400; % density of frozen bluffs. in kg/m3
% T_ice=1e4;
% T_b=2e5;

%geomtry
% z_top=5; %height of the frozen bluff
z_p=0; % niche point
i=0;
counter=0;
func1=@(x)x_p-x;
```

```
i=0;

for x_p=0:.001:x_edge
    i=i+1;
    counter(i)=i+1;
    func1=@(x)x_p-x;
    z=integral(func1,0,x_p);
    T_d(i)=p_b*g*(z_top-z_p)*z;
    T_r(i)=0.5*p_b*g*(z_top-z_p)*((x_p-x_edge)).^2;
    T_i(i)=T_ice*(x_edge-x_p)*(z_top-z_p);
    T_f(i)=T_b*integral(func1,x_edge,x_p);
    Result(i)=T_r(i)+T_i(i)+T_f(i)-T_d(i);
    if Result(i)<0
        break;
    end
end
y=x_p;
end
```

Probabilistic sensitivity analysis

```
n=10000;
x_edge= randn(n,1)*1.6+16; %mean 16, std 1.6
s_x_edge=sort(x_edge);
norm1=normpdf(s_x_edge,16,1.6);

p_b=(randn(n,1) * 140 ) + 1400; %mean 1400, std 140
s_p_b=sort(p_b);
norm2=normpdf(s_p_b,1400,140);

m=1e4;
v=100;
mu=log((m^2)/sqrt(v+m^2));
sigma=sqrt(log(v/(m^2)+1));
T_ice=lognrnd(mu,sigma,1,n); %mean 1e4, std 1e2
s_T_ice=sort(T_ice);
norm3=lognpdf(s_T_ice,mu,sigma);

m=2e5;
v=200;
mu=log((m^2)/sqrt(v+m^2));
sigma=sqrt(log(v/(m^2)+1));
T_b=lognrnd(mu,sigma,1,n);  %mean 1e5, std 2e3
s_T_b=sort(T_b);
norm4=lognpdf(s_T_b,mu,sigma);


z_top=(randn(n,1) * 0.5 ) + 5;
s_z_top=sort(z_top);
```

```
norm5=normpdf(s_z_top,5,0.5);

figure
title('Distribution of the input parameters')
ax1=subplot(2,2,1)
histogram(s_x_edge,20,'Normalization','pdf')
hold on,
plot(s_x_edge,norm1,'linewidth',1.5)
grid on;
grid minor;
% title('critical niche depth for various ice wedge sizes')
xlabel('ice wedge size
(m)','FontSize',12,'FontWeight','bold','Color','b')
ylabel('Probability','FontSize',12,'FontWeight','bold','Color','b')
% legend({'wedge size'},'Location','northeast')

ax2=subplot(2,2,2)
histogram(s_p_b,20,'Normalization','pdf')
hold on,
plot(s_p_b,norm2,'linewidth',1.5)
grid on;
grid minor;
% title('critical niche depth for various frozen bluff density')
xlabel('frozen bluff
density','FontSize',12,'FontWeight','bold','Color','b')
ylabel('Probability','FontSize',12,'FontWeight','bold','Color','b')

ax3=subplot(2,2,3)
histogram(T_ice,20,'Normalization','pdf')
hold on,
plot(s_T_ice,norm3,'linewidth',1)
grid on;
grid minor;
% title('ciritical niche depth for various frozen bluff strength')
xlabel('frozen bluff strength
(Pa)','FontSize',12,'FontWeight','bold','Color','b')
ylabel('Probability','FontSize',12,'FontWeight','bold','Color','b')

ax4=subplot(2,2,4)
histogram(s_z_top,20,'Normalization','pdf')
hold on,
plot(s_z_top,norm5,'linewidth',1)
grid on;
grid minor;
% title('ciritical niche depth for various frozen bluff height')
xlabel('frozen bluff height
(m)','FontSize',12,'FontWeight','bold','Color','b')
ylabel('Probability','FontSize',12,'FontWeight','bold','Color','b')
```

```
for i=1:1:n

result(i)=critical_niche(x_edge(i),p_b(i),T_ice(i),T_b(i),z_top(i));

end
 figure;
% normplot(y);
% y_mean = mean(result)
% y_std = std(result)

h1=subplot(1,1,1)

zx=tabulate(result);
result_B=sort(result);
histogram(result_B,'Normalization','pdf')
hold on,
[mean, std,mean95,std95]=normfit(result_B,0.05);
dim=[0.6,.7,0.3,0.2];
str={strcat('mean=', num2str(mean)),strcat('std=',
num2str(std)),strcat('95% confidence lowerbound=',
num2str(mean95(1))),strcat('95% confidence upperbound=',
num2str(mean95(2)))};
annotation('textbox',dim,'String',str)


f = exp(-(result_B-mean).^2./(2*std^2))./(std*sqrt(2*pi));
plot(result_B,f,'LineWidth',1.5)
xlabel('critical niche
growth','FontSize',12,'FontWeight','bold','Color','b')
ylabel('probability','FontSize',12,'FontWeight','bold','Color','b')
```